Klimaänderung I

4. Das zukünftige globale Klima: Szenarien-basierte Projektionen und kurzfristiger Ausblick

Robert Sausen

Institut für Physik der Atmosphäre
Deutsches Zentrum für Luft- und Raumfahrt
Oberpfaffenhofen

Vorlesung WS 2021/22

LMU München

Technical information

- http://www.pa.op.dlr.de/~RobertSausen/vorlesung/index.html
  - Most recent update on the lecture
  - Slides of the lecture (with some delay)

  - See also LSF https://lsf.verwaltung.uni-muenchen.de/

- Contact: robert.sausen@dlr.de

- Further information:
  - www.ipcc.ch
  - www.de-ipcc.de

Contents of IPCC AR 6 2021: Working Group I: the Physical Science Basis

Chapters

IPCC 2021

Chapter 4: Future global climate: scenario-based projections and near-term information

Coordinating Lead Authors:

June-Yi Lee (Republic of Korea), Jochem Marotzke (Germany)

Lead Authors:

Govindasamy Bala (India/United States of America), Long Cao (China), Susanna Corti (Italy), John P. Dunne (United States of America), Francois Engelbrecht (South Africa), Erich Fischer (Switzerland), John C. Fyfe (Canada), Christopher Jones (United Kingdom), Amanda Maycock (United Kingdom), Joseph Mutemi (Kenya), Ousmane Ndiaye (Senegal), Swapna Panickal (India), Tianjun Zhou (China)

Chapter 3: Human influence on the climate system

Contributing Authors:

Sebastian Milinski (Germany), Kyung-Sook Yun (Republic of Korea), Kyle Armour (United States of America), Nicolas Bellouin (United Kingdom/France), Ingo Bethke (Norway/Germany), Michael P. Byrne (United Kingdom /Ireland), Christophe Cassou (France), Deliang Chen (Sweden), Annalisa Cherchi (Italy), Hannah M. Christensen (United Kingdom), Sarah L. Connors (France/United Kingdom), Alejandro Di Luca (Australia, Canada/Argentina), Sybren S. Drijfhout (The Netherlands), Christopher G. Fletcher (Canada/United Kingdom, Canada), Piers Forster (United Kingdom), Javier García-Serrano (Spain), Nathan P. Gillett (Canada), Darrell S. Kaufmann (United States of America), David P. Keller (Germany/United States of America), Ben Kravitz (United States of America), Hongmei Li (Germany/China), Yongxiao Liang (Canada/China), Andrew H. MacDougall (Canada), Elizaveta Malinina (Canada/Russian Federation), Matthew Menary (France/United Kingdom), William J. Merryfield (Canada/United States of America), Seung-Ki Min (Republic of Korea), Zebedee R.J. Nicholls (Australia), Dirk Notz (Germany), Brodie Pearson (United States of America/United Kingdom), Matthew D. K. Priestley (United Kingdom), Johannes Quaas (Germany), Aurélien Ribes (France), Alex C. Ruane (United States of America), Jean-Baptiste Sallée (France), Emilia Sanchez-Gomez (France/Spain), Sonia I. Seneviratne (Switzerland), Aimée B. A. Slangen (The Netherlands), Chris Smith (United Kingdom), Malte F. Stuecker (United States of America/Germany), Ranjini Swaminathan (United Kingdom/India), Peter W. Thorne (Ireland/ United Kingdom), Katarzyna B. Tokarska (Switzerland/Poland), Matthew Toohey (Canada, Germany/Canada), Andrew Turner (United Kingdom), Danila Volpi (Italy), Cunde Xiao (China), Giuseppe Zappa (Italy)

Review Editors:

Krishna Kumar Kanikicharla (Qatar/India), Vladimir Kattsov (Russian Federation), Masahide Kimoto (Japan)

IPCC AR6 WG I, 2021, Chapter 4

Evaluation and communication of degree of certainty in AR6 findings

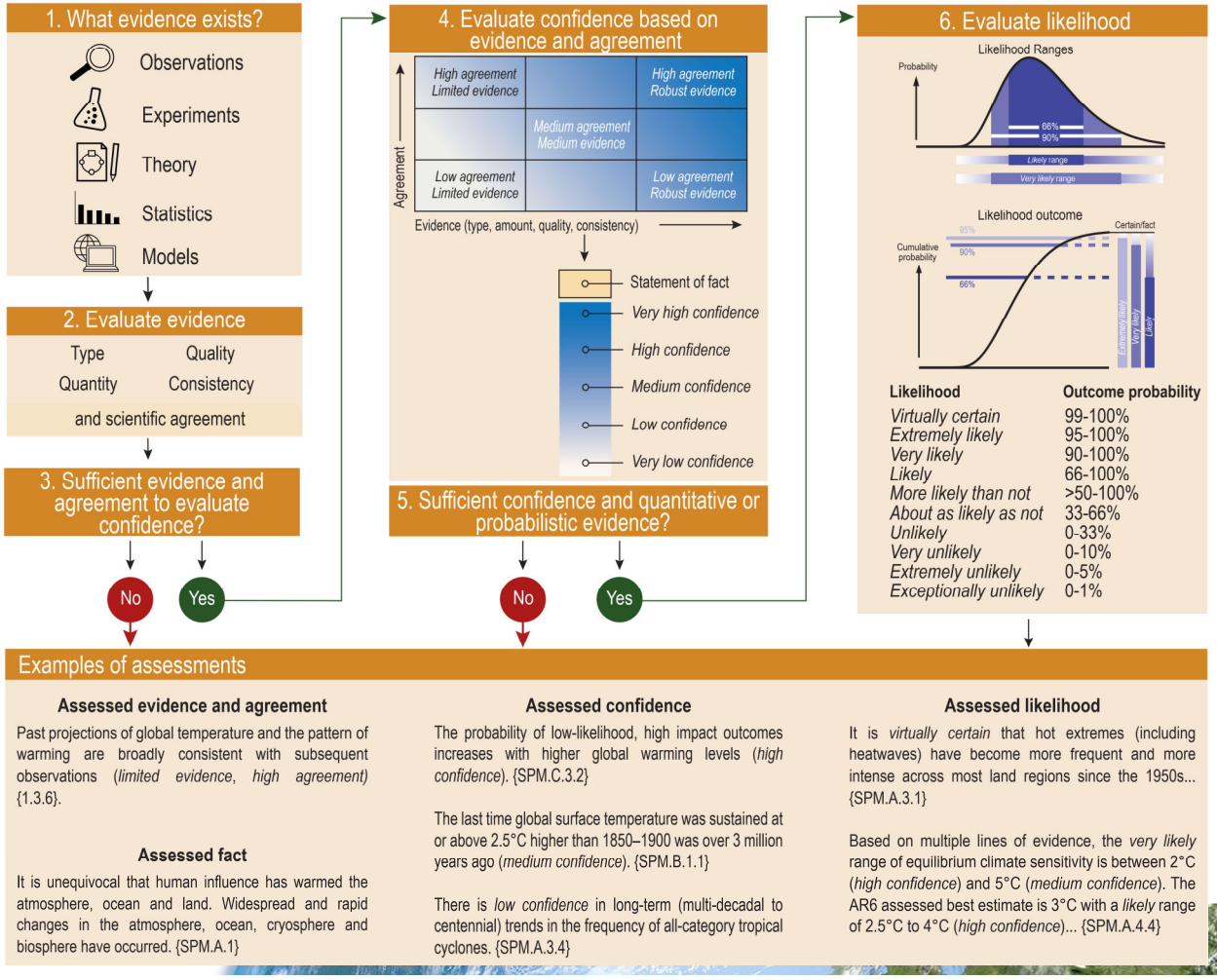

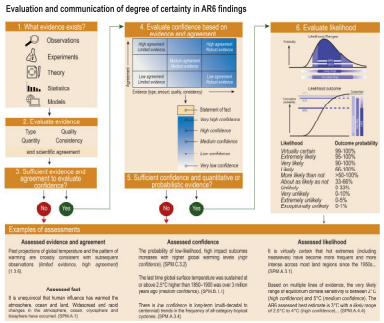

4. Evaluate confidence based on evidence and agreement

Agreement \ Evidence (type, amount, quality, consistency)		
		High agreement Robust evidence
	Medium agreement Medium evidence	
Low agreement Limited evidence		Low agreement Robust evidence

- Statement of fact
- Very high confidence
- High confidence
- Medium confidence
- Low confidence
- Very low confidence

5. Sufficient confidence and quantitative or probabilistic evidence?

No

Yes

6. Evaluate likelihood

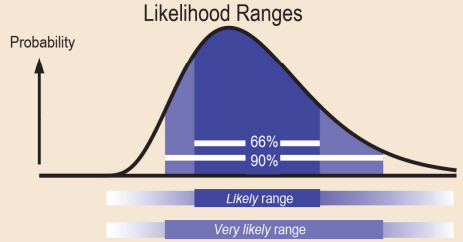

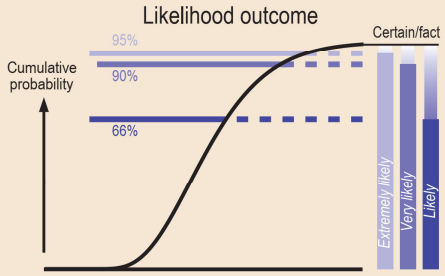

Likelihood	Outcome probability
Virtually certain	99-100%
Extremely likely	95-100%
Very likely	90-100%
Likely	66-100%
More likely than not	>50-100%
About as likely as not	33-66%
Unlikely	0-33%
Very unlikely	0-10%
Extremely unlikely	0-5%
Exceptionally unlikely	0-1%

IPCC 2021, Chap. 1

Chapter 4: Future global climate

Chapter 4 assesses simulations of future global climate change over the near, mid- and long term and out to year 2300.

Section 4.1
Overview

Section 4.2
Methodology

Section 4.3
Selected key indicators over the 21st century

Section 4.4
Near-term (2021–2040)

Section 4.5
Mid-term (2041–2060) and long-term (2081–2100)

Section 4.6
Policy implications

Section 4.7
Beyond 2100

Section 4.8
High warming storylines

FAQs

Chapter 4: **Quick guide**

Key topics and corresponding sub-sections

- Arctic sea ice and global sea level
  4.3.2 | **4.4.2**
- Climate models and forcing scenarios
  4.2.1 | **4.2.2** | **Box 4.1**
- Commitment, irreversibility and abrupt change
  4.7.1 | **4.7.2**
- Global monsoons
  4.4.1.4 | **4.5.1.5**
- Global surface temperature
  4.3.1 | **4.3.4** | **4.4.1** | **4.5.1** | **4.7.1**
- Global warming levels
  4.3.4 | **4.6.1**
- Mitigation, CO_2 removal and solar radiation modification
  4.6.3
- Modes of variability
  4.3.3 | **4.4.3** | **4.5.3**

Boxes

Box 4.1
Ensemble evaluation and weighting

Cross-chapter boxes

CC Box 4.1
The climate effects of volcanic eruptions

Figure 4.1 | Visual guide to Chapter 4.

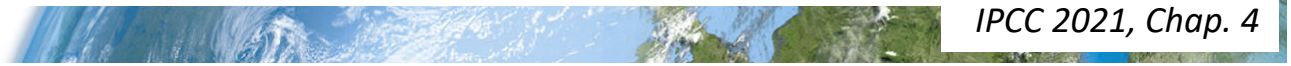

IPCC 2021, Chap. 4

Statements in the Executive Summary

This chapter assesses simulations of future global climate change, spanning time horizons from the near term (2021–2040), mid-term (2041–2060), and long term (2081–2100) out to the year 2300. Changes are assessed relative to both the recent past (1995–2014) and the 1850–1900 approximation to the pre-industrial period.

The projections assessed here are mainly based on a new range of scenarios, the Shared Socio-economic Pathways (SSPs) used in the Coupled Model Intercomparison Project Phase 6 (CMIP6). Among the SSPs, the focus is on the five scenarios SSP1-1.9, SSP1-2.6, SSP2-4.5, SSP3-7.0, and SSP5-8.5. In the SSP labels, the first number refers to the assumed shared socio-economic pathway, and the second refers to the approximate global effective radiative forcing (ERF) in 2100. Where appropriate, this chapter also assesses new results from CMIP5, which used scenarios based on Representative Concentration Pathways (RCPs). Additional lines of evidence enter the assessment, especially for change in globally averaged surface air temperature (GSAT) and global mean sea level (GMSL), while assessment for changes in other quantities is mainly based on CMIP6 results. Unless noted otherwise, the assessments assume that there will be no major volcanic eruption in the 21st century. {1.6, 4.2.2, 4.3.2, 4.3.4, 4.6.2, BOX 4.1: Cross-17 Chapter Box 4.1, Cross-Chapter Box 7.1, 9.6}

Die SSP-Szenarien
Shared Socioeconomic Pathways

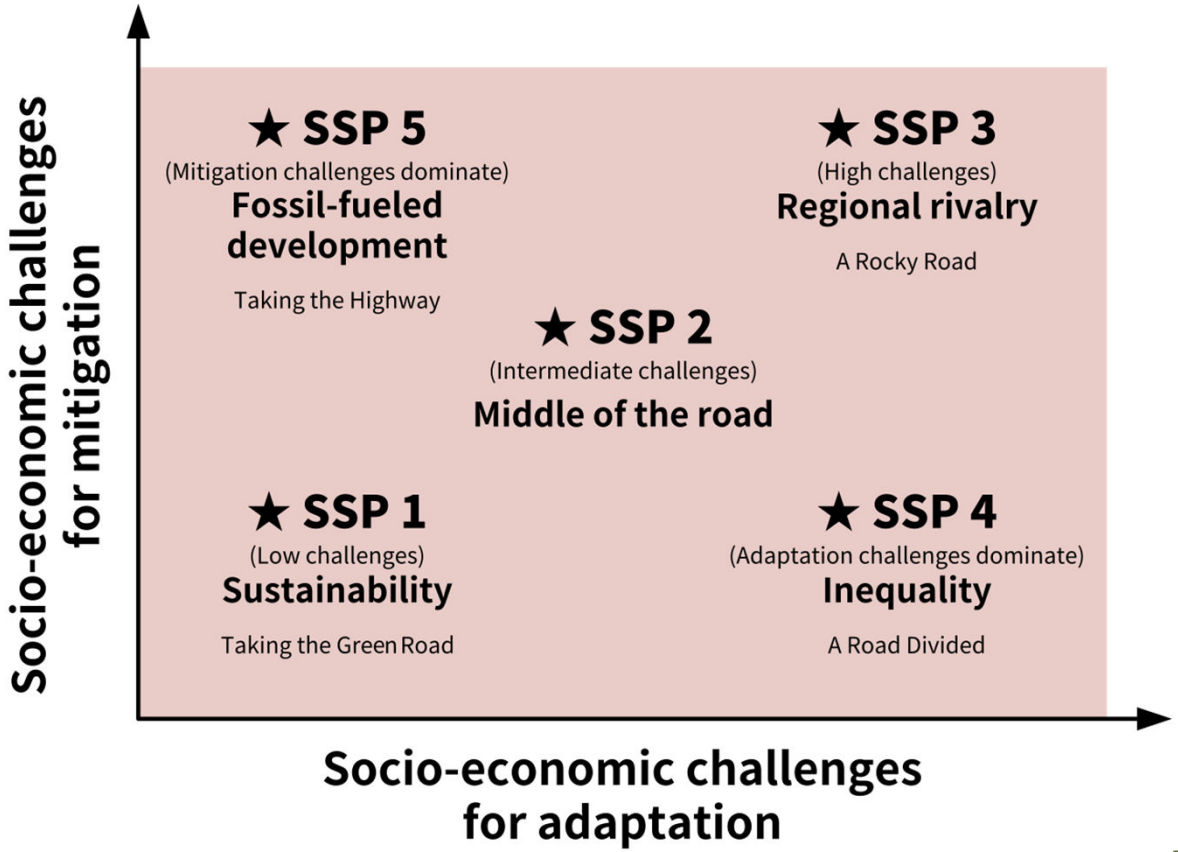

https://en.wikipedia.org

Die SSP-Szenarien – Shared Socioeconomic Pathways

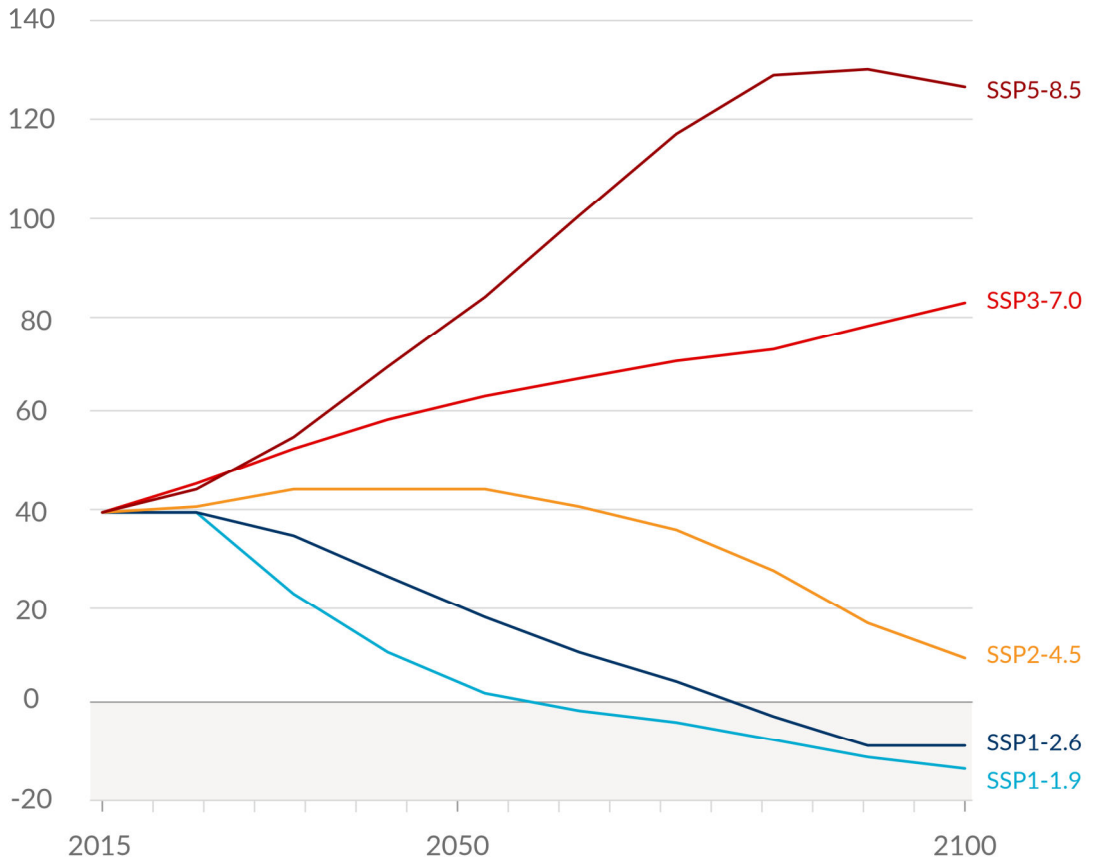

IPCC 2021, SPM

Statements in the Executive Summary

Temperature (1)

Assessed future change in GSAT is, for the first time in an IPCC report, explicitly constructed by combining scenario-based projections with observational constraints based on past simulated warming, as well as an updated assessment of equilibrium climate sensitivity (ECS) and transient climate response (TCR). Climate forecasts initialized using recent observations have also been used for the period 2019–2028. The inclusion of additional lines of evidence has reduced the assessed uncertainty ranges for each scenario. {4.3.1, 4.3.4, 4.4.1, 7.5}

IPCC 2021, Chap. 4

Statements in the Executive Summary

Temperature (2a)

In the near term (2021–2040), a 1.5°C increase in the 20-year average of GSAT, relative to the average over the period 1850–1900, is *very likely* to occur in scenario SSP5-8.5, *likely* to occur in scenarios SSP2-4.5 and SSP3-7.0, and *more likely than not* to occur in scenarios SSP1-1.9 and SSP1-2.6. The threshold-crossing time is defined as the midpoint of the first 20-year period during which the average GSAT exceeds the threshold. In all scenarios assessed here except SSP5-8.5, the central estimate of crossing the 1.5°C threshold lies in the early 2030s. This is about ten years earlier than the midpoint of the *likely* range (2030–2052) assessed in the SR1.5, which assumed continuation of the then-current warming rate; this rate has been confirmed in the AR6. Roughly half of the ten-year difference between assessed crossing times arises from a larger historical warming diagnosed in AR6. ...

SR1.5

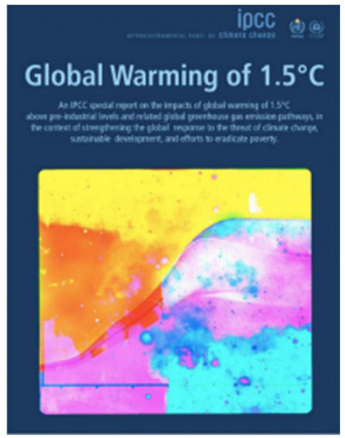

IPCC 2021, Chap. 4

Statements in the Executive Summary

Temperature (2b)

... The other half arises because for central estimates of climate sensitivity, most scenarios show stronger warming over the near term than was assessed as ‘current’ in SR1.5 (*medium confidence*). It is *more likely than not* that under SSP1-1.9, GSAT relative to 1850–1900 will remain below 1.6°C throughout the 21st century, implying a potential temporary overshoot of 1.5°C global warming of no more than 0.1°C. If climate sensitivity lies near the lower end of the assessed *very likely* range, crossing the 1.5°C warming threshold is avoided in scenarios SSP1-1.9 and SSP1-2.6 (*medium confidence*). {2.3.1, Cross-chapter Box 2.3, 3.3.1, 4.3.4, BOX 4.1:, 7.5}

IPCC 2021, Chap. 4

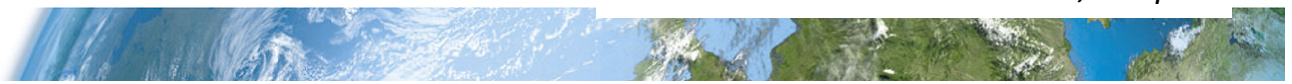

CMIP6 annual-mean GSAT simulations and various contributions to uncertainty in the projections ensemble

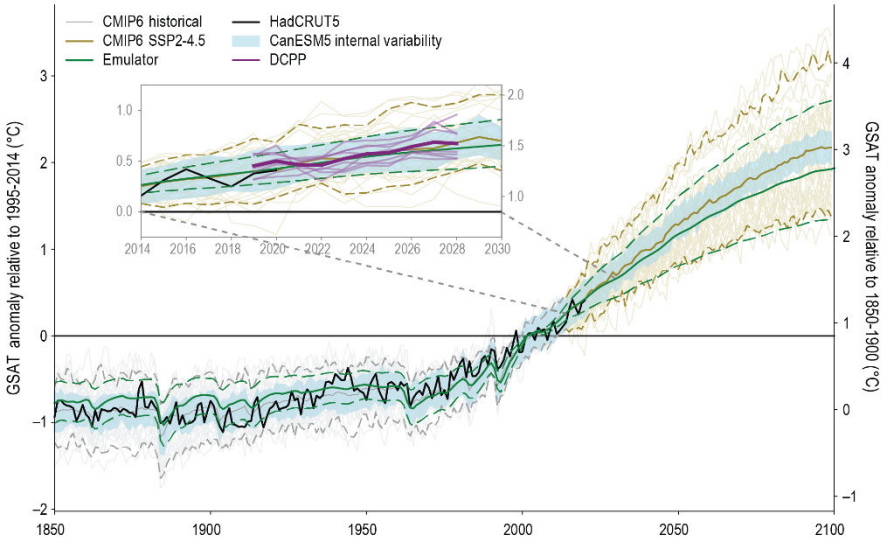

Box 4.1 Figure 1 | CMIP6 annual mean global surface air temperature (GSAT) simulations and various contributions to uncertainty in the projections ensemble. The figure shows anomalies relative to the period 1995–2014 (left y-axis), converted to anomalies relative to 1850–1900 (right y-axis); the difference between the y-axes is 0.85°C (Cross-Chapter Box 2.3). Shown are historical simulations with 39 CMIP6 models (grey) and projections following scenario SSP2-4.5 (dark yellow; thin lines: individual simulations; heavy line; ensemble mean; dashed lines: 5% and 95% ranges). The black curve shows the observations-based estimate (HadCRUT5; Morice et al., 2021). Light blue shading shows the 50-member ensemble CanESM5, such that the deviations from the CanESM5 ensemble mean have been added to the CMIP6 multi-model mean. The green curves are from the emulator and show the central estimate (solid) and *very likely* range (dashed) for GSAT. The inset shows a cut-out from the main plot and additionally in light purple for the period 2019–2028 the initialized forecasts from eight models contributing to DCPP (Boer et al., 2016); the deep-purple curve shows the average of the forecasts. Further details on data sources and processing are available in the chapter data table (Table 4.SM.1).

IPCC 2021, Chap. 4

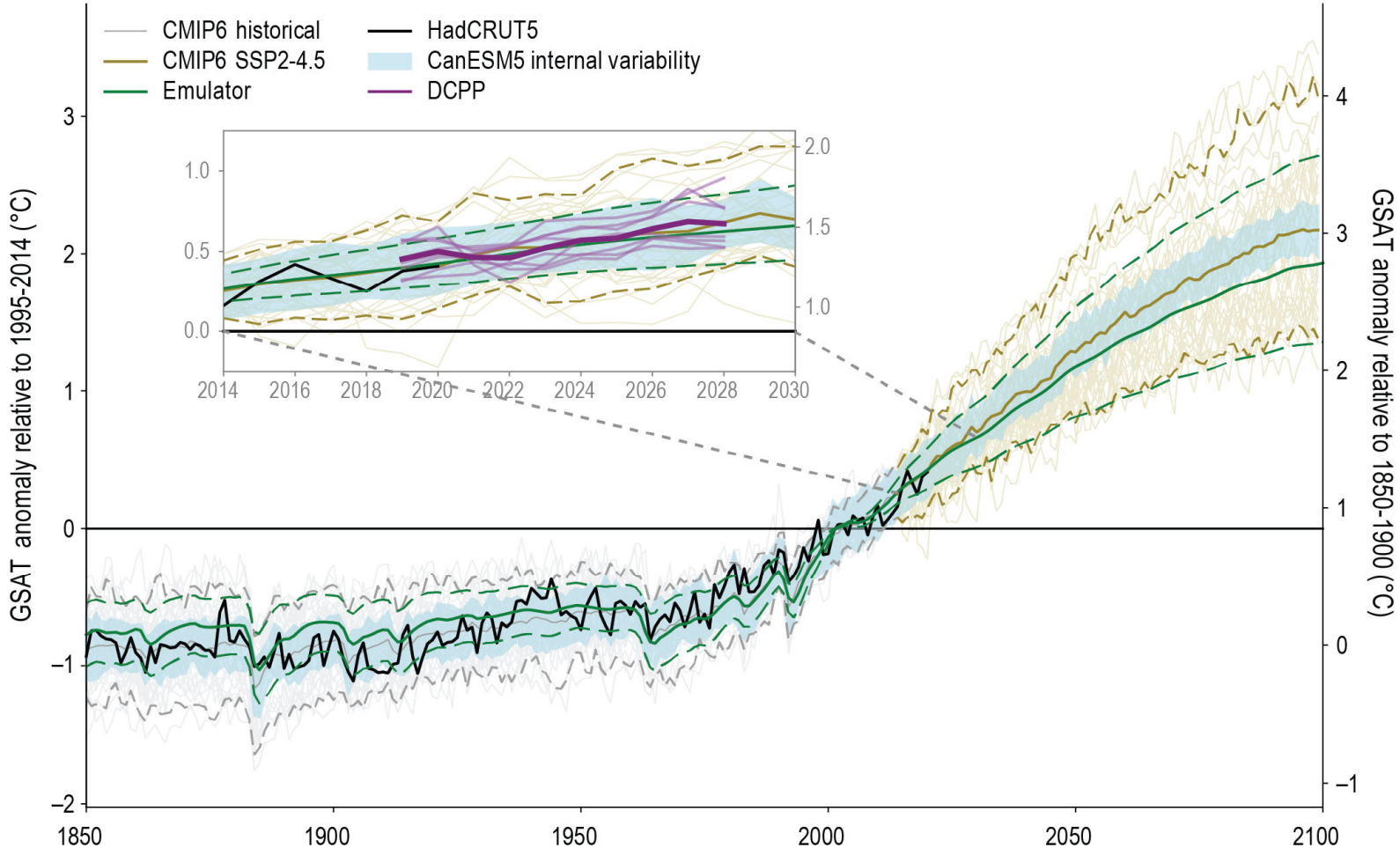

IPCC 2021, Chap. 4

Selected indicators of global climate change from CMIP6 historical and scenario simulations

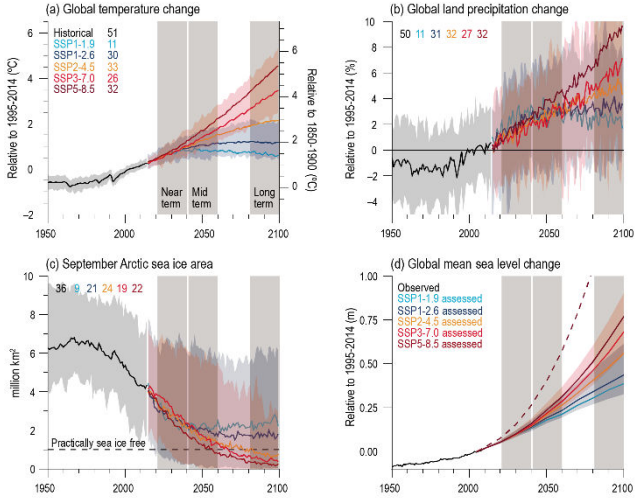

Figure 4.2 | Selected indicators of global climate change from CMIP6 historical and scenario simulations. (a) Global surface air temperature changes relative to the 1995–2014 average (left axis) and relative to the 1850–1900 average (right axis; offset by 0.82°C, which is the multi-model mean and close to observed best estimate, Cross-Chapter Box 2.1, Table 1). **(b)** Global land precipitation changes relative to the 1995–2014 average. **(c)** September Arctic sea ice area. **(d)** Global mean sea level (GMSL) change relative to the 1995–2014 average. (a), (b) and (d) are annual averages, (c) are September averages. In (a–c), the curves show averages over the CMIP6 simulations, the shadings around the SSP1-2.6 and SSP3-7.0 curves show 5–95% ranges, and the numbers near the top show the number of model simulations used. Results are derived from concentration-driven simulations. In (d), the barystatic contribution to GMSL (i.e., the contribution from land-ice melt) has been added offline to the CMIP6 simulated contributions from thermal expansion (thermosteric). The shadings around the SSP1-2.6 and SSP3-7.0 curves show 5–95% ranges. The dashed curve is the *low confidence* and low likelihood outcome at the high end of SSP5-8.5 and reflects deep uncertainties arising from potential ice-sheet and ice-cliff instabilities. This curve at year 2100 indicates 1.7 m of GMSL rise relative to 1995–2014. More information on the calculation of GMSL is available in Chapter 9, and further regional details are provided in the Atlas. Further details on data sources and processing are available in the chapter data table (Table 4.SM.1).

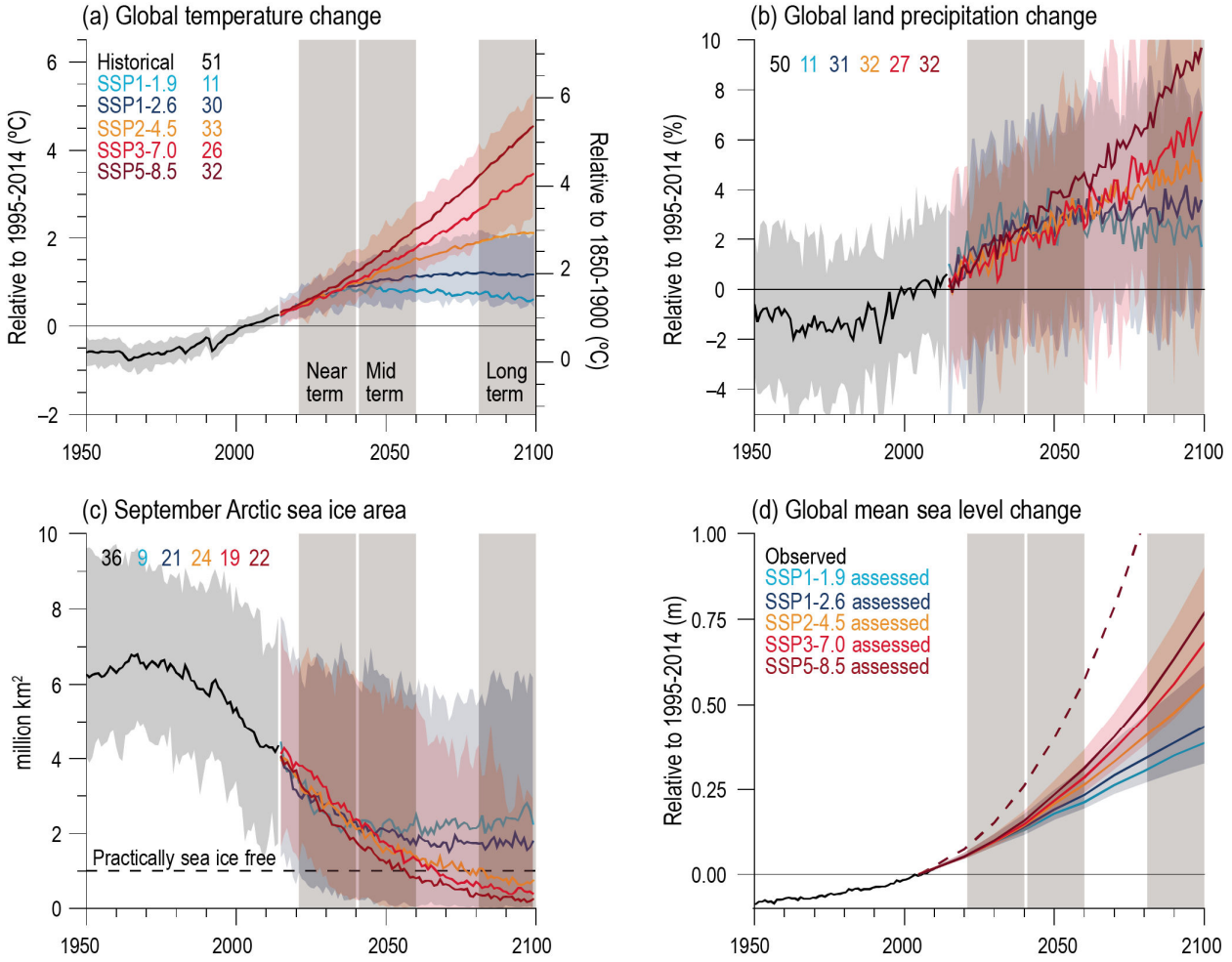

IPCC 2021, Chap. 4

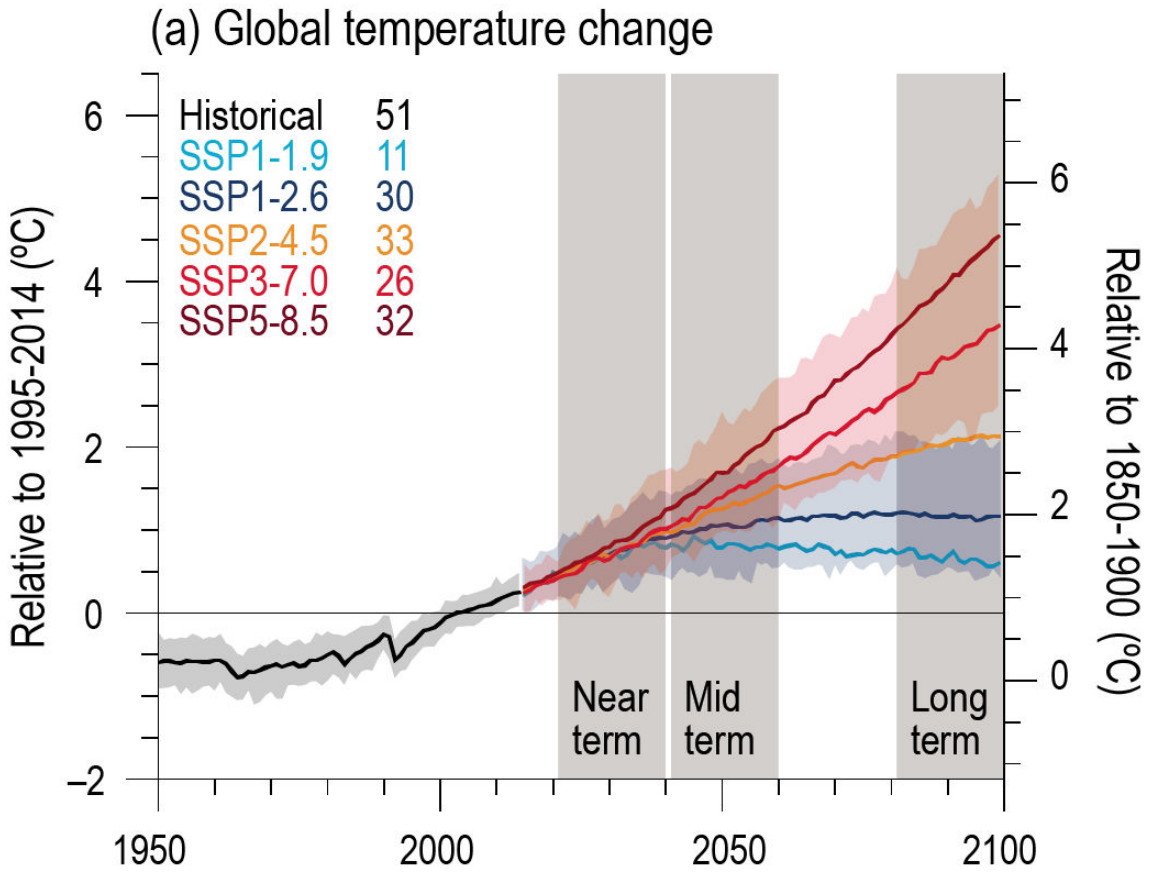

IPCC 2021, Chap. 4

Statements in the Executive Summary

Temperature (3)

By 2030, GSAT in any individual year could exceed 1.5°C relative to 1850–1900 with a likelihood between 40% and 60%, across the scenarios considered here (*medium confidence*). Uncertainty in near-term projections of annual GSAT arises in roughly equal measure from natural internal variability and model uncertainty (*high confidence*). By contrast, near-term annual GSAT levels depend less on the scenario chosen, consistent with the AR5 assessment. Forecasts initialized from recent observations simulate annual GSAT changes for the period 2019–2028 relative to the recent past that are consistent with the assessed *very likely* range (*high confidence*). {4.4.1, BOX 4.1:}

IPCC 2021, Chap. 4

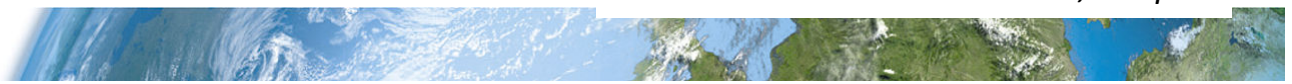

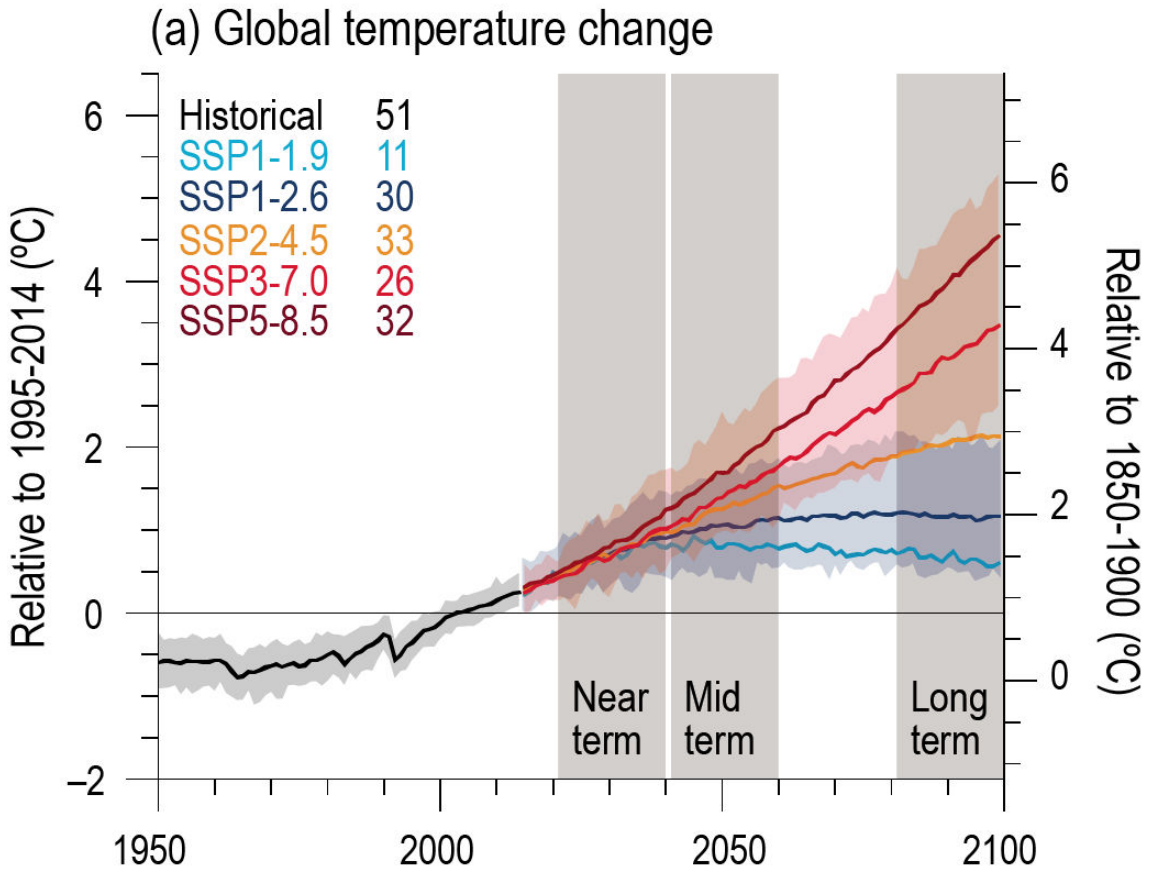

IPCC 2021, Chap. 4

Statements in the Executive Summary

Temperature (4)

Compared to the recent past (1995–2014), GSAT averaged over the period 2081–2100 is *very likely* to be higher by 0.2°C–1.0°C in the low-emission scenario SSP1-1.9 and by 2.4°C–4.8°C in the high-emission scenario SSP5-8.5. For the scenarios SSP1-2.6, SSP2-4.5, and SSP3-7.0, the corresponding *very likely* ranges are 0.5°C–1.5°C, 1.2°C–2.6°C, and 2.0°C–3.7°C, respectively. The uncertainty ranges for the period 2081–2100 continue to be dominated by the uncertainty in ECS and TCR (*very high confidence*). Emissions-driven simulations for SSP5-8.5 show that carbon-cycle uncertainty is too small to change the assessment of GSAT projections (*high confidence*). {4.3.1, 4.3.4, 4.6.2, 7.5}

IPCC 2021, Chap. 4

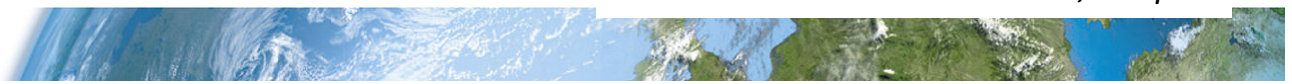

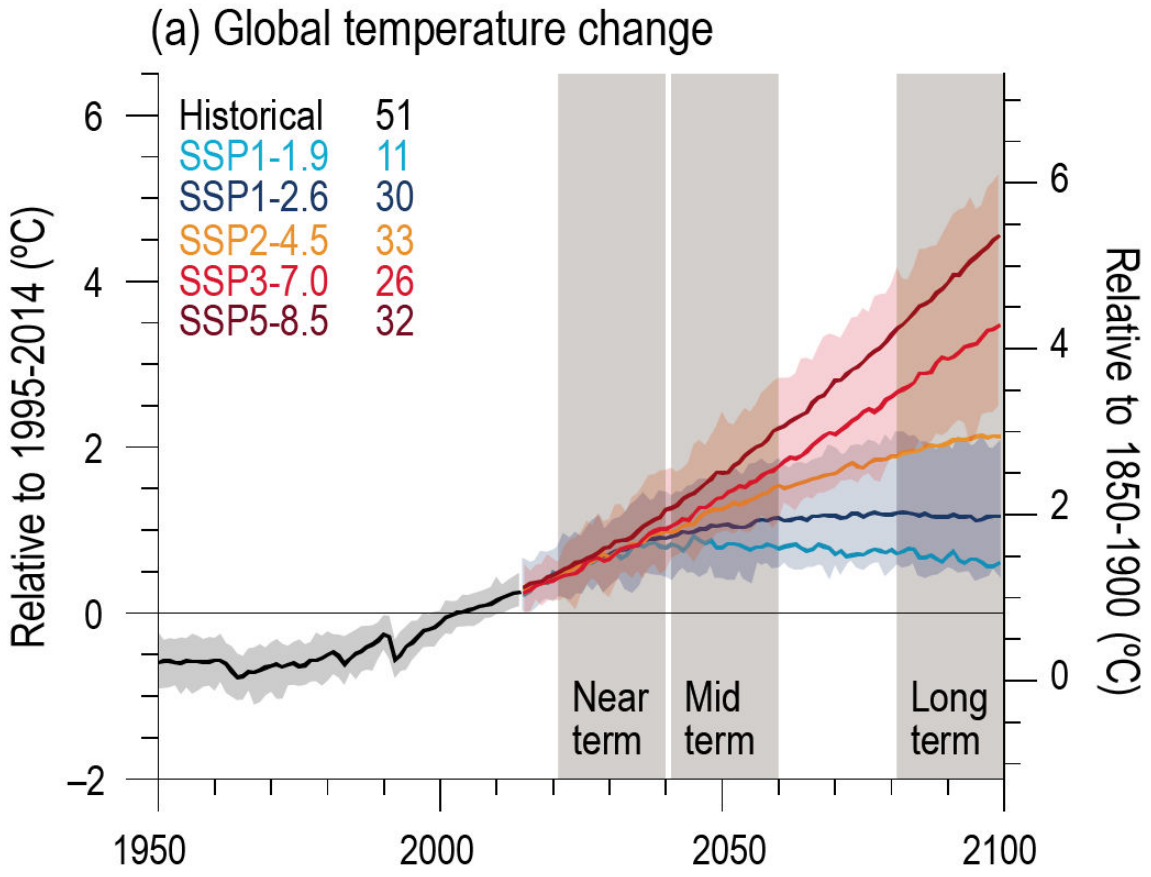

IPCC 2021, Chap. 4

Comparison of concentration-driven and emission-driven simulation

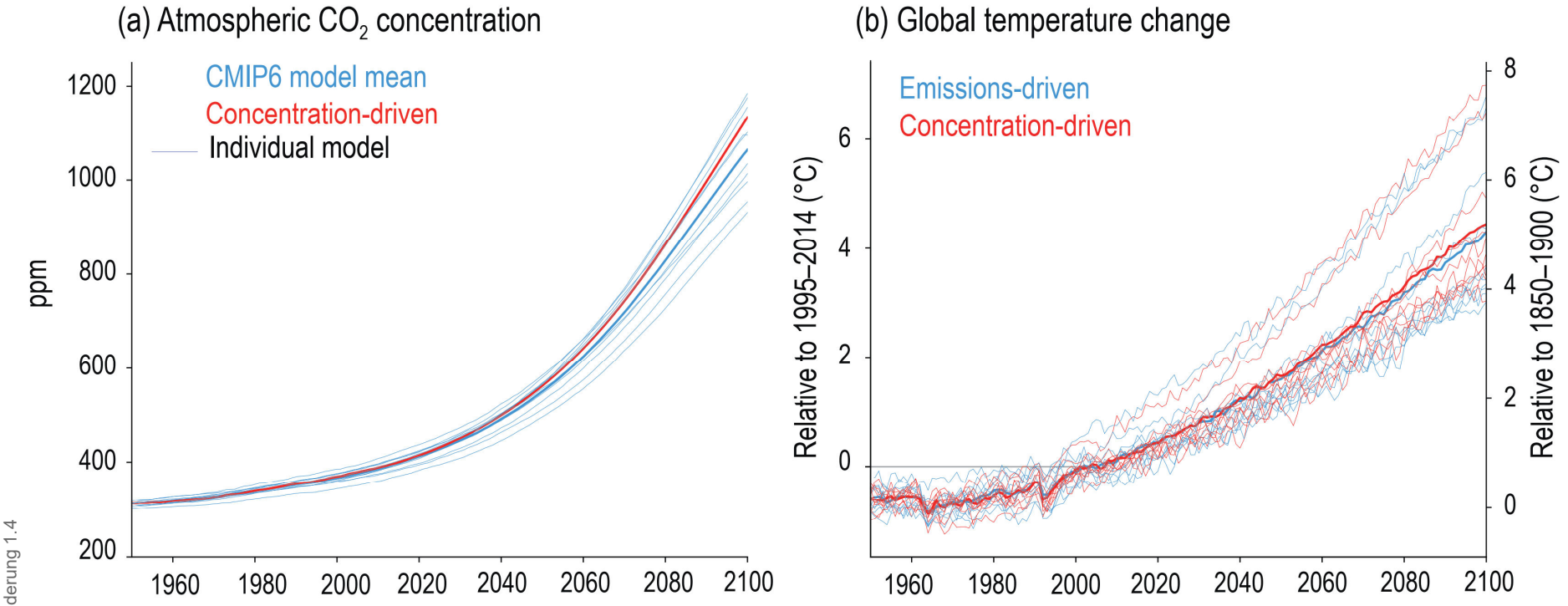

Figure 4.3 | Comparison of concentration-driven and emissions-driven simulation. (a) Atmospheric CO_2 concentration; **(b)** global surface air temperature from models which performed SSP5-8.5 scenario simulations in both emissions-driven (blue) and concentration-driven (red) configurations. For concentration driven simulations, CO_2 concentration is prescribed, and follows the red line in panel (a) in all models. For emissions-driven simulations, CO_2 concentration is simulated and can therefore differ for each model, blue lines in panel (a). Further details on data sources and processing are available in the chapter data table (Table 4.SM.1).

IPCC 2021, Chap. 4

Statements in the Executive Summary

Temperature (5)

The CMIP6 models project a wider range of GSAT change than the assessed range (*high confidence*); furthermore, the CMIP6 GSAT increase tends to be larger than in CMIP5 (*very high confidence*). About half of the increase in simulated warming has occurred because higher climate sensitivity is more prevalent in CMIP6 than in CMIP5; the other half arises from higher ERF in nominally comparable scenarios (e.g., RCP8.5 and SSP5-8.5; *medium confidence*). In SSP1-2.6 and SSP2-4.5, ERF changes also explain about half of the changes in the range of warming (*medium confidence*). For SSP5-8.5, higher climate sensitivity is the primary reason behind the upper end of the warming being higher than in CMIP5 (*medium confidence*). {4.3.1, 4.3.4, 4.6.2, 7.5.6}

IPCC 2021, Chap. 4

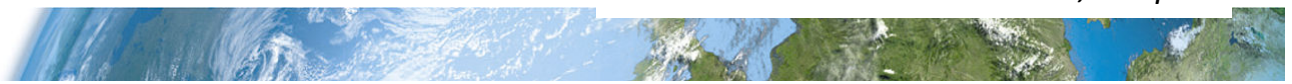

Statements in the Executive Summary

Temperature (6)

While high-warming storylines – those associated with GSAT levels above the upper bound of the assessed *very likely* range – are by definition *extremely unlikely*, they cannot be ruled out. For SSP1-2.6, such a high-warming storyline implies long-term (2081–2100) warming well above, rather than well below, 2° C (*high confidence*). Irrespective of scenario, high-warming storylines imply changes in many aspects of the climate system that exceed the patterns associated with the central estimate of GSAT changes by up to more than 50% (*high confidence*). {4.3.4, 4.8}

IPCC 2021, Chap. 4

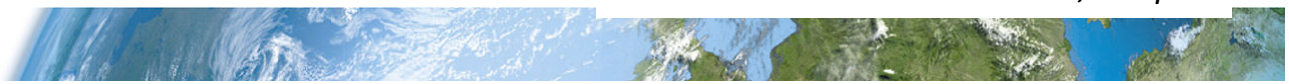

Statements in the Executive Summary

Temperature (7)

It is *virtually certain* that the average surface warming will continue to be higher over land than over the ocean and that the surface warming in the Arctic will continue to be more pronounced than the global average over the 21st century. The warming pattern likely varies across seasons, with northern high latitudes warming more during boreal winter than summer (*medium confidence*). Regions with increasing or decreasing year-to-year variability of seasonal mean temperatures will *likely* increase in their spatial extent. {4.3.1, 4.5.1, 7.4.4}

IPCC 2021, Chap. 4

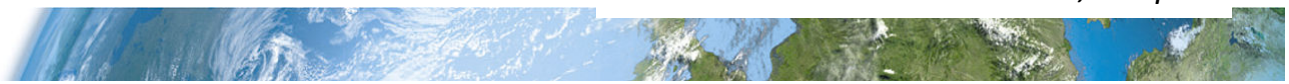

Near-term change of seasonal mean surface temperature

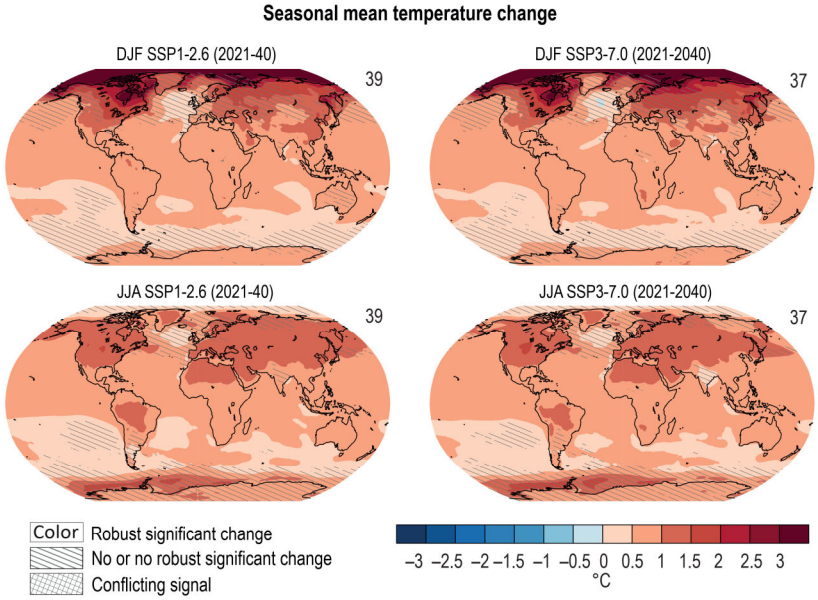

Figure 4.12 | Near-term change of seasonal mean surface temperature. Displayed are projected spatial patterns of CMIP6 multi-model mean change (°C) in **(top)** December–January–February (DJF) and **(bottom)** June–July–August (JJA) near-surface air temperature for 2021–2040 from SSP1-2.6 and SSP3-7.0 relative to 1995–2014. The number of models used is indicated in the top right of the maps. No overlay indicates regions where the change is robust and *likely* emerges from internal variability, that is, where at least 66% of the models show a change greater than the internal-variability threshold (Section 4.2.6) and at least 80% of the models agree on the sign of change. Diagonal lines indicate regions with no change or no robust significant change, where fewer than 66% of the models show change greater than the internal-variability threshold. Crossed lines indicate areas of conflicting signals where at least 66% of the models show change greater than the internal-variability threshold but fewer than 80% of all models agree on the sign of change. Further details on data sources and processing are available in the chapter data table (Table 4.SM.1).

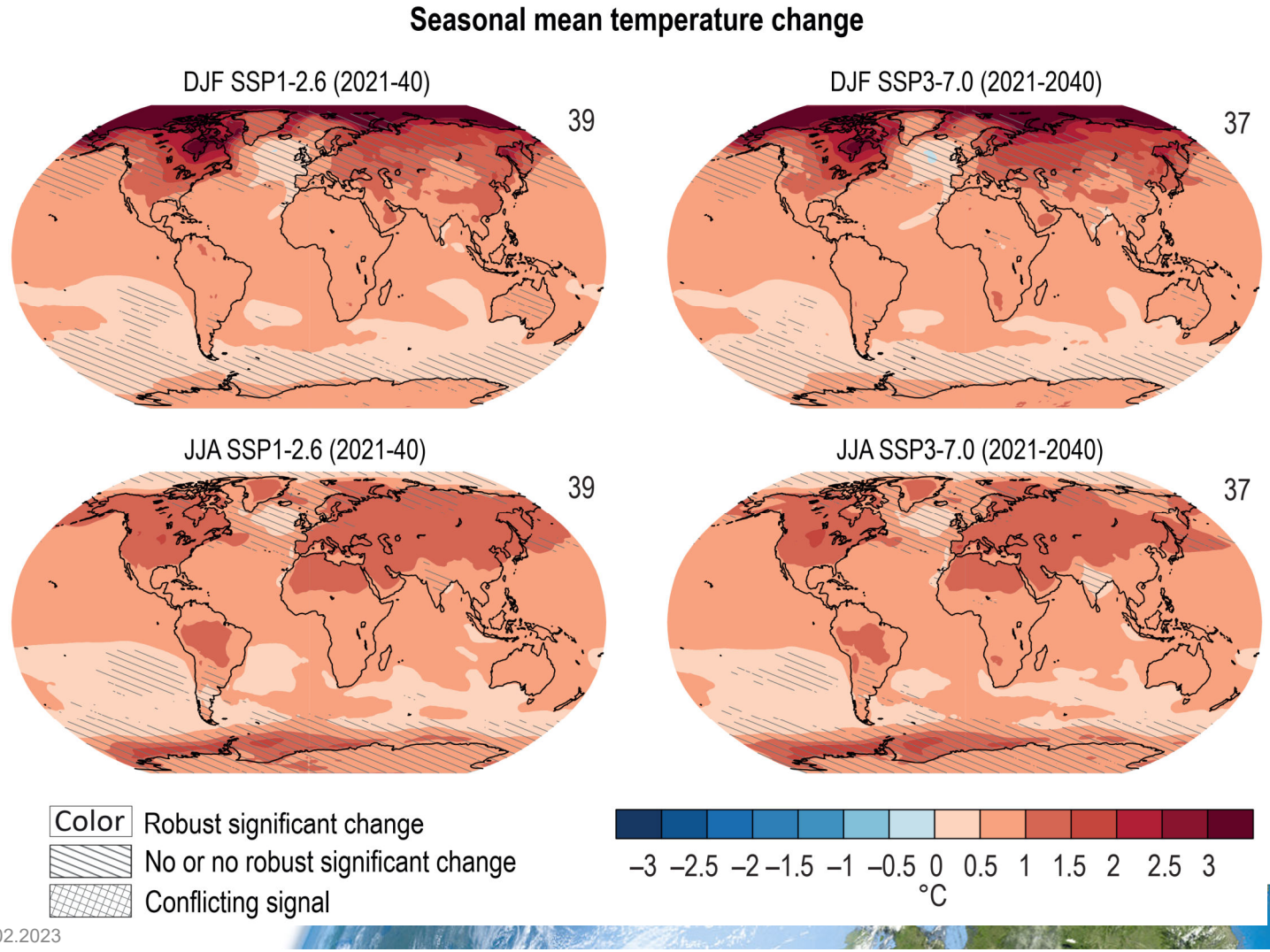

IPCC 2021, Chap. 4

Simulations over the period 1995–2040, encompassing the recent past and the next twenty years, of two important indicators of global climate change

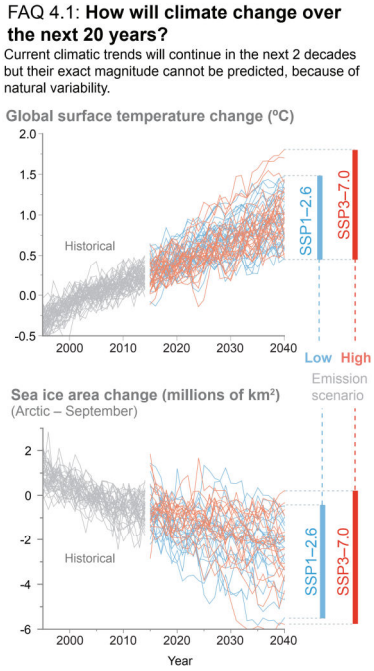

FAQ 4.1, Figure 1 | Simulations over the period 1995–2040, encompassing the recent past and the next twenty years, of two important indicators of global climate change. (Top) Global surface temperature, and **(bottom)**, the area of Arctic sea ice in September. Both quantities are shown as deviations from the average over the period 1995–2014. The grey curves are for the historical period ending in 2014; the blue curves represent a low-emissions scenario (SSP1-2.6) and the red curves one high-emissions scenario (SSP3-7.0).

IPCC 2021, Chap. 4

FAQ 4.1: **How will climate change over the next 20 years?**

Current climatic trends will continue in the next 2 decades but their exact magnitude cannot be predicted, because of natural variability.

Global surface temperature change (ºC)

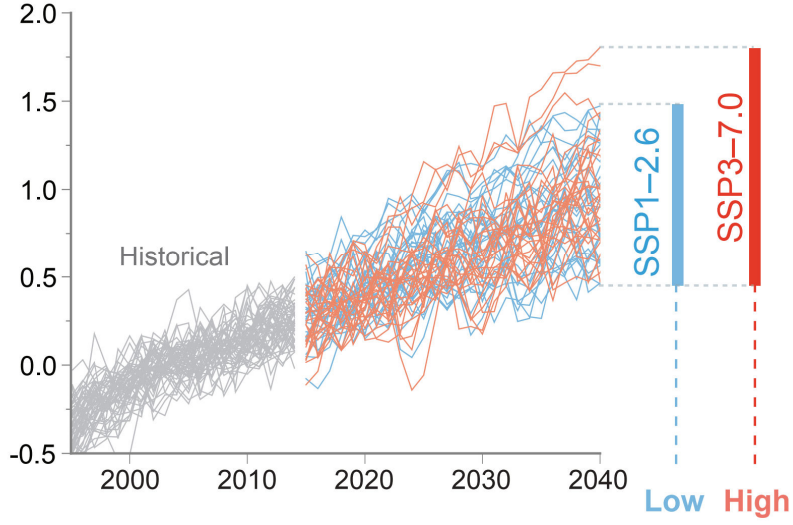

Sea ice area change (millions of km²)
(Arctic – September)

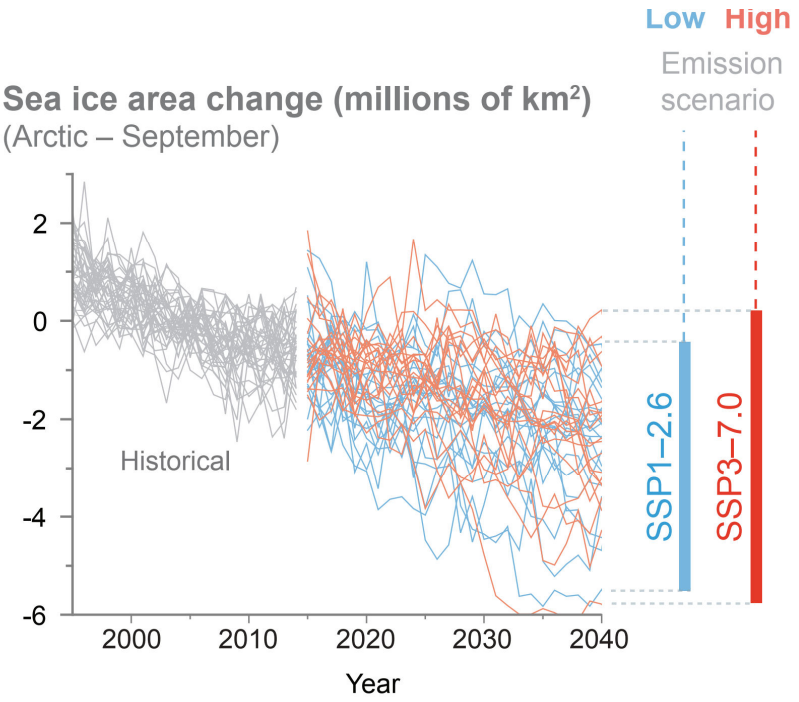

IPCC 2021, Chap. 4

Mid- and long-term change of annual mean surface temperature

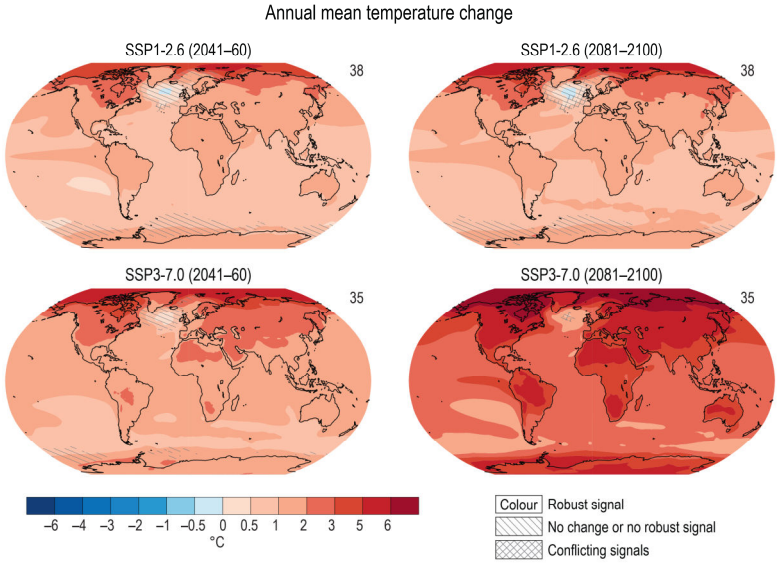

Figure 4.19 | Mid- and long-term change of annual mean surface temperature. Displayed are projected spatial patterns of multi-model mean change in annual mean near-surface air temperature (°C) in 2041–2060 and 2081–2100 relative to 1995–2014 for **(top)** SSP1-2.6 and **(bottom)** SSP3-7.0. The number of models used is indicated in the top right of the maps. No overlay indicates regions where the change is robust and *likely* emerges from internal variability, that is, where at least 66% of the models show a change greater than the internal-variability threshold (see Section 4.2.6) and at least 80% of the models agree on the sign of change. Diagonal lines indicate regions with no change or no robust significant change, where fewer than 66% of the models show change greater than the internal-variability threshold. Crossed lines indicate areas of conflicting signals where at least 66% of the models show change greater than the internal-variability threshold but fewer than 80% of all models agree on the sign of change. Further details on data sources and processing are available in the chapter data table (Table 4.SM.1).

Annual mean temperature change

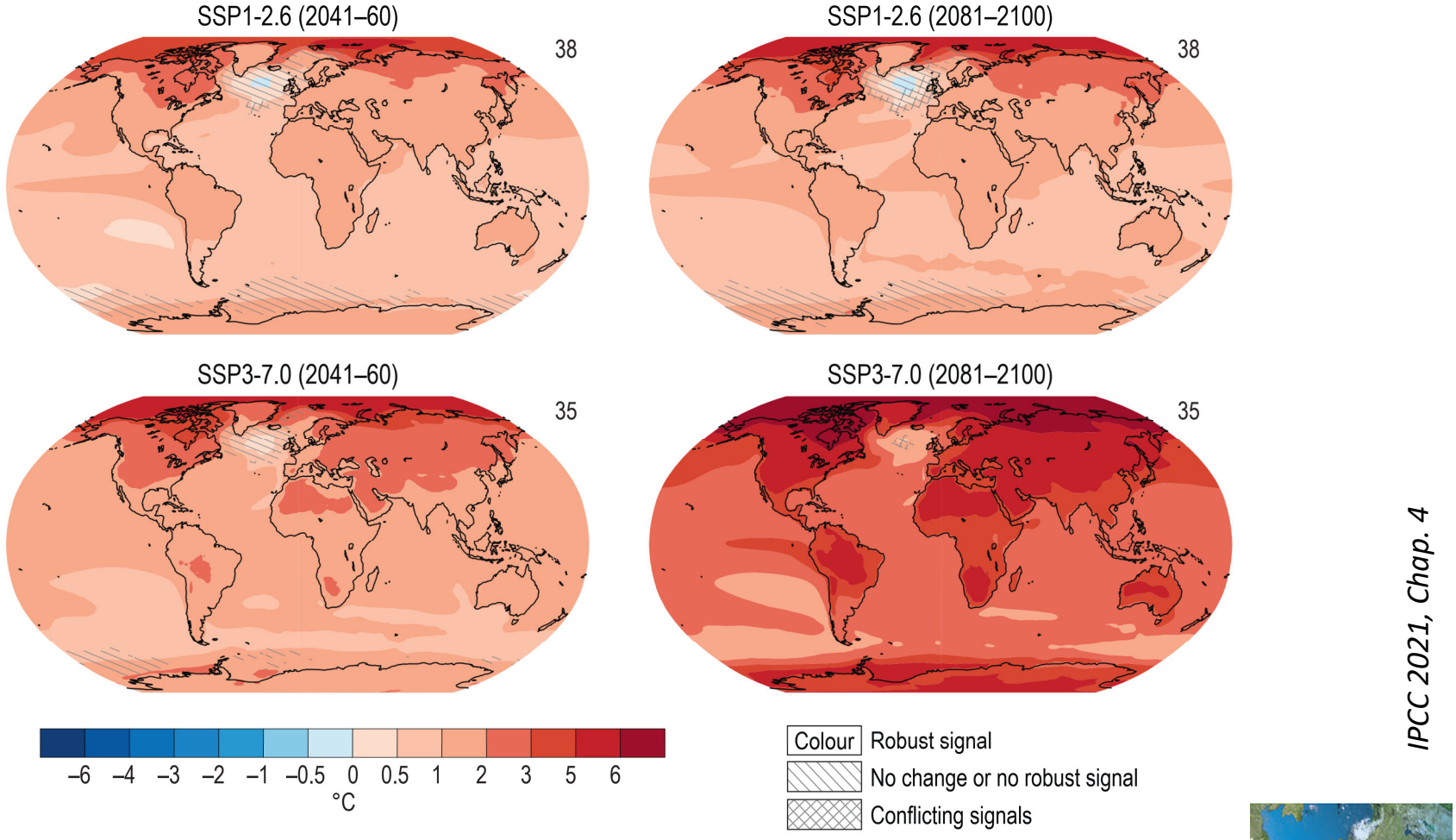

IPCC 2021, Chap. 4

Projected spatial patterns of change in annual average near-surface temperature (°C) at different levels of global warming.

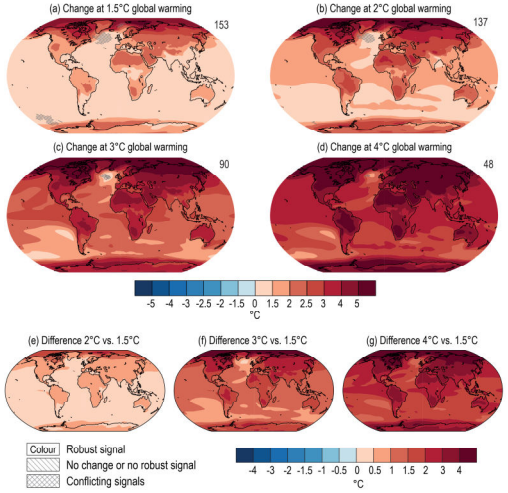

Figure 4.31 | Projected spatial patterns of change in annual average near-surface temperature (°C) at different levels of global warming. Displayed are **(a–d)** spatial patterns of change in annual average near-surface temperature at 1.5°C, 2°C, 3°C, and 4°C of global warming relative to the period 1850–1900 and **(e–g)** spatial patterns of differences in temperature change at 2°C, 3°C, and 4°C of global warming compared to 1.5°C of global warming. The number of models used is indicated in the top right of the maps. No overlay indicates regions where the change is robust and *likely* emerges from internal variability. That is, where at least 66% of the models show a change greater than the internal-variability threshold (Section 4.2.6) and at least 80% of the models agree on the sign of change. Diagonal lines indicate regions with no change or no robust significant change, where fewer than 66% of the models show change greater than the internal-variability threshold. Crossed lines indicate areas of conflicting signals where at least 66% of the models show change greater than the internal-variability threshold but fewer than 80% of all models agree on the sign of change. Values were assessed from a 20-year period at a given warming level, based on model simulations under the Tier-1 SSPs of CMIP6. Further details on data sources and processing are available in the chapter data table (Table 4.SM.1).

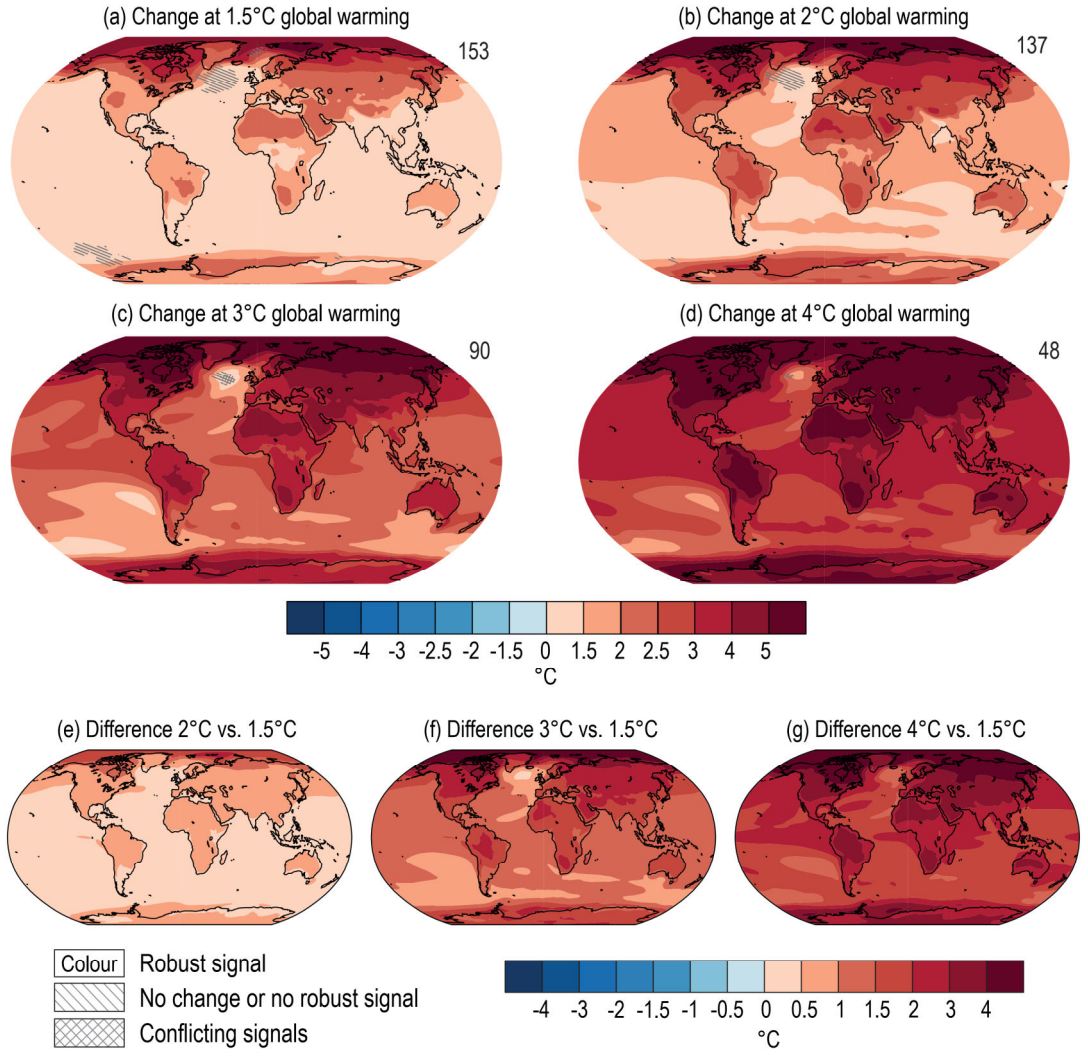
(a) Change at 1.5°C global warming
153
(b) Change at 2°C global warming
137
(c) Change at 3°C global warming
90
(d) Change at 4°C global warming
48
-5 -4 -3 -2.5 -2 -1.5 0 1.5 2 2.5 3 4 5
°C
(e) Difference 2°C vs. 1.5°C
(f) Difference 3°C vs. 1.5°C
(g) Difference 4°C vs. 1.5°C
Colour
Robust signal
No change or no robust signal
Conflicting signals
-4 -3 -2 -1.5 -1 -0.5 0 0.5 1 1.5 2 3 4
°C

Difference of surface temperature change between JJA and DJF

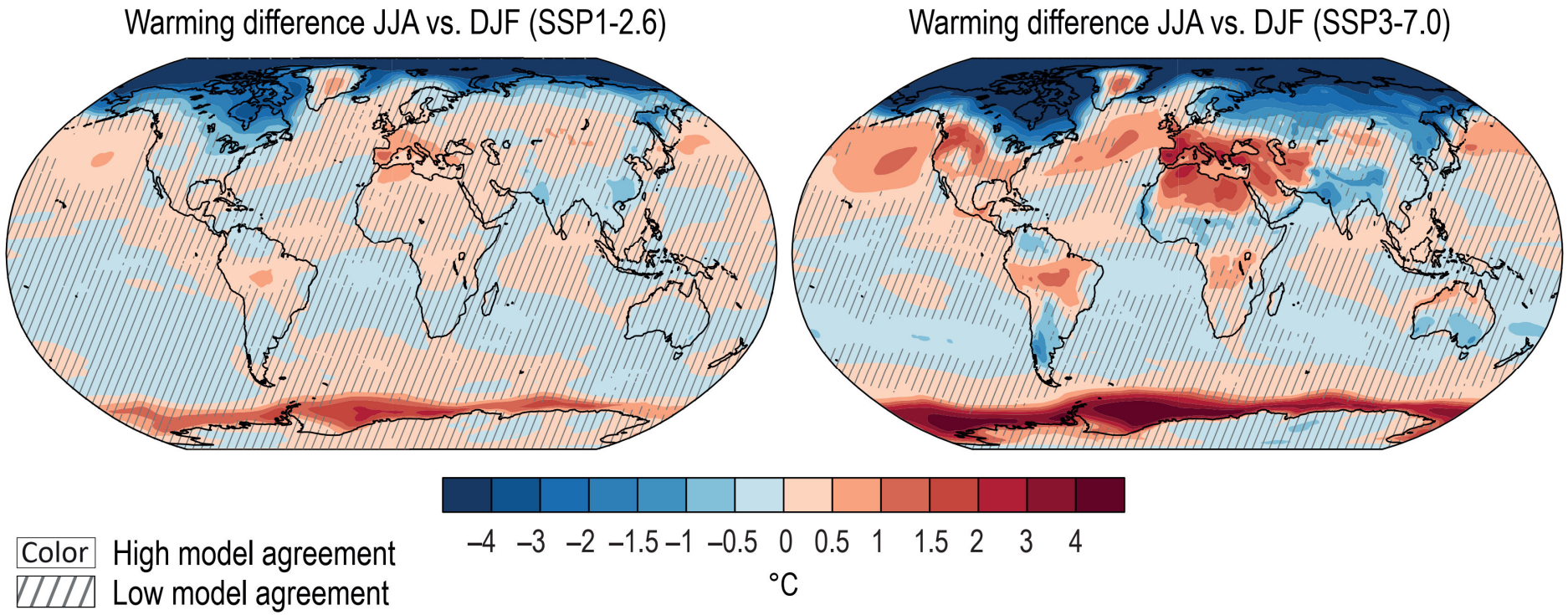

Figure 4.20 | Difference of surface temperature change between June–July–August (JJA) and December–January–February (DJF). Displayed are spatial patterns of multi-model mean difference in projected warming in JJA minus warming in DJF in 2081–2100 relative to 1995–2014 for **(left)** SSP1-2.6 and **(right)** SSP3-7.0. Diagonal lines mark areas where fewer than 80% of the models agree on the sign of change, and no overlay where at least 80% of the models agree. Further details on data sources and processing are available in the chapter data table (Table 4.SM.1).

IPCC 2021, Chap. 4

Potential impact of volcanic eruption on future global temperature change

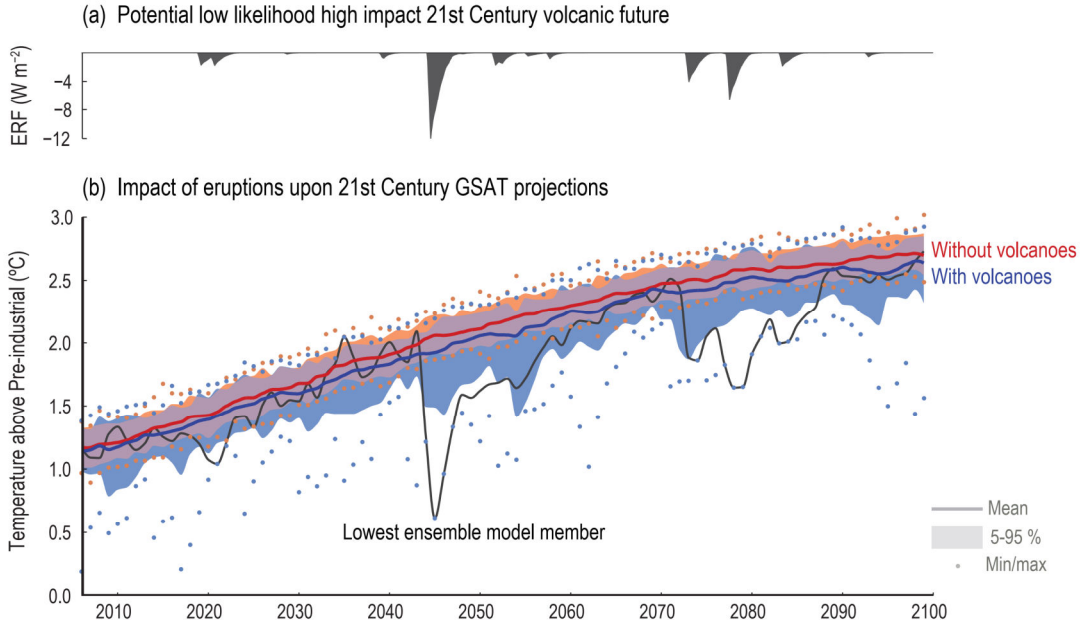

Cross-Chapter Box 4.1, Figure 1 | Potential impact of volcanic eruption on future global temperature change. CMIP5 projections of possible 21st-century futures under RCP4.5 after a 1257 Samalas magnitude volcanic eruption in 2044, from Bethke et al. (2017). **(a)** Volcanic ERF of the most volcanically active ensemble member, estimated from SAOD. **(b)** Annual mean global surface air temperature. Ensemble mean (solid) of future projections including volcanoes (blue) and excluding volcanoes (red) with 5–95% range (shading) and ensemble minima/maxima (dots); evolution of the most volcanically active member (black). Data created using a SMILE approach with NorESM1 in its CMIP5 configuration. See Sections 2.2.2 and 4.4.4 for more details. Further details on data sources and processing are available in the chapter data table (Table 4.SM.1).

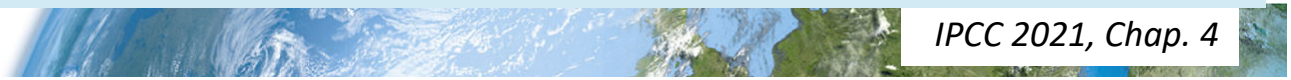

IPCC 2021, Chap. 4

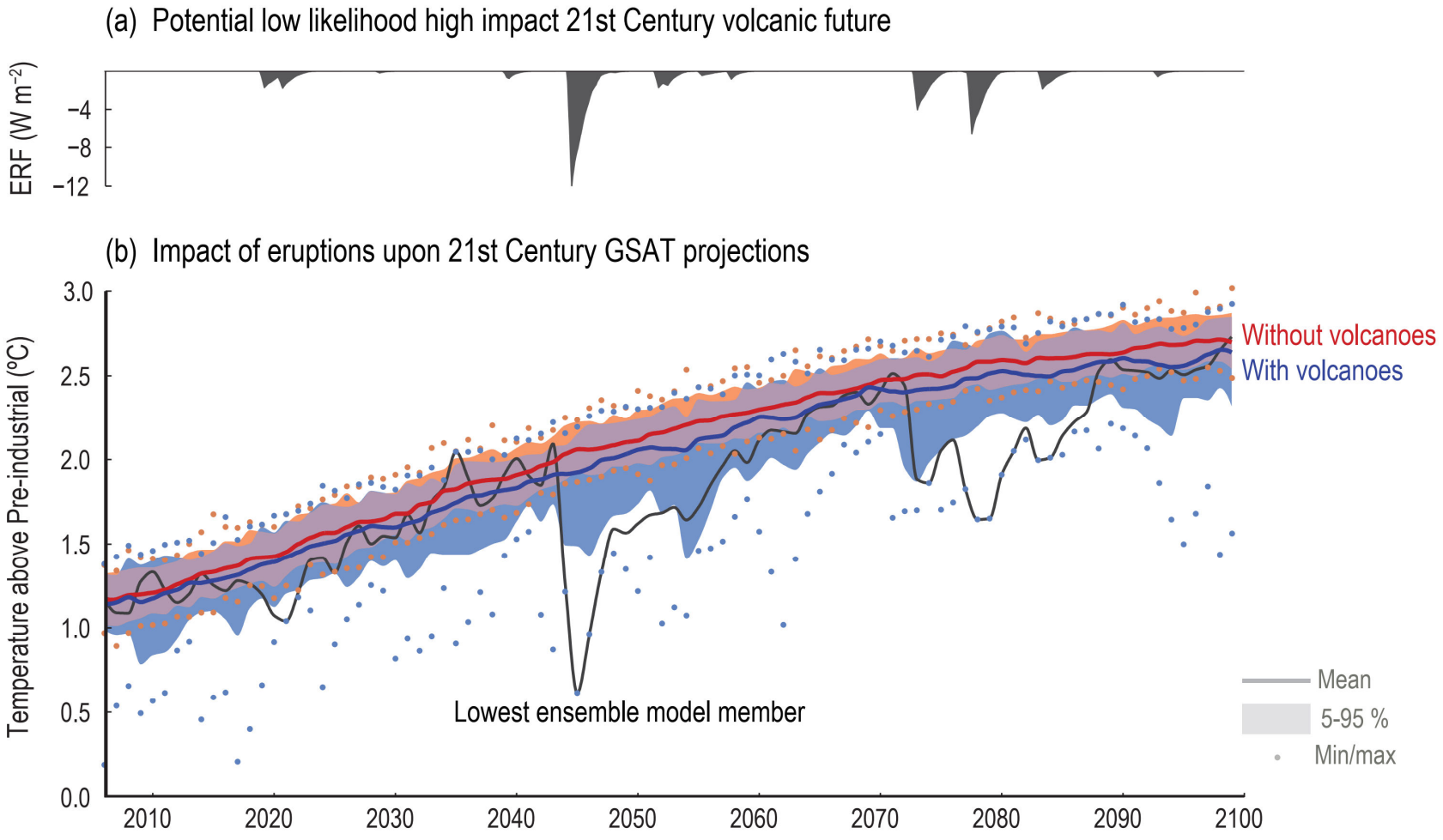

IPCC 2021, Chap. 4

Statements in the Executive Summary

Temperature (8)

It is very likely that long-term lower-tropospheric warming will be larger in the Arctic than in the global mean. It is *very likely* that global mean stratospheric cooling will be larger by the end of the 21st century in a pathway with higher atmospheric CO_2 concentrations. It is *likely* that tropical upper tropospheric warming will be larger than at the tropical surface, but with an uncertain magnitude owing to the effects of natural internal variability and uncertainty in the response of the climate system to anthropogenic forcing. {4.5.1, 3.3.1.2}

IPCC 2021, Chap. 4

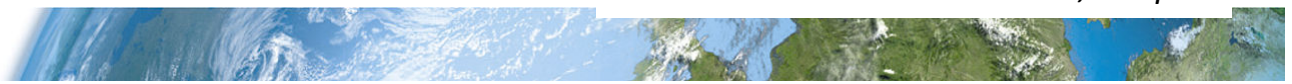

Long-term change of annual and zonal mean atmospheric tempe

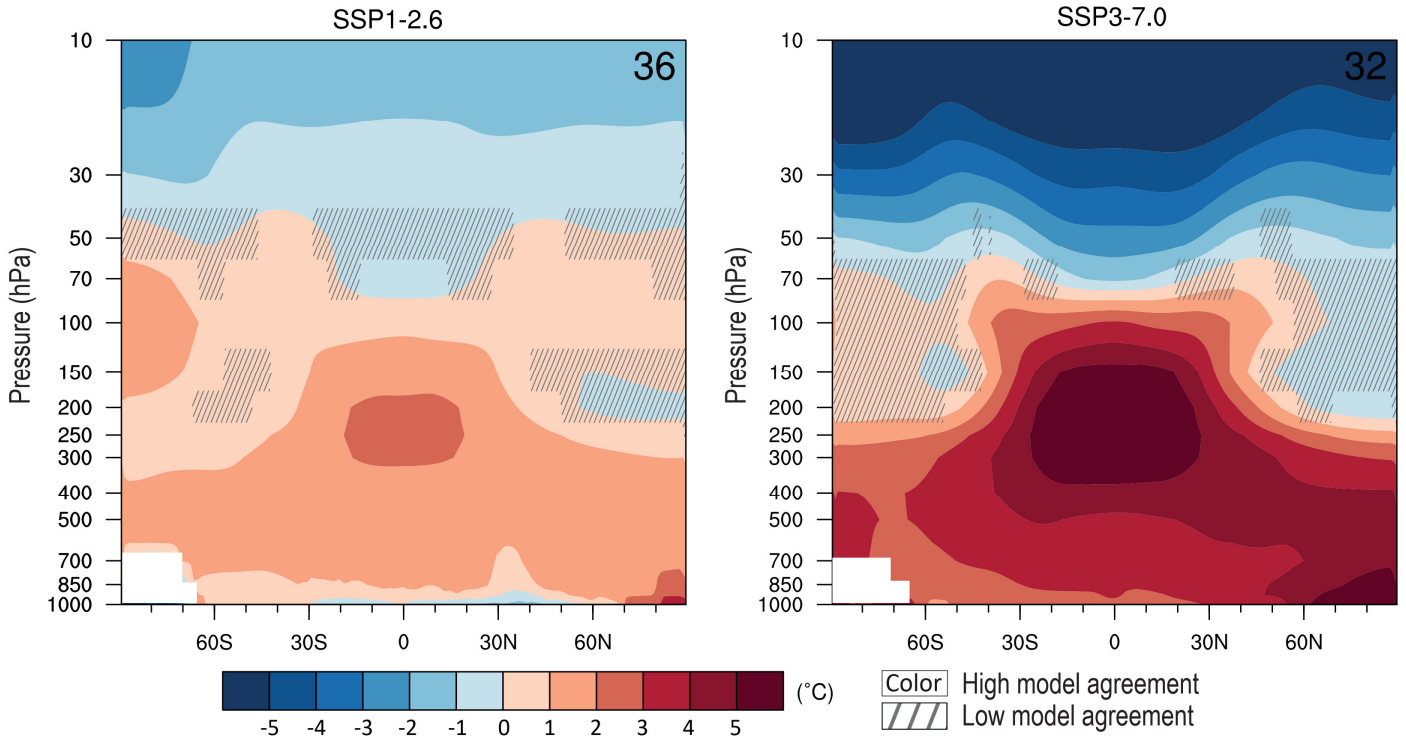

Figure 4.22 | Long-term change of annual and zonal mean atmospheric temperature. Displayed are multi-model mean change in annual and zonal mean atmospheric temperature (°C) in 2081–2100 relative to 1995–2014 for **(left)** SSP1-2.6 and **(right)** SSP3-7.0. The number of models used is indicated in the top right of the maps. Diagonal lines indicate regions where less than 80% of the models agree on the sign of the change and no overlay where 80% or more of the models agree on the sign of the change. Further details on data sources and processing are available in the chapter data table (Table 4.SM.1).

Statements in the Executive Summary

Precipitation (1)

Annual global land precipitation will increase over the 21st century as GSAT increases (*high confidence*). The likely range of change in globally averaged annual land precipitation during 2081– 2100 relative to 1995–2014 is –0.2–4.7% in the low-emission scenario SSP1-1.9 and 0.9–12.9% in the high-emission scenario SSP5-8.5, based on all available CMIP6 models. The corresponding *likely* ranges are 0.0–6.6% in SSP1-2.6, 1.5–8.3% in SSP2-4.5, and 0.5–9.6% in SSP3-7.0. {4.3.1, 4.5.1, 4.6.1, 8.4.1}

IPCC 2021, Chap. 4

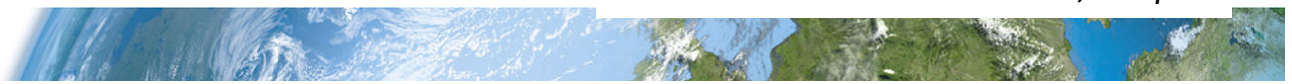

Selected indicators of global climate change from CMIP6 historical and scenario simulations

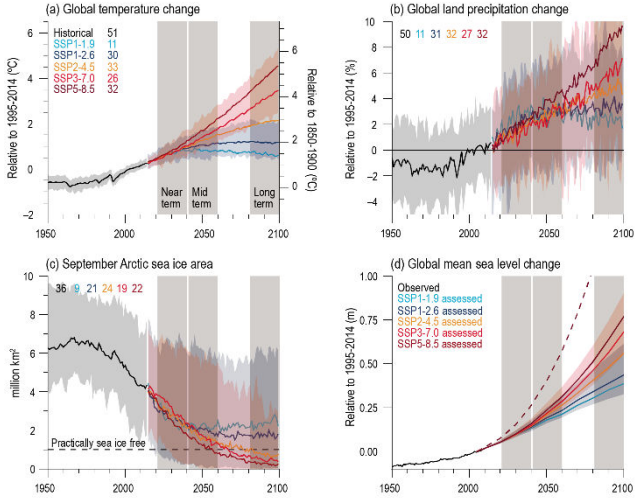

Figure 4.2 | Selected indicators of global climate change from CMIP6 historical and scenario simulations. (a) Global surface air temperature changes relative to the 1995–2014 average (left axis) and relative to the 1850–1900 average (right axis; offset by 0.82°C, which is the multi-model mean and close to observed best estimate, Cross-Chapter Box 2.1, Table 1). **(b)** Global land precipitation changes relative to the 1995–2014 average. **(c)** September Arctic sea ice area. **(d)** Global mean sea level (GMSL) change relative to the 1995–2014 average. (a), (b) and (d) are annual averages, (c) are September averages. In (a–c), the curves show averages over the CMIP6 simulations, the shadings around the SSP1-2.6 and SSP3-7.0 curves show 5–95% ranges, and the numbers near the top show the number of model simulations used. Results are derived from concentration-driven simulations. In (d), the barystatic contribution to GMSL (i.e., the contribution from land-ice melt) has been added offline to the CMIP6 simulated contributions from thermal expansion (thermosteric). The shadings around the SSP1-2.6 and SSP3-7.0 curves show 5–95% ranges. The dashed curve is the *low confidence* and low likelihood outcome at the high end of SSP5-8.5 and reflects deep uncertainties arising from potential ice-sheet and ice-cliff instabilities. This curve at year 2100 indicates 1.7 m of GMSL rise relative to 1995–2014. More information on the calculation of GMSL is available in Chapter 9, and further regional details are provided in the Atlas. Further details on data sources and processing are available in the chapter data table (Table 4.SM.1).

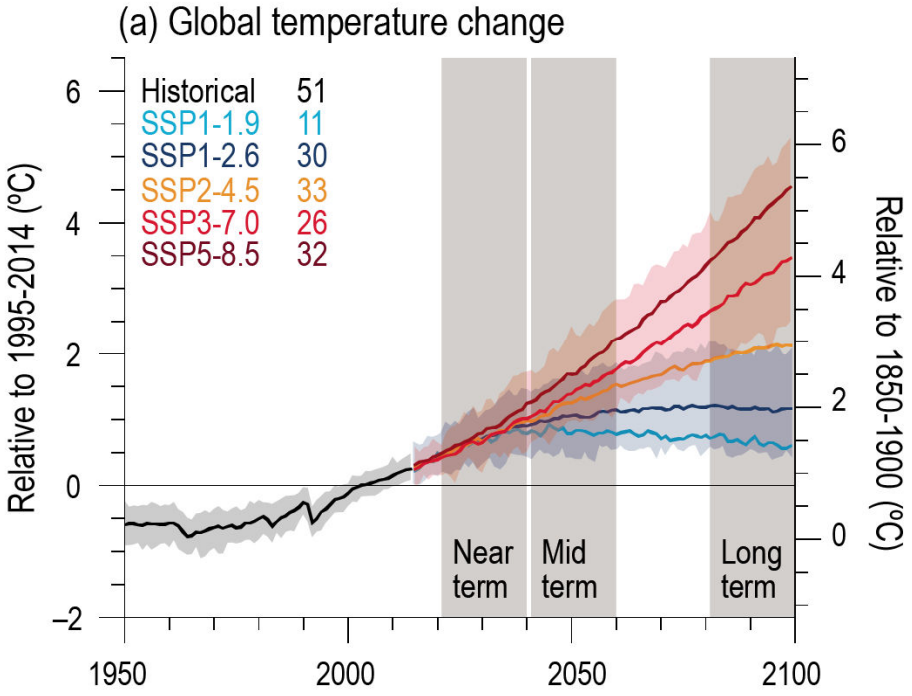
(a) Global temperature change
Historical 51
SSP1-1.9 11
SSP1-2.6 30
SSP2-4.5 33
SSP3-7.0 26
SSP5-8.5 32
Near term
Mid term
Long term
Relative to 1995-2014 (°C)
Relative to 1850-1900 (°C)
6
4
2
0
−2
1950
2000
2050
2100

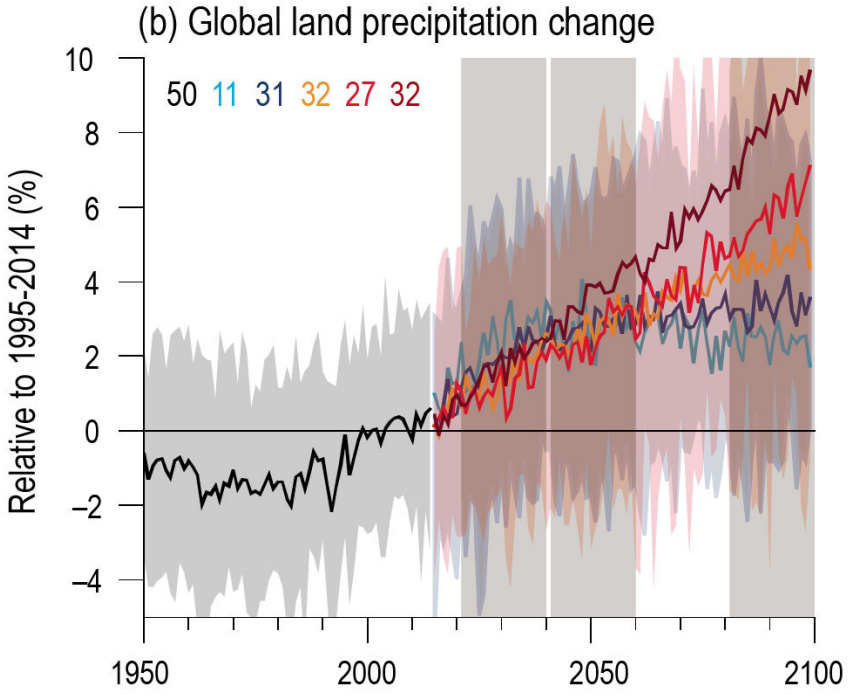
(b) Global land precipitation change
50 11 31 32 27 32
Relative to 1995-2014 (%)
10
8
6
4
2
0
−2
−4
1950
2000
2050
2100


IPCC 2021, Chap. 4

Statements in the Executive Summary

Precipitation (1)

Annual global land precipitation will increase over the 21st century as GSAT increases (*high confidence*). The likely range of change in globally averaged annual land precipitation during 2081– 2100 relative to 1995–2014 is –0.2–4.7% in the low-emission scenario SSP1-1.9 and 0.9–12.9% in the high-emission scenario SSP5-8.5, based on all available CMIP6 models. The corresponding *likely* ranges are 0.0–6.6% in SSP1-2.6, 1.5–8.3% in SSP2-4.5, and 0.5–9.6% in SSP3-7.0. {4.3.1, 4.5.1, 4.6.1, 8.4.1}

Precipitation change will exhibit substantial regional differences and seasonal contrast as GSAT increases over the 21st century (*high confidence*). As warming increases, a larger land area will experience statistically significant increases or decreases in precipitation (*medium confidence*). Precipitation will *very likely* increase over high latitudes and the tropical oceans, and *likely* increase in large parts of the monsoon region, but *likely* decrease over large parts of the subtropics in response to greenhouse gas-induced warming. Interannual variability of precipitation over many land regions will increase with global warming (*medium confidence*). {4.5.1, 4.6.1, 8.4.1}

IPCC 2021, Chap. 4

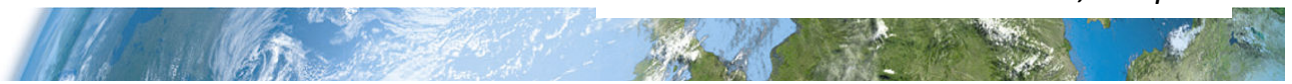

CMIP6 precipitation anomalies (%) relative to averages over 1995–2014 for selected future periods, regions and SSPs.

Table 4.3 | CMIP6 precipitation anomalies (%) relative to averages over 1995–2014 for selected future periods, regions and SSPs. Displayed are the multi-model averages across the individual models and, in parentheses, the 5–95% ranges. Also shown are land precipitation anomalies at the time when global increase in GSAT relative to 1850–1900 exceeds 1.5°C, 2.0°C, 3.0°C, and 4.0°C, and the percentage of simulations for which such exceedances are true (to the right of the parentheses). Here, the time of GSAT exceedance is determined as the first year at which 21-year running averages of GSAT exceed the given threshold. Land precipitation percent anomalies are then computed as 21-year averages about the year of the first GSAT crossing. The numbers of models used are indicated in Figure 4.4.

Time Period and Region		SSP1-1.9 (%)	SSP1-2.6 (%)	SSP2-4.5 (%)	SSP3-7.0 (%)	SSP5-8.5 (%)
Land	2021–2040	2.4 (0.7, 4.1)	2.0 (–0.6, 3.6)	1.5 (–0.4, 3.6)	1.2 (–1.0, 3.4)	1.7 (–0.1, 4.1)
	2041–2060	2.7 (0.6, 5.0)	2.8 (–0.4, 5.2)	2.7 (0.3, 5.2)	2.5 (–0.8, 5.1)	3.7 (–0.1, 6.9)
	2081–2100	2.4 (–0.2, 4.7)	3.3 (0.0, 6.6)	4.6 (1.5, 8.3)	5.8 (0.5, 9.6)	8.3 (0.9, 12.9)
Global	2081–2100	2.0 (0.4, 4.2)	2.9 (1.0, 5.2)	4.0 (2.3, 6.7)	4.7 (2.3, 8.2)	6.5 (3.4, 10.9)
Ocean	2081–2100	1.9 (0.6, 4.1)	2.8 (1.1, 5.4)	3.8 (2.0, 6.8)	4.4 (2.1, 7.9)	6.0 (2.9, 10.5)
Land	ΔT > 1.5°C	2.0 (0.6, 4.4) 55	1.7 (–2.0, 6.9) 87	1.7 (–2.9, 6.2) 100	1.5 (–3.9, 6.6) 100	1.5 (–3.5, 6.4) 100
	ΔT > 2.0°C	3.8 (2.4, 5.8) 36	2.2 (–2.0, 4.6) 58	2.8 (–2.2, 8.1) 97	2.4 (–4.4, 7.7) 100	2.8 (–2.8, 8.3) 100
	ΔT > 3.0°C	– (–, –) 0	– (–, –) 0	4.9 (1.5, 9.6) 54	4.3 (–4.4, 11.5) 97	4.9 (–2.6, 11.0) 100
	ΔT > 4.0°C	– (–, –) 0	– (–, –) 0	4.2 (1.3, 6.3) 9	5.1 (–2.5, 11.1) 57	6.4 (–3.4, 15.0) 85

IPCC 2021, Chap. 4

CMIP6 annual mean precipitation changes (%) from historical and scenario simulations

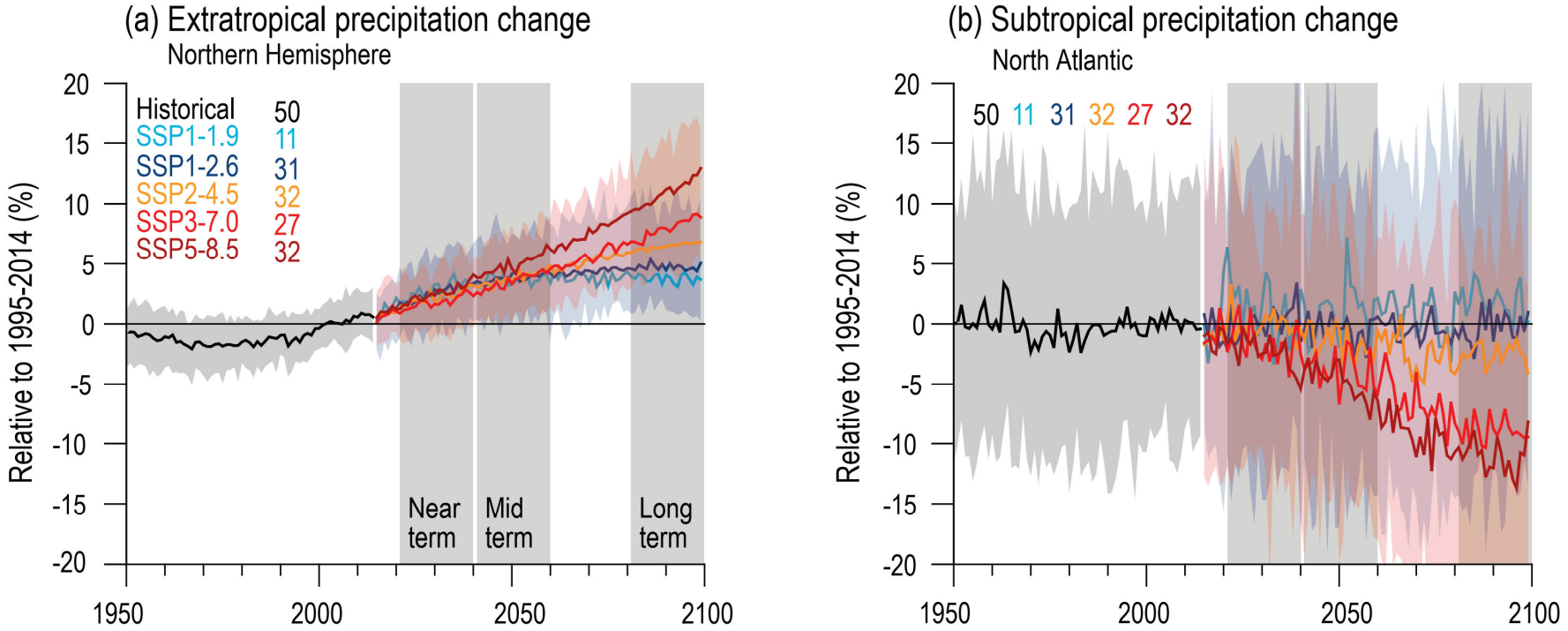

Figure 4.4 | CMIP6 annual mean precipitation changes (%) from historical and scenario simulations. (a) Northern Hemisphere extratropics (30°N–90°N). **(b)** North Atlantic subtropics (5°N–30°N, 80°W–0°). Changes are relative to 1995–2014 averages. Displayed are multi-model averages and, in parentheses, 5–95% ranges. The numbers inside each panel are the number of model simulations. Results are derived from concentration-driven simulations. Further details on data sources and processing are available in the chapter data table (Table 4.SM.1).

Long-term change of seasonal mean precipitation

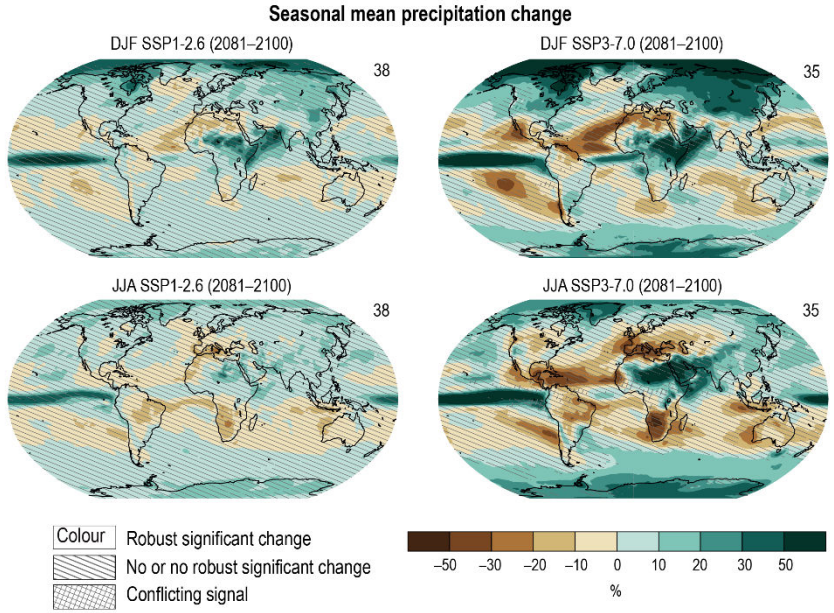

Figure 4.24 | Long-term change of seasonal mean precipitation. Displayed are projected spatial patterns of multi-model mean change (%) in **(top)** December–January–February (DJF) and **(bottom)** June–July–August (JJA) mean precipitation in 2081–2100 relative to 1995–2014, for (left) SSP1-2.6 and (right) SSP3-7.0. The number of models used is indicated in the top right of the maps. No map overlay indicates regions where the change is robust and *likely* emerges from internal variability, that is, where at least 66% of the models show a change greater than the internal-variability threshold (Section 4.2.6) and at least 80% of the models agree on the sign of change. Diagonal lines indicate regions with no change or no robust significant change, where fewer than 66% of the models show change greater than the internal-variability threshold. Crossed lines indicate areas of conflicting signals where at least 66% of the models show change greater than the internal-variability threshold but fewer than 80% of all models agree on the sign of change. Further details on data sources and processing are available in the chapter data table (Table 4.SM.1).

Seasonal mean precipitation change

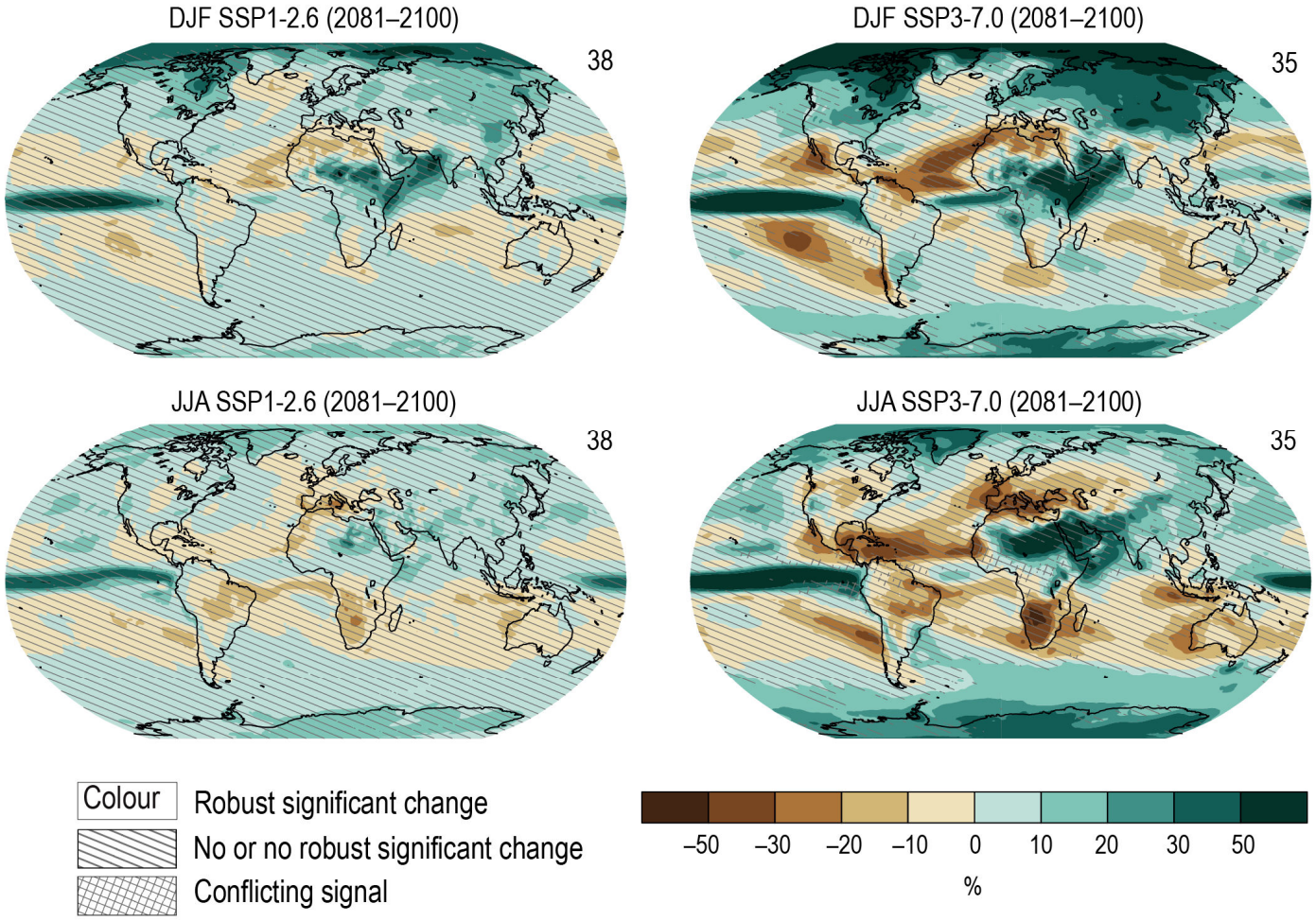

IPCC 2021, Chap. 4

Long-term changes in seasonal mean relative humidity

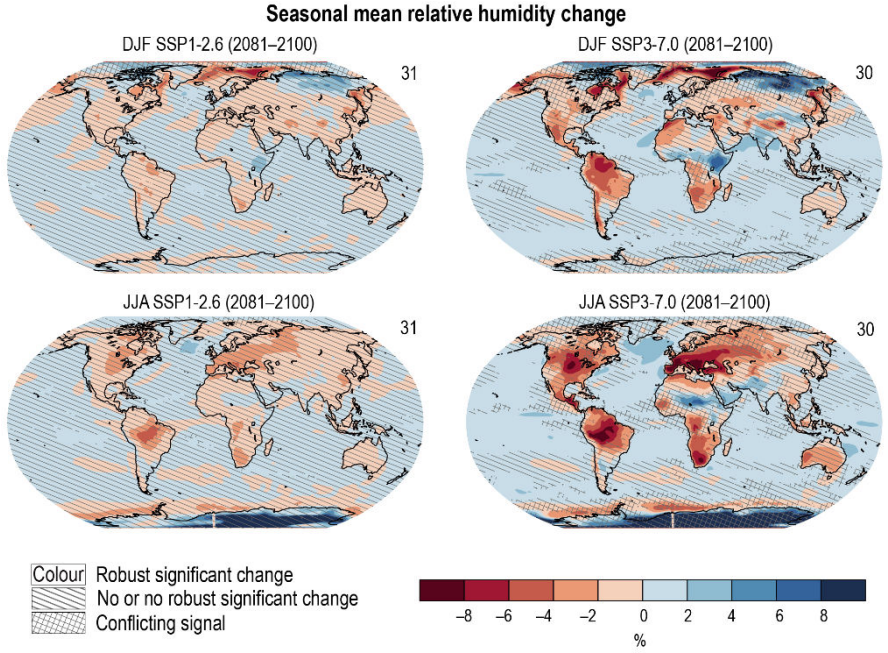

Figure 4.23 | Long-term changes in seasonal mean relative humidity. Displayed are projected spatial patterns of multi-model mean change (%) in seasonal **(top)** December–January–February (DJF) and **(bottom)** June–July–August (JJA) mean near-surface relative humidity in 2081–2100 relative to 1995–2014, for (left) SSP1-2.6 and (right) SSP3-7.0. The number of models used is indicated in the top right of the maps. No overlay indicates regions where the change is robust and *likely* emerges from internal variability, that is, where at least 66% of the models show a change greater than the internal variability threshold (Section 4.2.6) and at least 80% of the models agree on the sign of change. Diagonal lines indicate regions with no change or no robust significant change, where fewer than 66% of the models show change greater than the internal-variability threshold. Crossed lines indicate areas of conflicting signals where at least 66% of the models show change greater than the internal-variability threshold but fewer than 80% of all models agree on the sign of change. Further details on data sources and processing are available in the chapter data table (Table 4.SM.1).

Seasonal mean relative humidity change

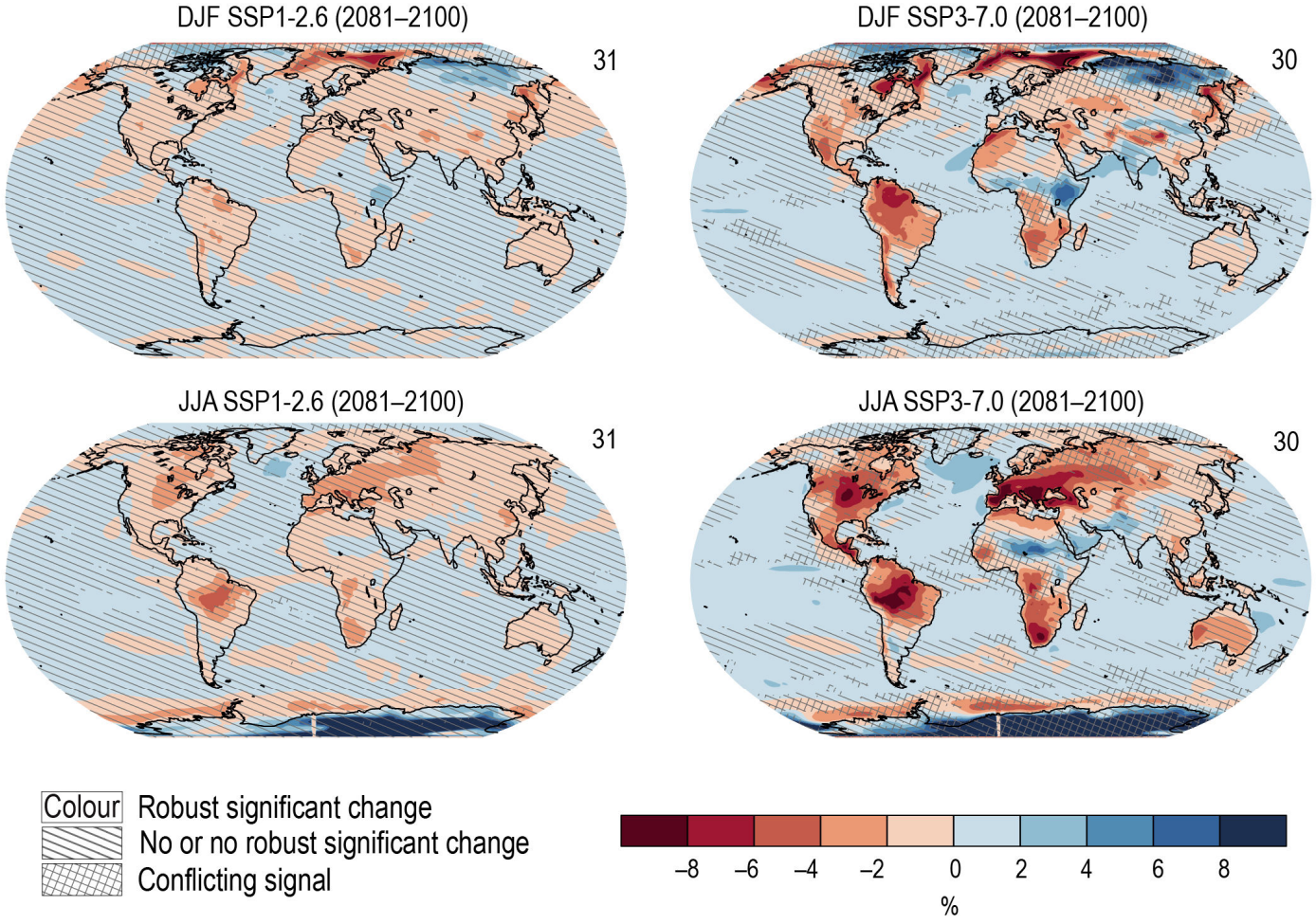

IPCC 2021, Chap. 4

Projected spatial patterns of change in annual average precipitation (expressed as a percentage change) at different levels of global warming

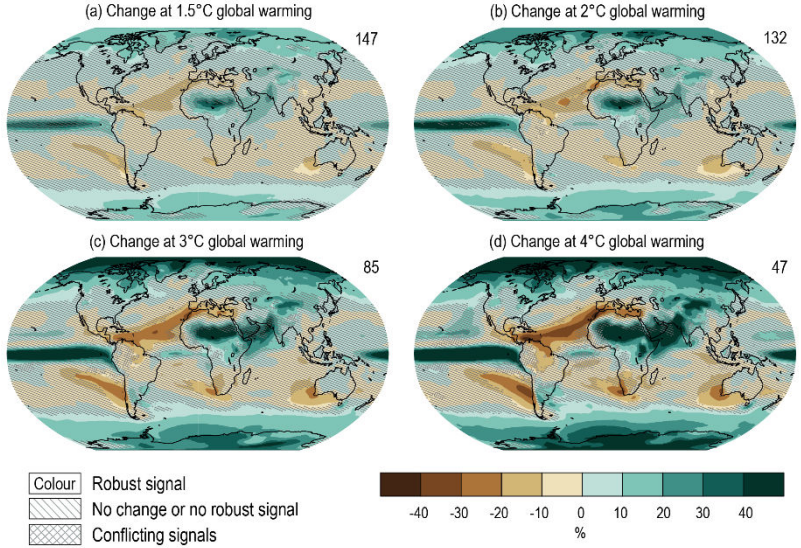

Figure 4.32 | Projected spatial patterns of change in annual average precipitation (expressed as a percentage change) at different levels of global warming. Displayed are **(a–d)** spatial patterns of change in annual precipitation at 1.5°C, 2°C, 3°C, and 4°C of global warming relative to the period 1850–1900. No map overlay indicates regions where the change is robust and *likely* emerges from internal variability, that is, where at least 66% of the models show a change greater than the internal-variability threshold (Section 4.2.6) and at least 80% of the models agree on the sign of change. Diagonal lines indicate regions with no change or no robust significant change, where fewer than 66% of the models show change greater than the internal-variability threshold. Crossed lines indicate areas of conflicting signals where at least 66% of the models show change greater than the internal-variability threshold but fewer than 80% of all models agree on the sign of change. Values were assessed from a 20-year period at a given warming level, based on model simulations under the Tier-1 SSPs of CMIP6. Further details on data sources and processing are available in the chapter data table (Table 4.SM.1).

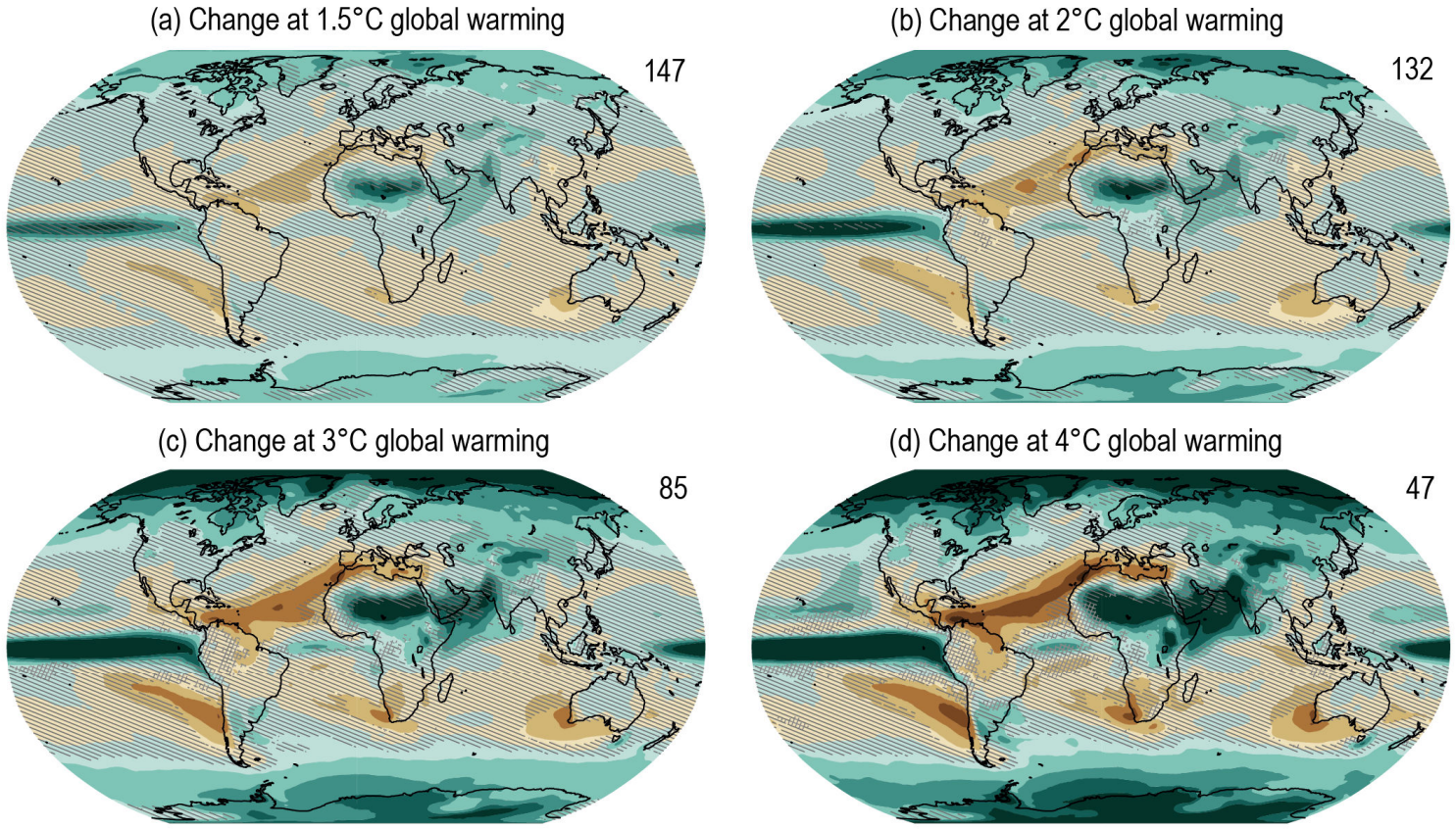

IPCC 2021, Chap. 4

Regional changes in temperature (left) and precipitation (right) are proportional to the level of global warming

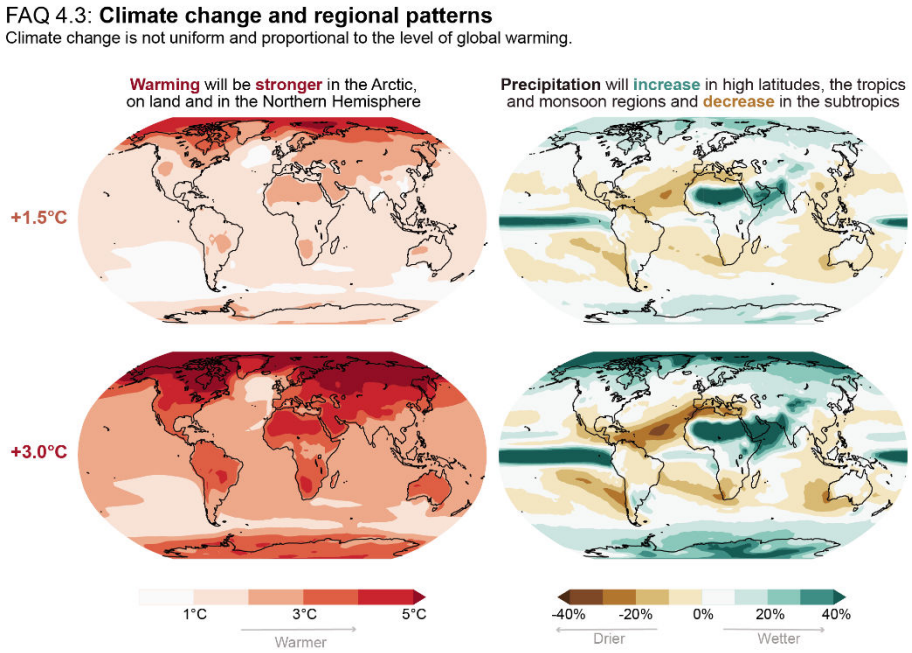

FAQ 4.3, Figure 1 | Regional changes in temperature (left) and precipitation (right) are proportional to the level of global warming, irrespective of the scenario through which the level of global warming is reached. Surface warming and precipitation change are shown relative to the 1850–1900 climate, and for time periods over which the globally averaged surface warming is 1.5°C **(top)** and 3°C **(bottom)**, respectively. Changes presented here are based on 31 CMIP6 models using the high-emissions scenario SSP3-7.0.

IPCC 2021, Chap. 4

FAQ 4.3: **Climate change and regional patterns**

Climate change is not uniform and proportional to the level of global warming.

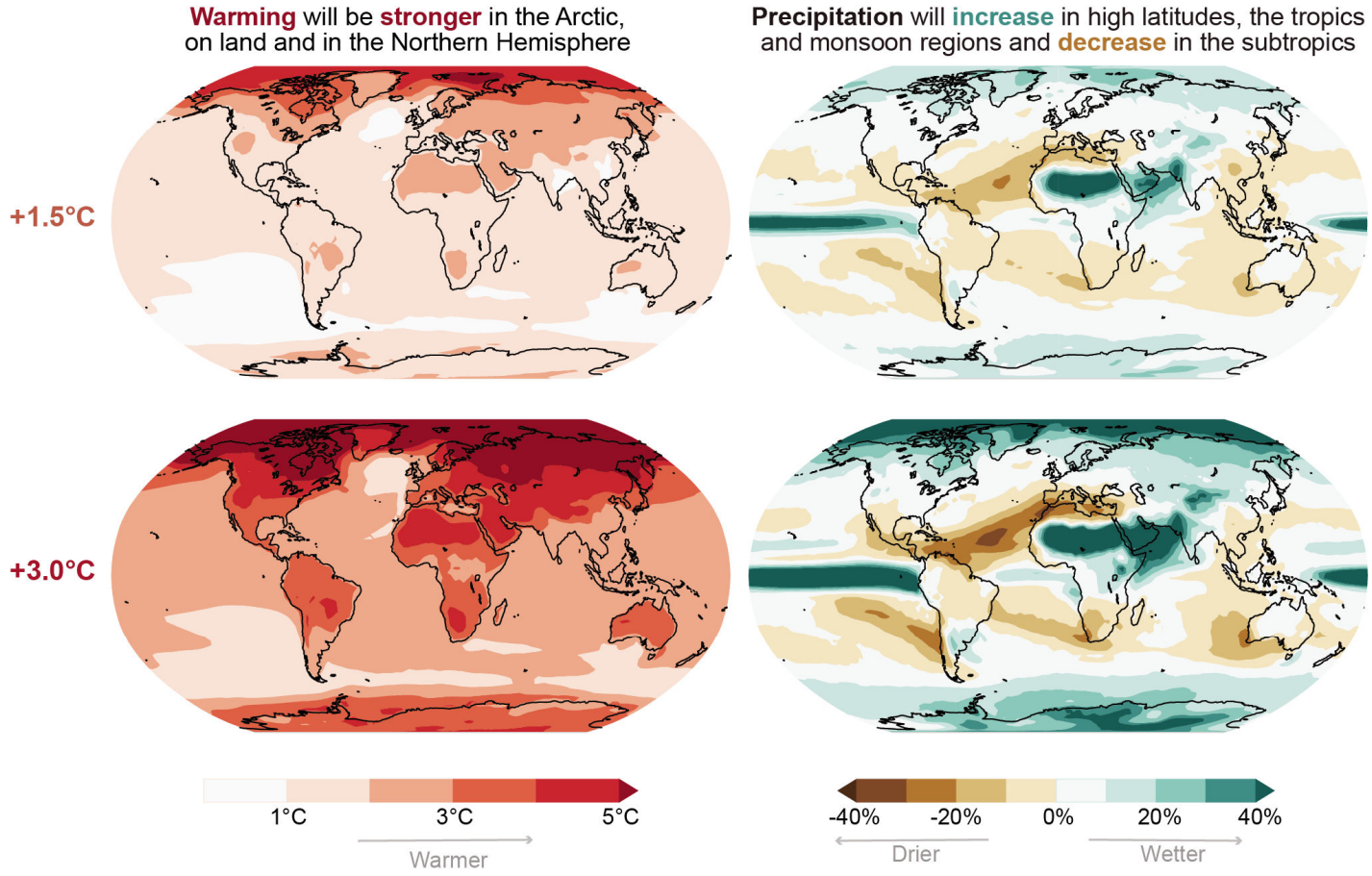

IPCC 2021, Chap. 4

Statements in the Executive Summary

Precipitation (2)

Near-term projected changes in precipitation are uncertain, mainly because of natural internal variability, model uncertainty, and uncertainty in natural and anthropogenic aerosol forcing (*medium confidence*). In the near term, no discernible differences in precipitation changes are projected between different SSPs (*high confidence*). The anthropogenic aerosol forcing decreases in most scenarios, contributing to increases in GSAT (*medium confidence*) and global-mean land precipitation (*low confidence*). {4.3.1, 4.4.1, 4.4.4, 8.5}

Near-term change of seasonal mean precipitation

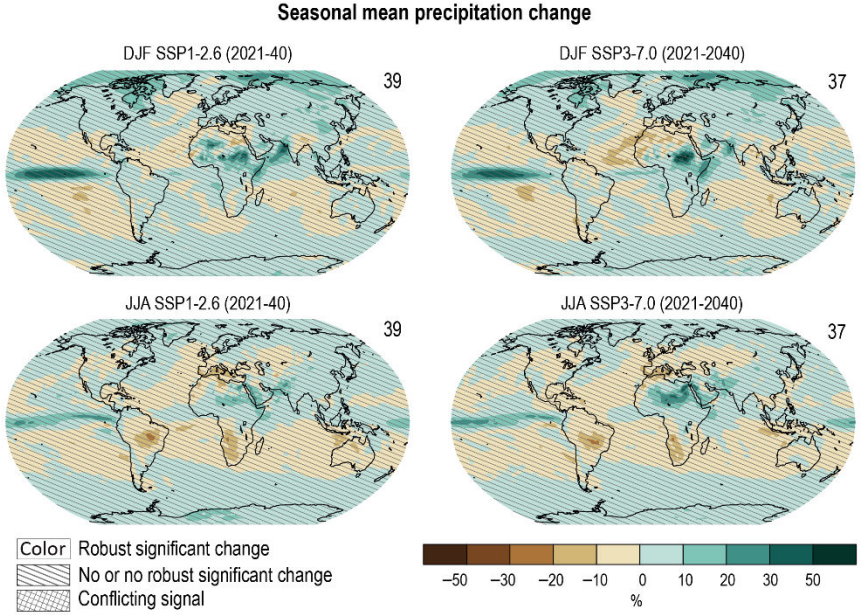

Figure 4.13 | Near-term change of seasonal mean precipitation. Displayed are projected spatial patterns of CMIP6 multi-model mean change (%) in **(top)** December–January–February (DJF) and **(bottom)** June–July–August (JJA) precipitation from SSP1-2.6 and SSP3-7.0 in 2021–2040 relative to 1995–2014. The number of models used is indicated in the top right of the maps. No overlay indicates regions where the change is robust and *likely* emerges from internal variability, that is, where at least 66% of the models show a change greater than the internal-variability threshold (Section 4.2.6) and at least 80% of the models agree on the sign of change. Diagonal lines indicate regions with no change or no robust significant change, where fewer than 66% of the models show change greater than the internal-variability threshold. Crossed lines indicate areas of conflicting signals where at least 66% of the models show change greater than the internal-variability threshold but fewer than 80% of all models agree on the sign of change. Further details on data sources and processing are available in the chapter data table (Table 4.SM.1).

Seasonal mean precipitation change

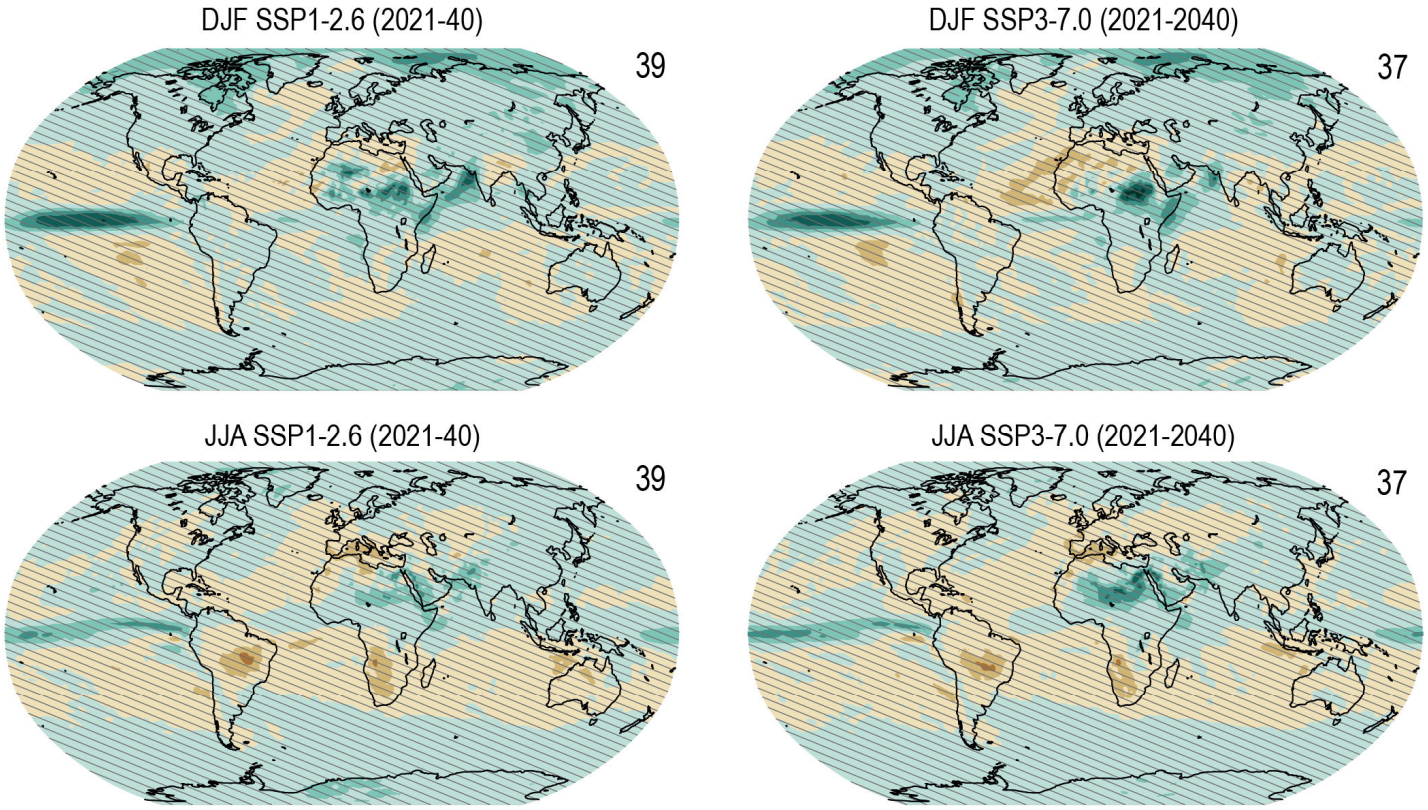

IPCC 2021, Chap. 4

Statements in the Executive Summary

Precipitation (3)

In response to greenhouse gas-induced warming, it is *likely* that global land monsoon precipitation will increase, particularly in the Northern Hemisphere, although Northern Hemisphere monsoon circulation will *likely* weaken. In the long term (2081–2100), monsoon rainfall change will feature a north–south asymmetry characterized by a greater increase in the Northern Hemisphere than in the Southern Hemisphere and an east–west asymmetry characterized by an increase in Asian-African monsoon regions and a decrease in the North American monsoon region (*medium confidence*). Near-term changes in global monsoon precipitation and circulation are uncertain due to model uncertainty and internal variability such as Atlantic Multi-decadal Variability and Pacific Decadal Variability (*medium confidence*). {4.4.1, 4.5.1, 8.4.1, 10.6.3}

Time series of global land monsoon precipitation and Northern Hemisphere summer monsoon (NHSM) circulation index anomalies.

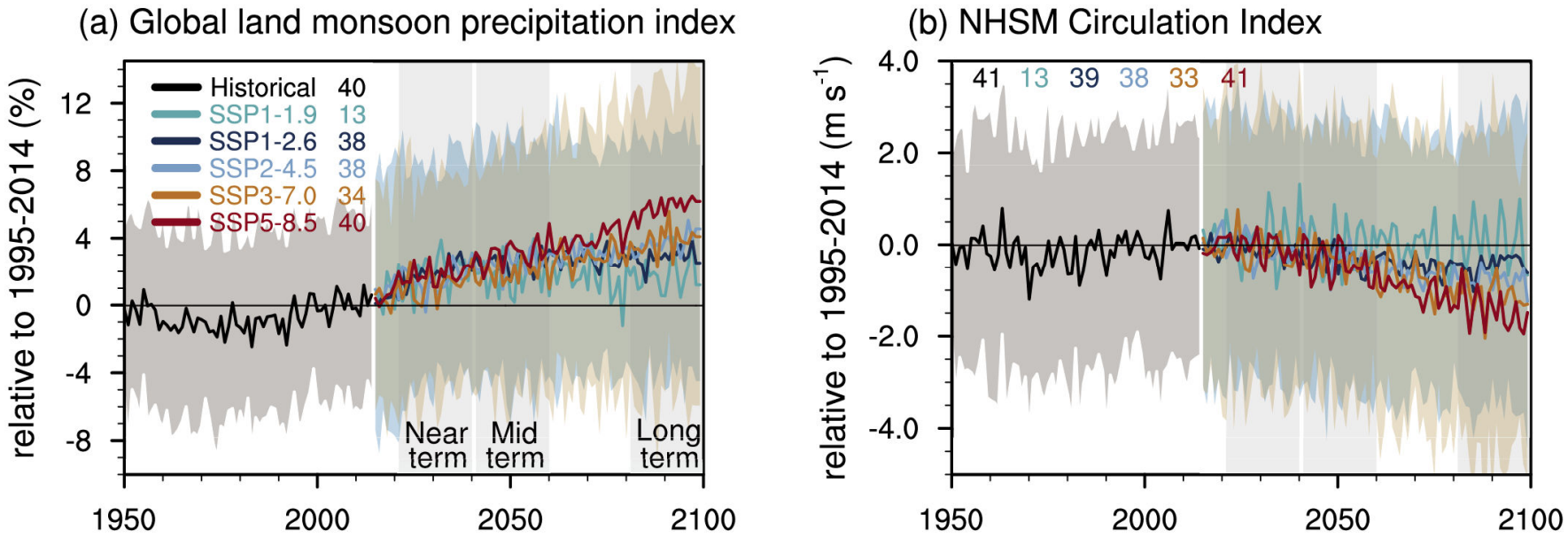

Figure 4.14 | Time series of global land monsoon precipitation and Northern Hemisphere summer monsoon (NHSM) circulation index anomalies. (a) Global land monsoon precipitation index anomalies (unit: %) defined as the area-weighted mean precipitation rate in the global land monsoon domain (as defined by Wang et al. (2013a) for the CMIP6 historical simulation (1950–2014) and five SSPs (2015–2100). **(b)** Anomalies in NHSM circulation index (unit: m s^{-1}), defined as the vertical shear of zonal winds between 850 and 200 hPa averaged in a zone stretching from Mexico eastward to the Philippines (0°–20°N, 120°W–120°E; Wang et al., 2013a) for the CMIP6 historical simulation and five SSPs. One realization is averaged from each model. Anomalies are shown relative to the present-day (1995–2014) mean. The curves show averages over the simulations, the shadings around the SSP1-2.6 and SSP3-7.0 curves show 5–95% ranges, and the numbers near the top show the number of model simulations used. Further details on data sources and processing are available in the chapter data table (Table 4.SM.1).

Statements in the Executive Summary

Precipitation (4)

It is likely that at least one large volcanic eruption will occur during the 21st century. Such an eruption would reduce GSAT for several years, decrease global-mean land precipitation, alter monsoon circulation, modify extreme precipitation, and change the profile of many regional climatic impact-drivers. A low-likelihood, high-impact outcome would be several large eruptions that would greatly alter the 21st century climate trajectory compared to SSP-based Earth system model projections. {Cross-Chapter Box 4.1}

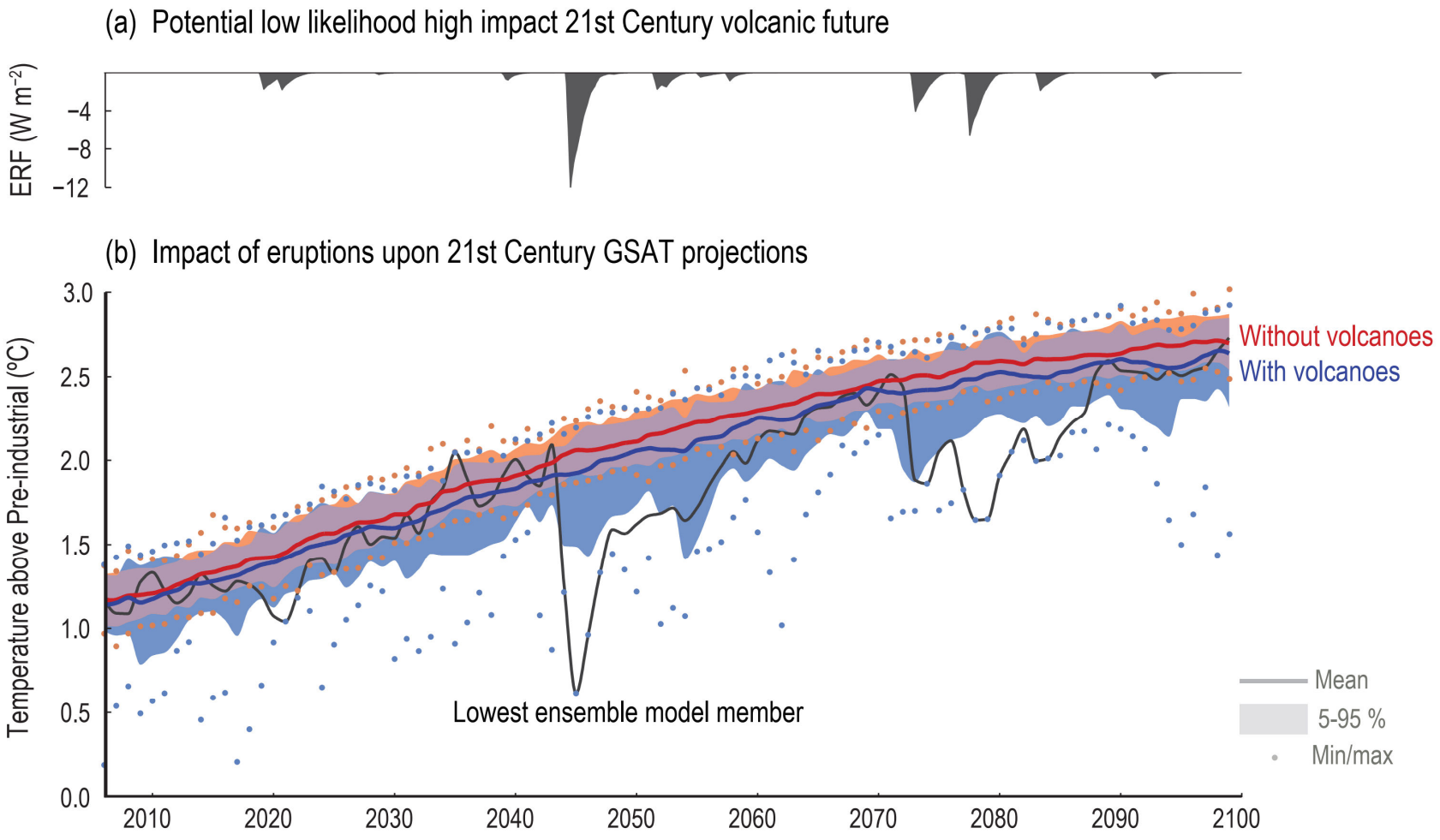

IPCC 2021, Chap. 4

Modes of variability (1)

The **Southern Annular Mode (SAM)** is a climate driver that can influence rainfall and temperature in Australia. The SAM refers to the (non-seasonal) north-south movement of the strong westerly winds that blow almost continuously in the mid- to high-latitudes of the southern hemisphere. The station-based index of the SAM is based on the zonal pressure difference between the latitudes of 40S and 65S.

The **Arctic oscillation (AO)** or **Northern Annular Mode/Northern Hemisphere Annular Mode (NAM)** is a weather phenomenon at the Arctic pole north of 20 degrees latitude. It is an important mode of climate variability for the Northern Hemisphere. The southern hemisphere analogue is called the Antarctic oscillation or Southern Annular Mode (SAM). The index varies over time with no particular periodicity, and is characterized by non-seasonal sea-level pressure anomalies of one sign in the Arctic, balanced by anomalies of opposite sign centered at about 37–45°N

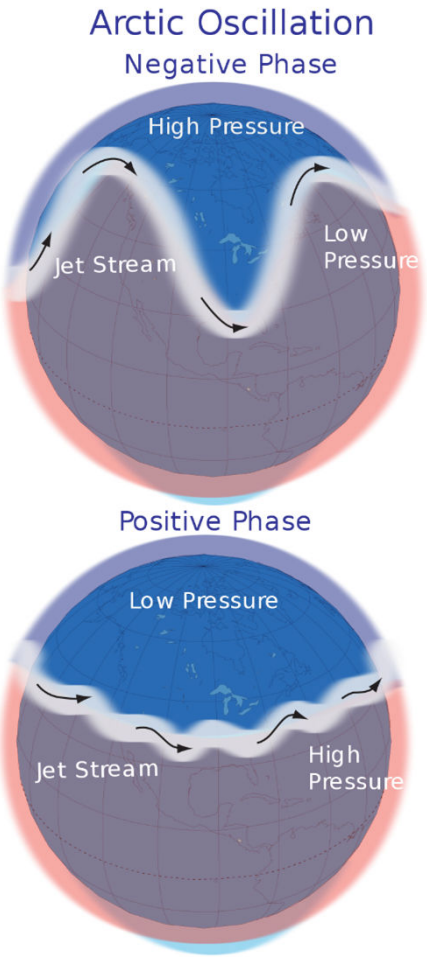

Statements in the Executive Summary

Large-scale Circulation and Modes of Variability (1)

In the near term, the forced change in Southern Annular Mode in austral summer is *likely* to be weaker than observed during the late 20th century under all five SSPs assessed. This is because of the opposing influence in the near- to mid-term from stratospheric ozone recovery and increases in other greenhouse gases on the Southern Hemisphere summertime mid-latitude circulation (*high confidence*). In the near term, forced changes in the Southern Annular Mode in austral summer are therefore *likely* to be smaller than changes due to natural internal variability. {4.3.3, 4.4.3}

IPCC 2021, Chap. 4

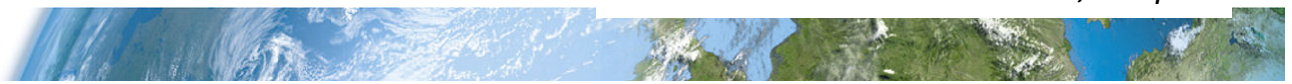

CMIP6 Annular Mode index change (hPa) from 1995–2014 to 2021–2040

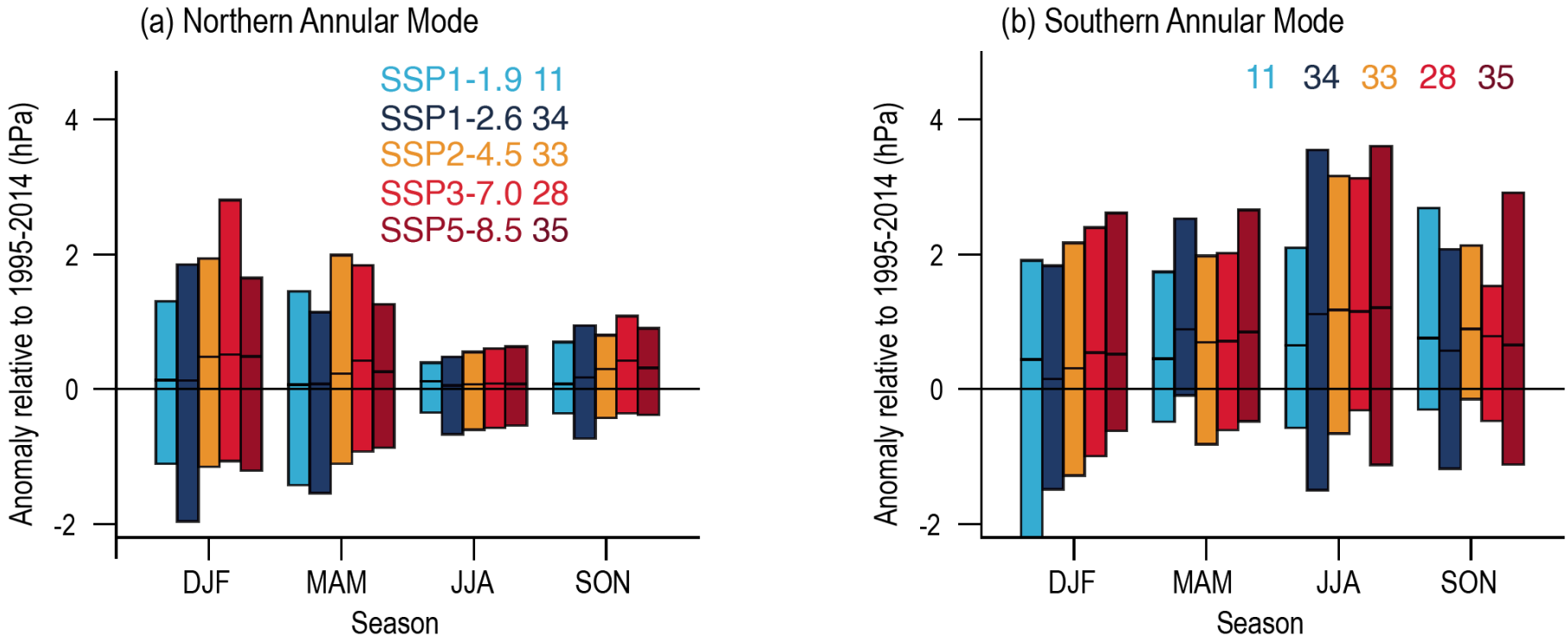

Figure 4.17 | CMIP6 Annular Mode index change (hPa) from 1995–2014 to 2021–2040. (a) Northern Annular Mode (NAM); **(b)** Southern Annular Mode (SAM). The NAM is defined as the difference in zonal mean sea level pressure (SLP) at 35°N and 65°N (Li and Wang, 2003) and the SAM as the difference in zonal mean SLP at 40°S and 65°S (Gong and Wang, 1999). The shadings are the 5–95% ranges across the simulations. The numbers near the top of each panel are the numbers of model simulations in each SSP ensemble. Further details on data sources and processing are available in the chapter data table (Table 4.SM.1).

IPCC 2021, Chap. 4

Statements in the Executive Summary

Large-scale Circulation and Modes of Variability (1)

In the near term, the forced change in Southern Annular Mode in austral summer is *likely* to be weaker than observed during the late 20th century under all five SSPs assessed. This is because of the opposing influence in the near- to mid-term from stratospheric ozone recovery and increases in other greenhouse gases on the Southern Hemisphere summertime mid-latitude circulation (*high confidence*). In the near term, forced changes in the Southern Annular Mode in austral summer are therefore *likely* to be smaller than changes due to natural internal variability. {4.3.3, 4.4.3}

In the long term, the Southern Hemisphere mid-latitude jet is *likely* to shift poleward and strengthen under SSP5-8.5 relative to 1995–2014. This is *likely* to be accompanied by an increase in the Southern Annular Mode index in all seasons relative to 1995–2014. For SSP1-2.6, CMIP6 models project no robust change in the Southern Annular Mode index in the long term. It is *likely* that wind speeds associated with extratropical cyclones will strengthen in the Southern Hemisphere storm track for SSP5-8.5. {4.5.1, 4.5.3}

IPCC 2021, Chap. 4

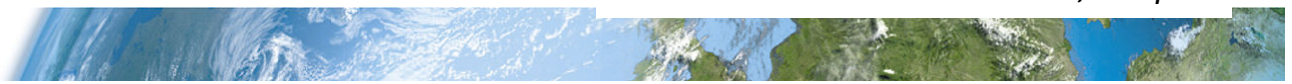

CMIP6 Annular Mode index change from 1995–2014 to 2081–2100

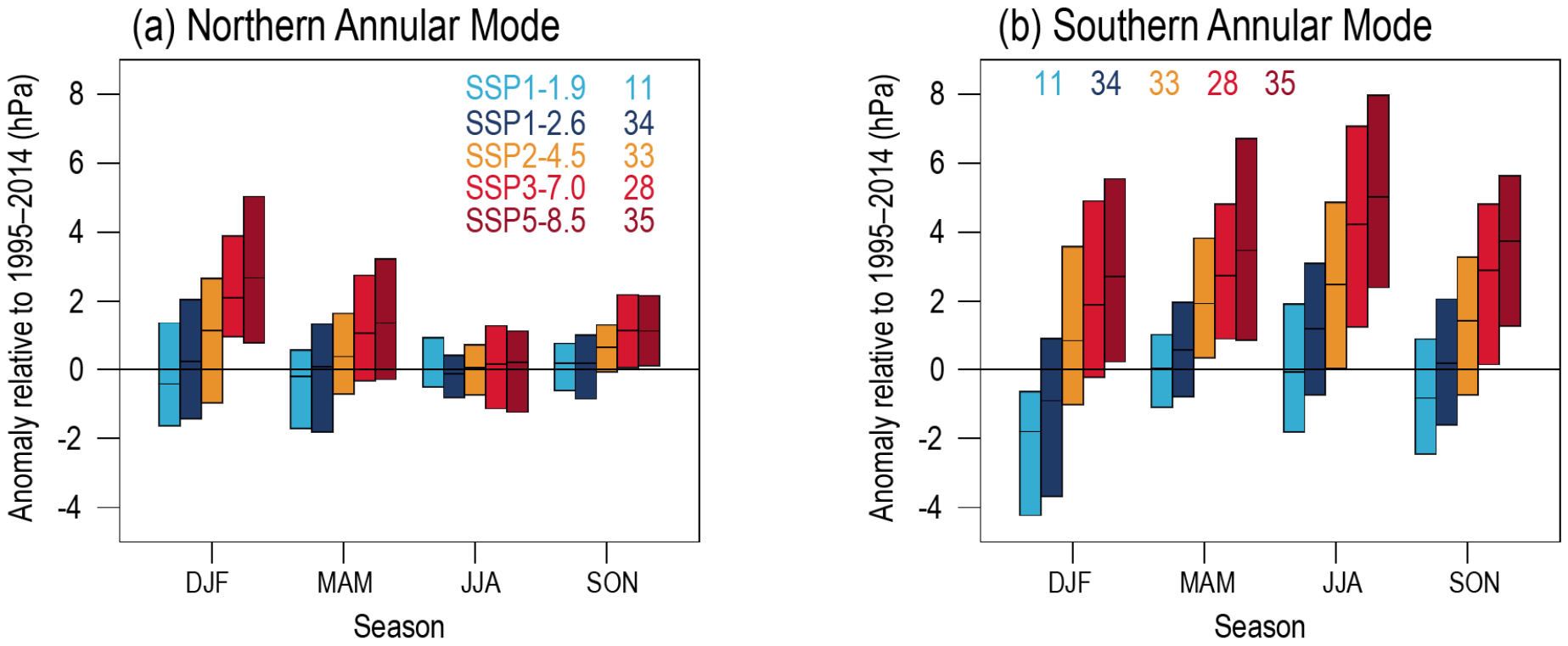

Figure 4.30 | CMIP6 Annular Mode index change from 1995–2014 to 2081–2100. (a) Northern Annular Mode (NAM) and **(b)** Southern Annular Mode (SAM). The NAM is defined as the difference in zonal mean SLP at 35°N and 65°N (Li and Wang, 2003) and the SAM as the difference in zonal mean SLP at 40°S and 65°S (Gong and Wang, 1999). The shadings are the 5–95% ranges across the simulations. The numbers near the top are the numbers of model simulations in each SSP ensemble. Further details on data sources and processing are available in the chapter data table (Table 4.SM.1).

IPCC 2021, Chap. 4

Statements in the Executive Summary

Large-scale Circulation and Modes of Variability (2)

The CMIP6 multi-model ensemble projects a long-term increase in the boreal wintertime Northern Annular Mode index under the high-emission scenarios of SSP3-7.0 and SSP5-8.5, but regional changes may deviate from a simple shift in the mid-latitude circulation. Substantial uncertainty and thus *low confidence* remain in projecting regional changes in Northern Hemisphere jet streams and storm tracks, especially for the North Atlantic basin in winter; this is due to large natural internal variability, the competing effects of projected upper- and lower-tropospheric temperature gradient changes, and new evidence of weaknesses in simulating past variations in North Atlantic atmospheric circulation on seasonal-to-decadal timescales. One exception is the expected decrease in frequency of atmospheric blocking events over Greenland and the North Pacific in boreal winter in SSP3-7.0 and SSP5-8.5 scenarios (*medium confidence*). {4.5.1}

IPCC 2021, Chap. 4

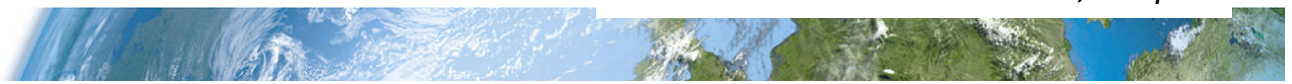

Long-term change of zonal mean zonal wind

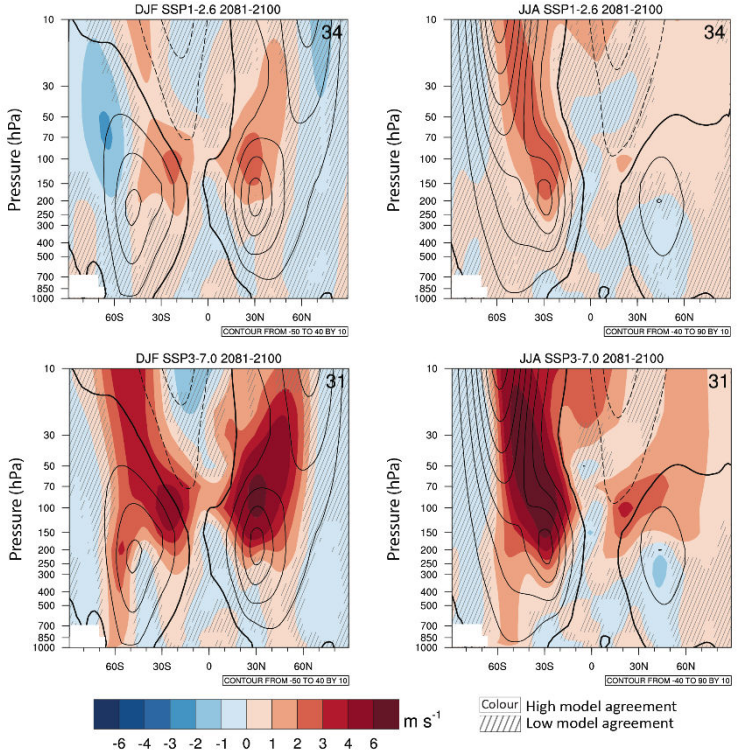

Figure 4.26 | Long-term change of zonal-mean, zonal wind. Displayed are multi-model mean changes in **(left)** boreal winter (December–January–February, DJF) and **(right)** austral winter (June–July–August, JJA) zonal mean, zonal wind (m s^{-1}) in 2081–2100 for (top) SSP1-2.6 and (bottom) SSP3-7.0 relative to 1995–2014. The 1995–2014 climatology is shown in contours with spacing 10 m s^{-1}. Diagonal lines indicate regions where less than 80% of the models agree on the sign of the change and no overlay where at least 80% of the models agree on the sign of the change. Further details on data sources and processing are available in the chapter data table (Table 4.SM.1).

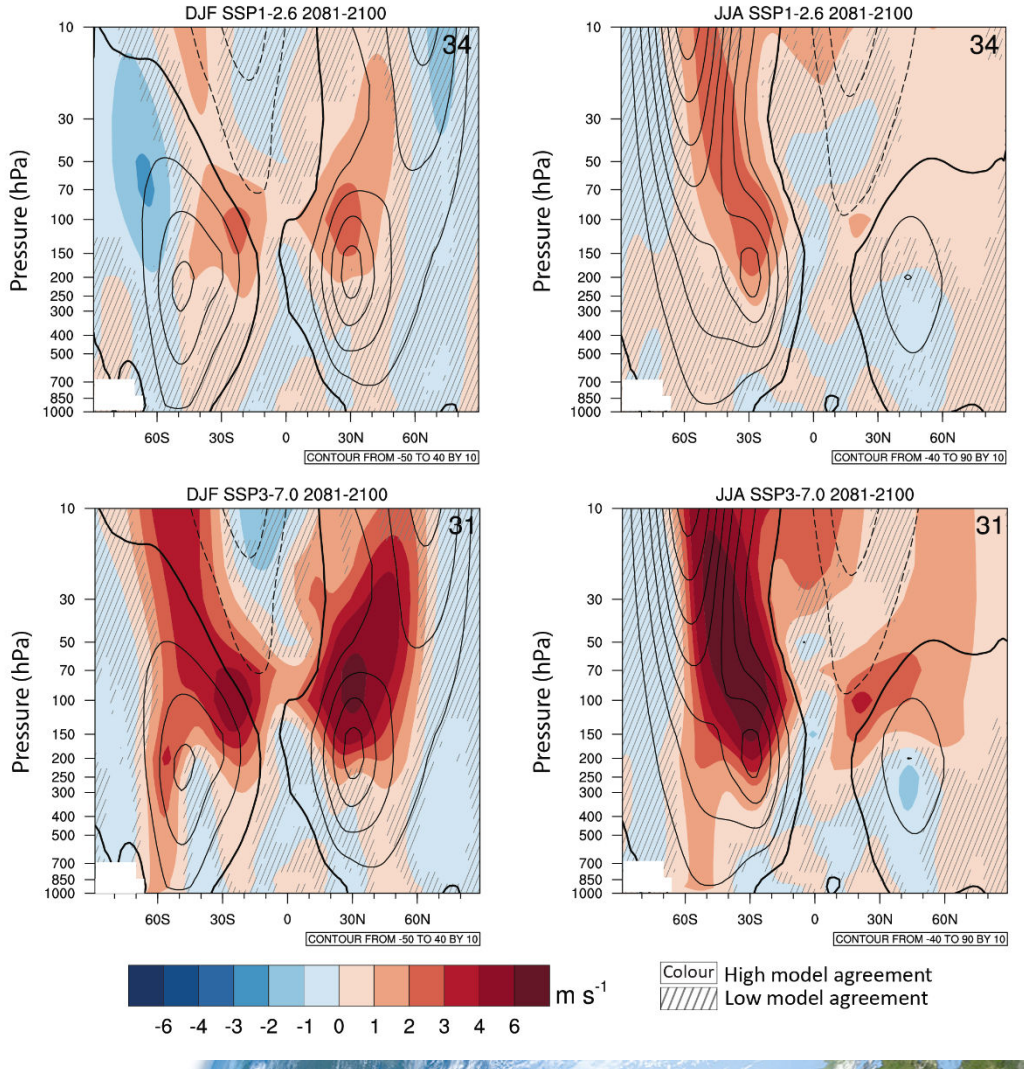

IPCC 2021, Chap. 4

Changes in extratropical storm track density

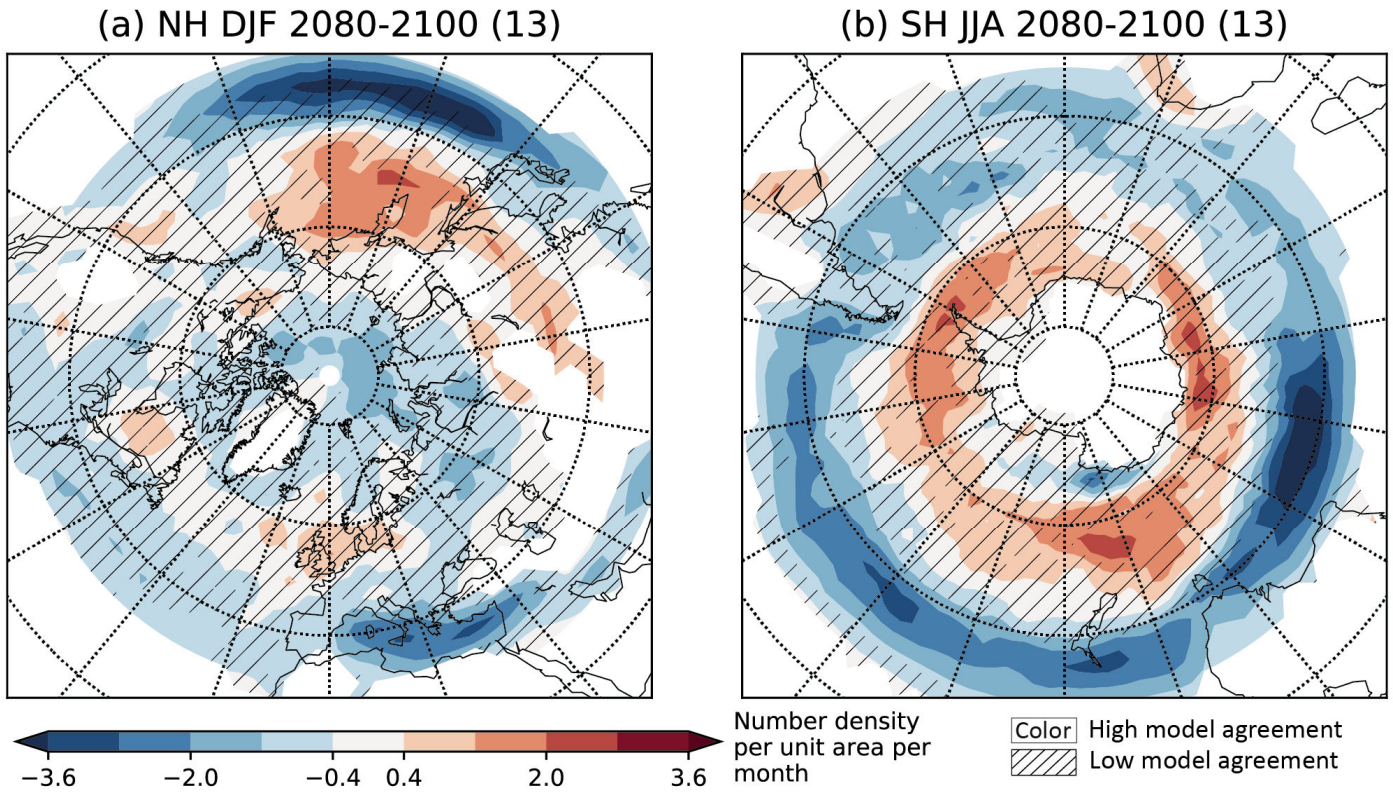

Figure 4.27 | Changes in extratropical storm track density. Displayed are projected spatial pattern of multi-model mean change of extratropical storm track density in winter (Northern Hemisphere December–January–Februrary, NH DJF, and Southern Hemisphere June–July–August, SH JJA) in 2080–2100 for SSP5-8.5 relative to 1979–2014 based on 13 CMIP6 models. Diagonal lines indicate regions where fewer than 80% of the models agree on the sign of the change and no overlay where at least 80% of the models agree on the sign of change. Units are number density per 5° spherical cap per month. Further details on data sources and processing are available in the chapter data table (Table 4.SM.1).

Modes of variability (2)

Blocks in meteorology are large-scale patterns in the atmospheric pressure field that are nearly stationary, effectively "**blocking**" or redirecting migratory cyclones. They are also known as blocking highs or blocking anticyclones. These blocks can remain in place for several days or even weeks, causing the areas affected by them to have the same kind of weather for an extended period of time.

Projected wintertime atmospheric blocking frequencies

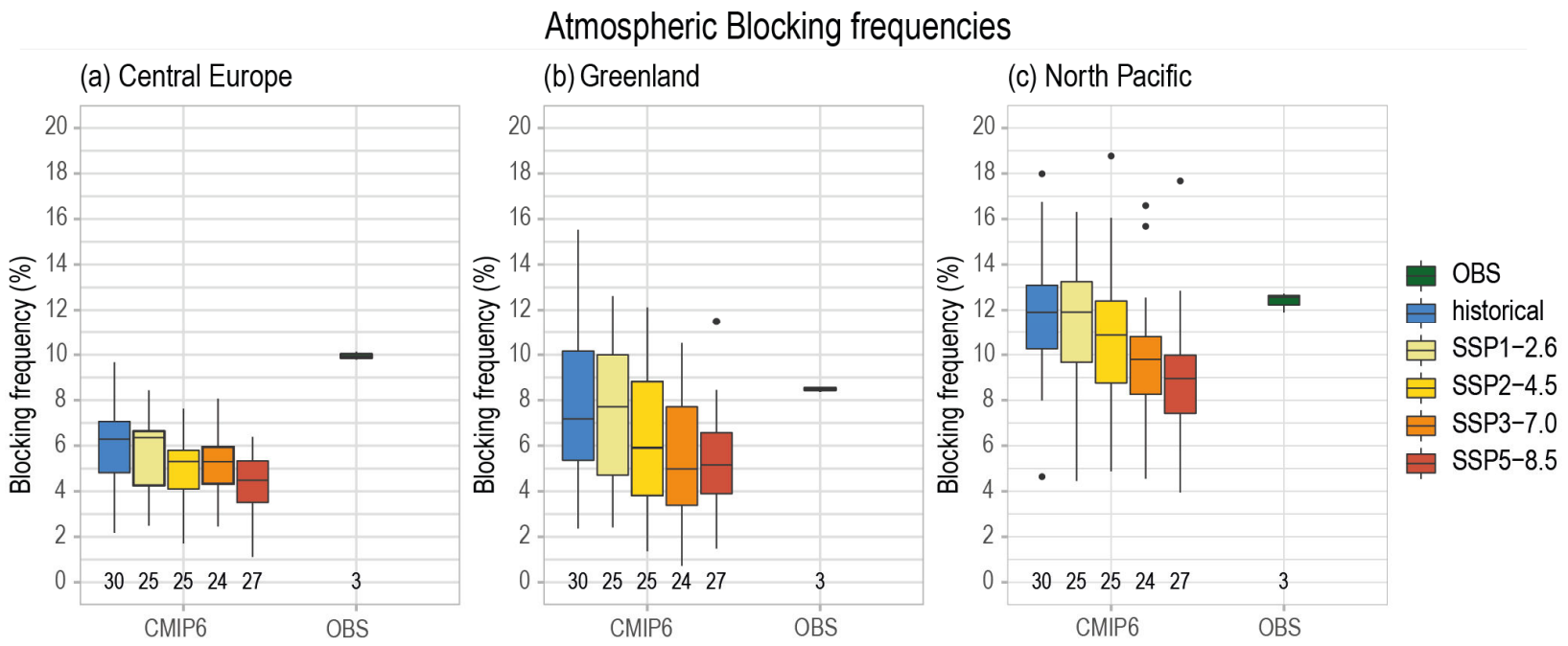

Figure 4.28 | Projected winter atmospheric blocking frequencies. Box plot showing December–March atmospheric blocking frequencies from historical simulations over 1995–2014 and projections over 2081–2100, over **(a)** the Central European region (20°W–20°E, 45°N–65°N); **(b)** the Greenland region (65°W–20°W, 62.5°N–72.5°N); **(c)** the North Pacific region (130°E–150°W, 60°N–75°N). Values show the percentage of blocked days per season following the (Davini et al., 2012) index. Median values are the thick black horizontal bar. The lower whiskers extend from the first quartile to the smallest value in the ensemble, and the upper whiskers extend from the third quartile to the largest value. The whiskers are limited to an upper bound that is 1.5 times the interquartile range (the distance between the third and first quartiles). Black dots show outliers from the whiskers. The numbers below each bar report the number of models included. Observationally-based values are obtained as the average of the ERA-Interim Reanalysis, the JRA-55 Reanalysis and the NCEP/NCAR Reanalysis. Adapted from Davini and D'Andrea (2020). Further details on data sources and processing are available in the chapter data table (Table 4.SM.1).

Projected wintertime atmospheric blocking frequencies

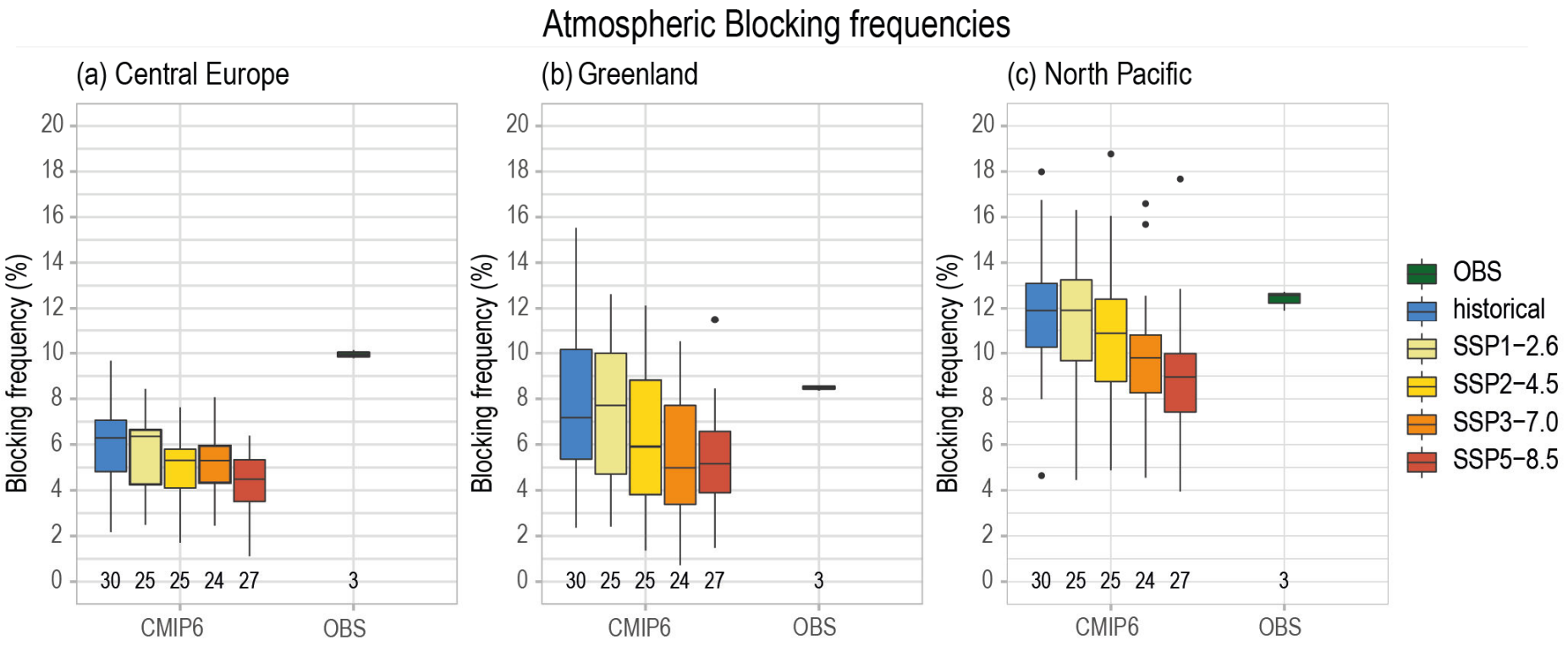

IPCC 2021, Chap. 4

Modes of variability (3)

The **Atlantic Multidecadal Oscillation (AMO)**, also known as **Atlantic Multidecadal Variability (AMV)**, is the theorized variability of the sea surface temperature (SST) of the North Atlantic Ocean on the timescale of several decades.

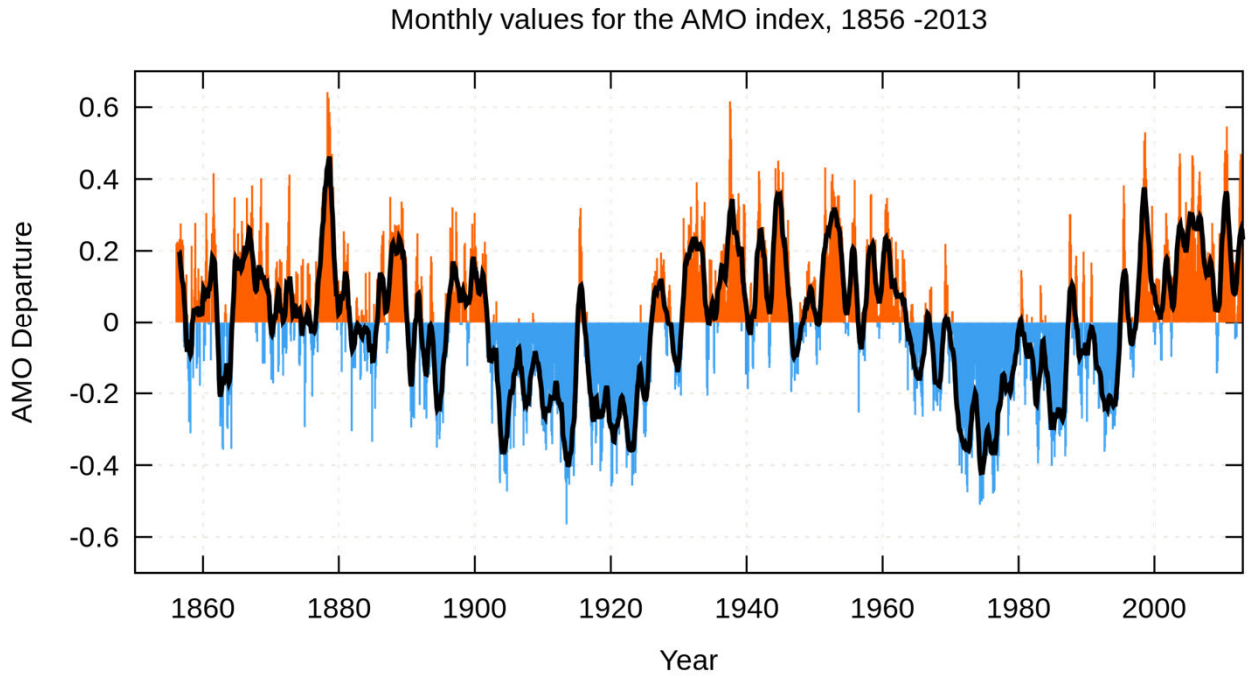

Statements in the Executive Summary

Large-scale Circulation and Modes of Variability (3)

Near-term predictions and projections of the sub-polar branch of the Atlantic Multi-decadal Variability (AMV) on the decadal timescale have improved in CMP6 models compared to CMIP5 (*high confidence*). This is likely to be related to a more accurate response to natural forcing in CMIP6 models. Initialization contributes to the reduction of uncertainty and to predicting subpolar sea surface temperature. AMV influences on the nearby regions can be predicted over lead times of 5–8 years (*medium confidence*). {4.4.3}

IPCC 2021, Chap. 4

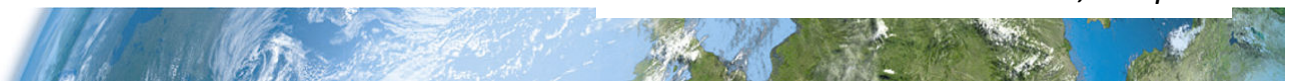

Modes of variability (4)

El Niño–Southern Oscillation (ENSO) is an irregular periodic variation in winds and sea surface temperatures over the tropical eastern Pacific Ocean, affecting the climate of much of the tropics and subtropics. The warming phase of the sea temperature is known as El Niño and the cooling phase as La Niña.

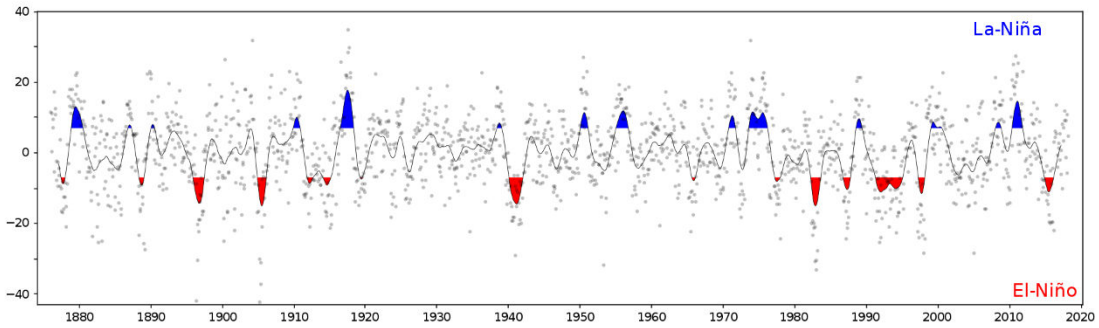

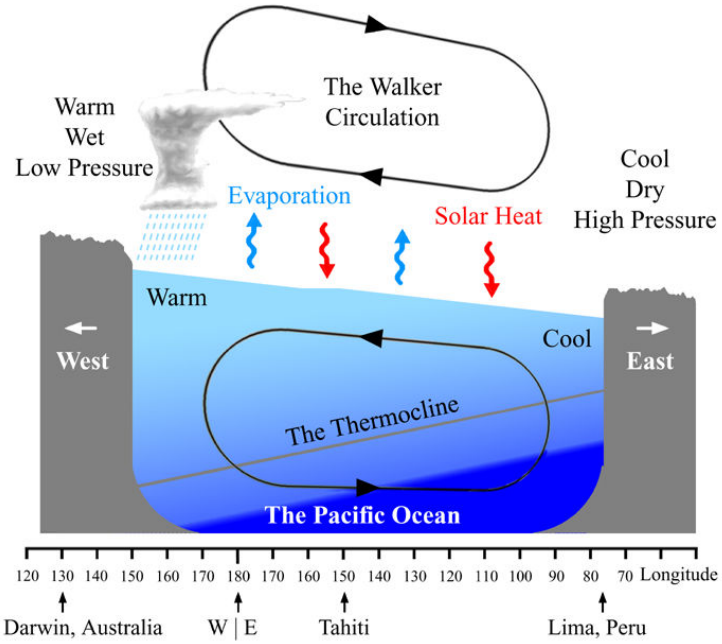

Statements in the Executive Summary

Large-scale Circulation and Modes of Variability (3)

Near-term predictions and projections of the sub-polar branch of the Atlantic Multi-decadal Variability (AMV) on the decadal timescale have improved in CMP6 models compared to CMIP5 (*high confidence*). This is likely to be related to a more accurate response to natural forcing in CMIP6 models. Initialization contributes to the reduction of uncertainty and to predicting subpolar sea surface temperature. AMV influences on the nearby regions can be predicted over lead times of 5–8 years (*medium confidence*). {4.4.3}

It is *virtually certain* that the El Niño–Southern Oscillation (ENSO) will remain the dominant mode of interannual variability in a warmer world. There is no model consensus for a systematic change in intensity of ENSO sea surface temperature (SST) variability over the 21st century in any of the SSP scenarios assessed (*medium confidence*). However, it is *very likely* that ENSO rainfall variability, used for defining extreme El Niños and La Niñas, will increase significantly, regardless of amplitude changes in ENSO SST variability, by the second half of the 21st century in scenarios SSP2-4.5, SSP3-7.0, and SSP5-8.5. {4.3.3, 4.5.3, 8.4.2}

IPCC 2021, Chap. 4

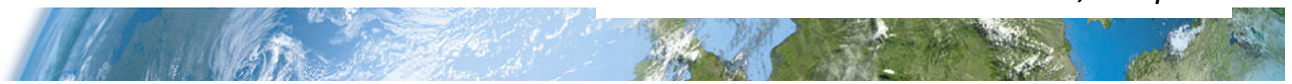

Statements in the Executive Summary

Cryosphere and Ocean (1)

Under the SSP2-4.5, SSP3-7.0, and SSP5-8.5 scenarios, it is *likely* that the Arctic Ocean in September, the month of annual minimum sea ice area, will become practically ice-free (sea ice area less than 1 million km^2) averaged over 2081–2100 and all available simulations. Arctic sea ice area in March, the month of annual maximum sea ice area, also decreases in the future under each of the considered scenarios, but to a much lesser degree (in percentage terms) than in September (*high confidence*). {4.3.2}

IPCC 2021, Chap. 4

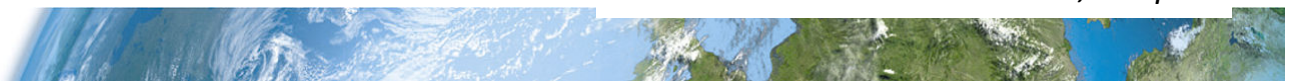

Selected indicators of global climate change from CMIP6 historical and scenario simulations

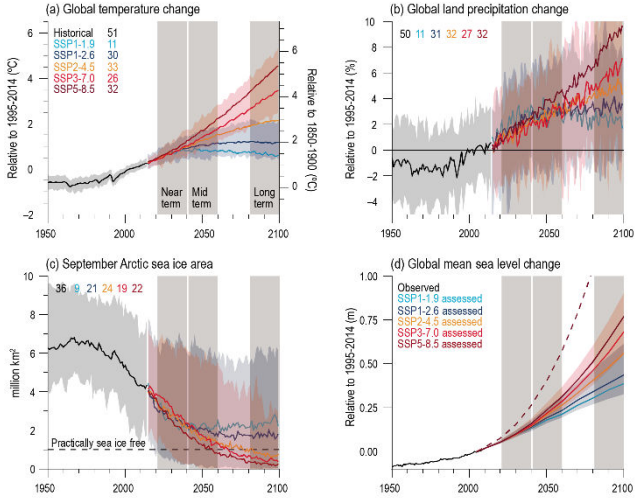

Figure 4.2 | Selected indicators of global climate change from CMIP6 historical and scenario simulations. (a) Global surface air temperature changes relative to the 1995–2014 average (left axis) and relative to the 1850–1900 average (right axis; offset by 0.82°C, which is the multi-model mean and close to observed best estimate, Cross-Chapter Box 2.1, Table 1). **(b)** Global land precipitation changes relative to the 1995–2014 average. **(c)** September Arctic sea ice area. **(d)** Global mean sea level (GMSL) change relative to the 1995–2014 average. (a), (b) and (d) are annual averages, (c) are September averages. In (a–c), the curves show averages over the CMIP6 simulations, the shadings around the SSP1-2.6 and SSP3-7.0 curves show 5–95% ranges, and the numbers near the top show the number of model simulations used. Results are derived from concentration-driven simulations. In (d), the barystatic contribution to GMSL (i.e., the contribution from land-ice melt) has been added offline to the CMIP6 simulated contributions from thermal expansion (thermosteric). The shadings around the SSP1-2.6 and SSP3-7.0 curves show 5–95% ranges. The dashed curve is the *low confidence* and low likelihood outcome at the high end of SSP5-8.5 and reflects deep uncertainties arising from potential ice-sheet and ice-cliff instabilities. This curve at year 2100 indicates 1.7 m of GMSL rise relative to 1995–2014. More information on the calculation of GMSL is available in Chapter 9, and further regional details are provided in the Atlas. Further details on data sources and processing are available in the chapter data table (Table 4.SM.1).

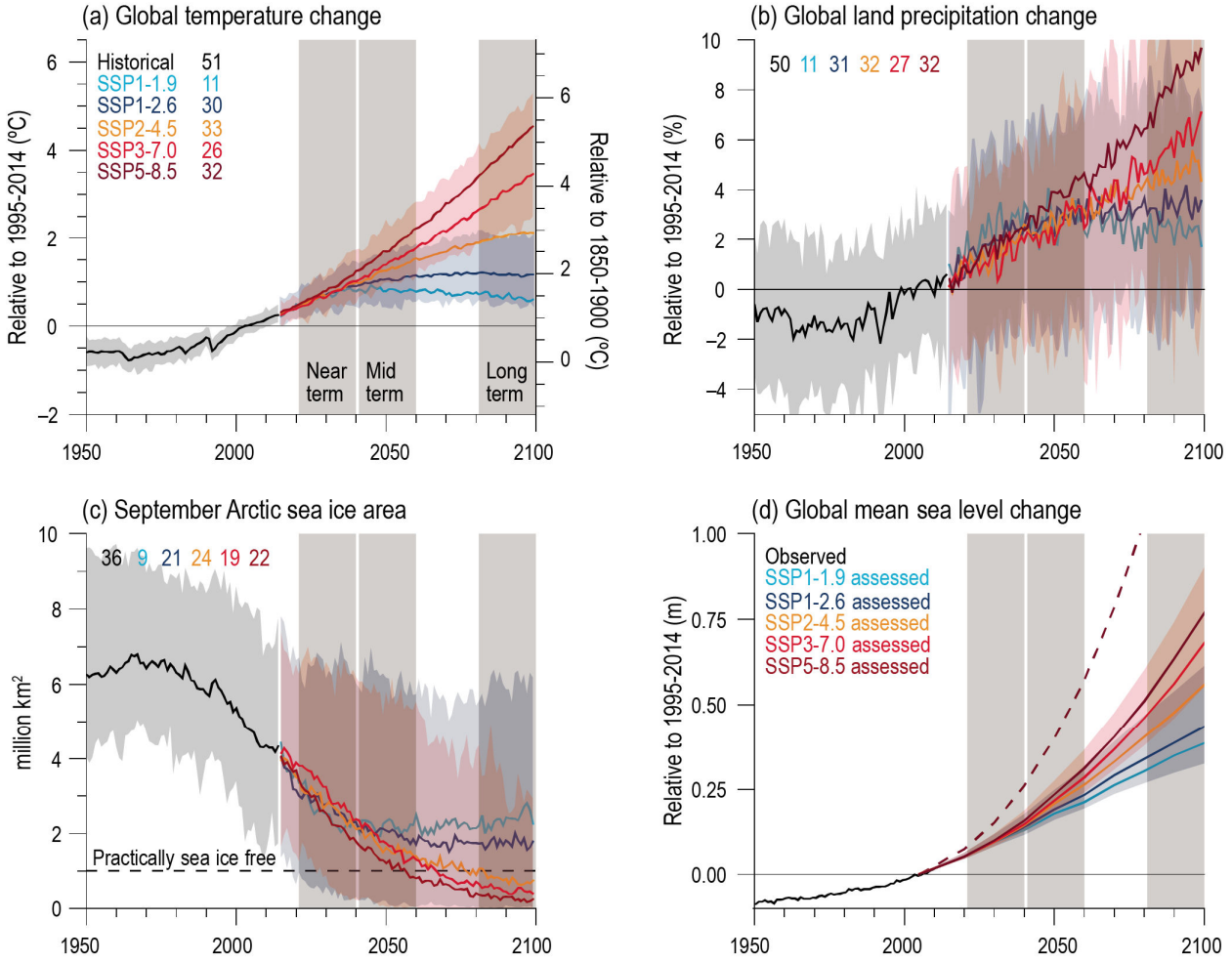

IPCC 2021, Chap. 4

Statements in the Executive Summary

Cryosphere and Ocean (1)

Under the SSP2-4.5, SSP3-7.0, and SSP5-8.5 scenarios, it is *likely* that the Arctic Ocean in September, the month of annual minimum sea ice area, will become practically ice-free (sea ice area less than 1 million km^2) averaged over 2081–2100 and all available simulations. Arctic sea ice area in March, the month of annual maximum sea ice area, also decreases in the future under each of the considered scenarios, but to a much lesser degree (in percentage terms) than in September (*high confidence*). {4.3.2}

Under the five scenarios assessed, it is *virtually certain* that global mean sea level (GMSL) will continue to rise through the 21st century. For the period 2081–2100 relative to 1995–2014, GMSL is *likely* to rise by 0.46–0.74 m under SSP3-7.0 and by 0.30–0.54 m under SSP1-2.6 (*medium confidence*). For the assessment of change in GMSL, the contribution from land-ice melt has been added offline to the CMIP6-simulated contributions from thermal expansion. {4.3.2. 9.6}

IPCC 2021, Chap. 4

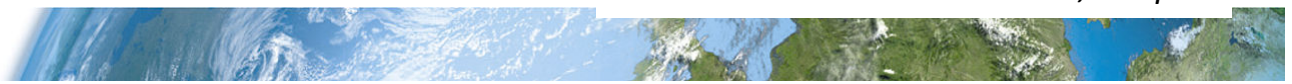

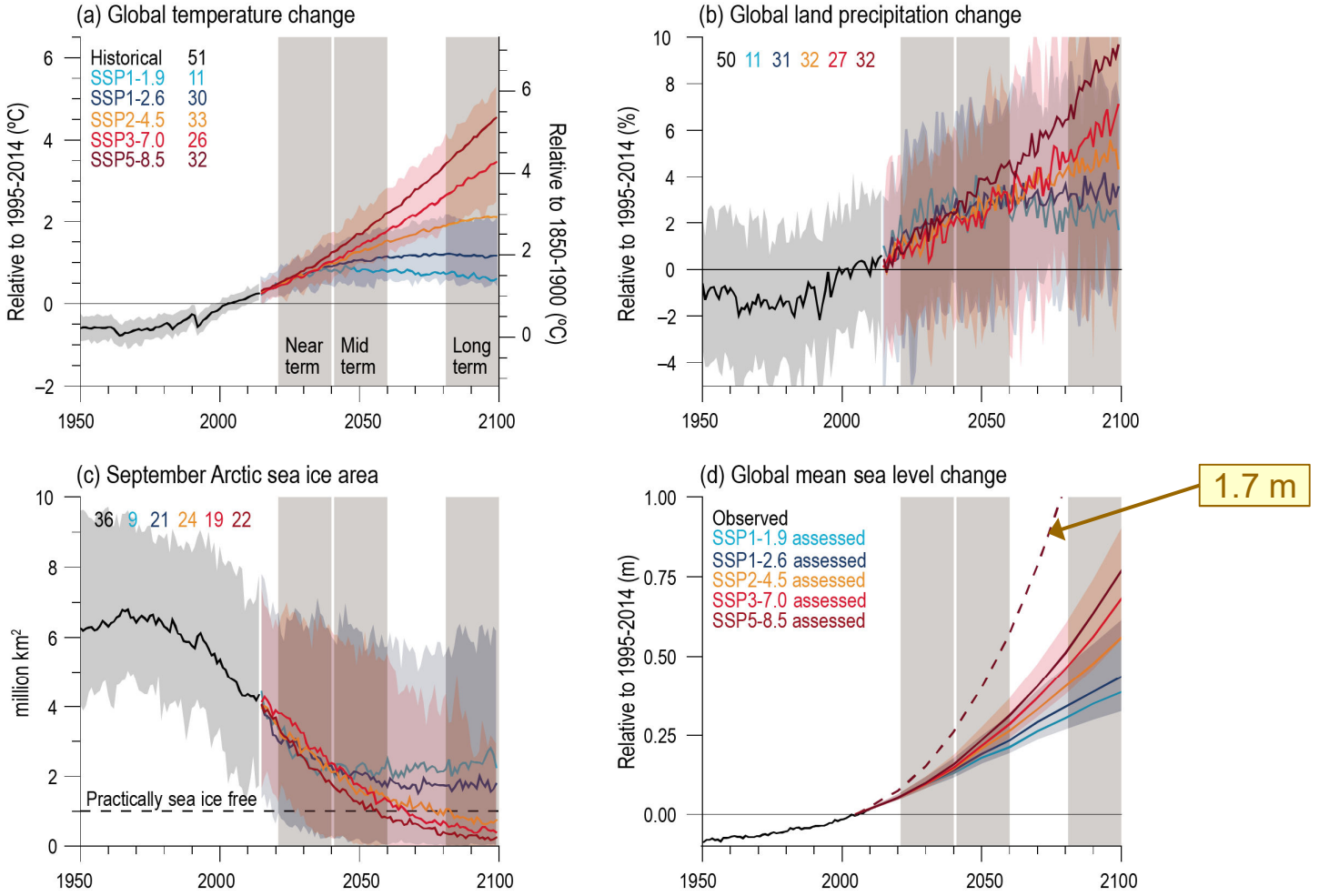

IPCC 2021, Chap. 4

Statements in the Executive Summary

Cryosphere and Ocean (2)

It is *very likely* that the cumulative uptake of carbon by the ocean and by land will increase through to the end of the 21st century. Carbon uptake by land shows greater increases but with greater uncertainties than for ocean carbon uptake. The fraction of emissions absorbed by land and ocean sinks will be smaller under high emission scenarios than under low emission scenarios (*high confidence*). Ocean surface pH will decrease steadily through the 21st century, except for SSP1-1.9 and SSP1-2.6 where values decrease until around 2070 and then increase slightly to 2100 (high confidence). {4.3.2, 5.4}

IPCC 2021, Chap. 4

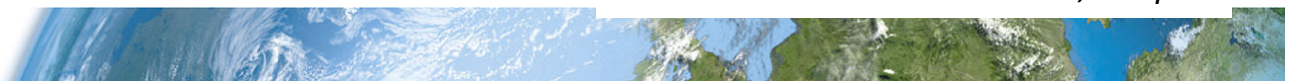

Long-term change of annual and zonal ocean pH

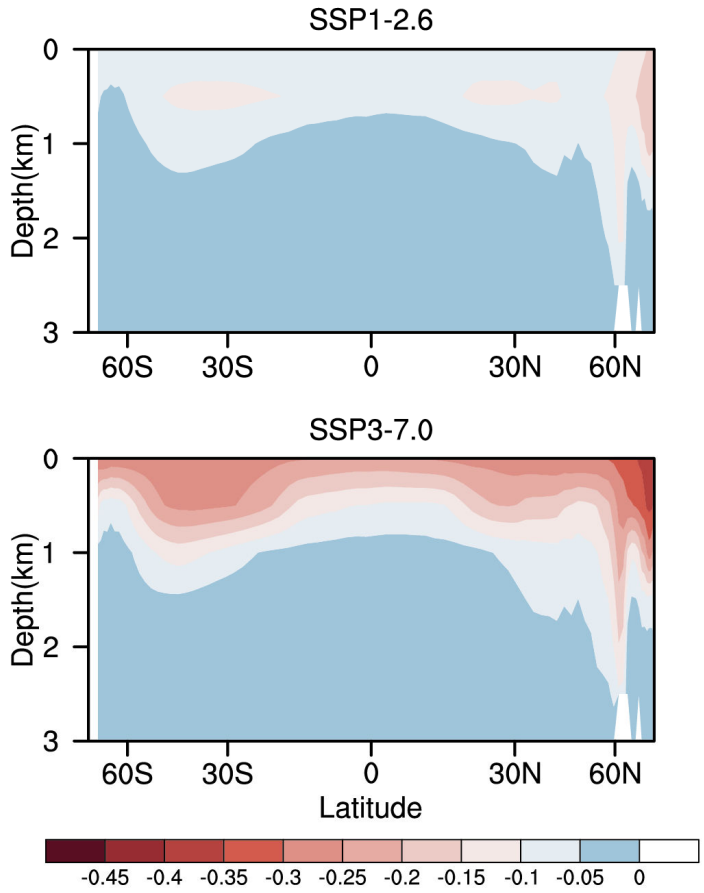

Figure 4.29 | Long-term change of annual and zonal ocean pH. Displayed are multi-model mean change in annual and zonal ocean pH in 2081–2100 relative to the mean of 1995–2014 for SSP1-2.6 and SSP3-7.0, respectively. Eleven CMIP6 model results are used. Diagonal lines indicate regions where fewer than 80% of the models agree on the sign of the change and no overlay where at least 80% of the models agree on the sign of change. Further details on data sources and processing are available in the chapter data table (Table 4.SM.1).

IPCC 2021, Chap. 4

Statements in the Executive Summary

Climate Response to Emission Reduction, Carbon Dioxide Removal, and Solar Radiation Modification (1)

If strong mitigation is applied from 2020 onward as reflected in SSP1-1.9, its effect on 20-year trends in GSAT would likely emerge during the near term (2021–2040), measured against an assumed non-mitigation scenario such as SSP3-7.0 and SSP5-8.5. However, the response of many other climate quantities to mitigation would be largely masked by internal variability during the near term, especially on the regional scale (*high confidence*). The mitigation benefits for these quantities would emerge only later during the 21st century (*high confidence*). During the near term, a small fraction of the surface can show cooling under all scenarios assessed here, so near-term cooling at any given location is fully consistent with GSAT increase (*high confidence*). Events of reduced and increased GSAT trends at decadal timescales will continue to occur in the 21st century but will not affect the centennial warming (*very high confidence*). {4.6.3, Cross-Chapter Box 3.1}

IPCC 2021, Chap. 4

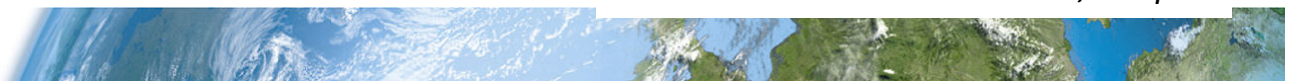

Statements in the Executive Summary

Climate Response to Emission Reduction, Carbon Dioxide Removal, and Solar Radiation Modification (2)

Because of the near-linear relationship between cumulative carbon emissions and GSAT change, the cooling or avoided warming from carbon dioxide removal (CDR) is proportional to the cumulative amount of CO_2 removed by CDR (*high confidence*). The climate system response to net negative CO_2 emissions is expected to be delayed by years to centuries. Net negative CO_2 emissions due to CDR will not reverse some climate change, such as sea level rise, at least for several centuries (*high confidence*). The climate effect of a sudden and sustained CDR termination would depend on the amount of CDR-induced cooling prior to termination and the rate of background CO_2 emissions at the time of termination (*high confidence*). {4.6.3, 5.5, 5.6}

IPCC 2021, Chap. 4

Delayed climate response to CDR-caused net negative CO_2 emissions

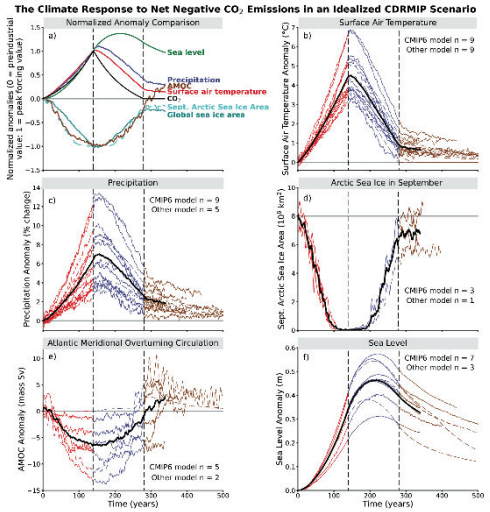

Figure 4.37 | Delayed climate response to carbon dioxide removal (CDR)-caused net negative CO_2 emissions. Multi-model simulated response in global and annual mean climate variables for a ramp-up followed by ramp-down of CO_2. Atmospheric CO_2 increases from the pre-industrial level at a rate of 1% yr^{-1} to 4×CO2, then decreases at the same rate to the pre-industrial level and then remains constant. The ramp-down phase represents the period of net negative CO_2 emissions. **(a)** Normalized ensemble mean anomaly of key variables as a function of year, including atmospheric CO_2, surface air temperature, precipitation, thermosteric sea level change (see Glossary), global sea ice area, Northern Hemisphere sea ice area in September, and Atlantic meridional overturning circulation (AMOC); **(b)** surface air temperature; **(c)** precipitation; **(d)** September Arctic sea ice area; **(e)** AMOC; **(f)** thermosteric sea level; five-year running means are shown for all variables except the sea level change. In (b, f), red lines represent the phase of CO_2 ramp-up, blue lines represent the phase of CO_2 ramp-down, brown lines represent the period after CO_2 has returned to pre-industrial level, and black lines represent the multi-model mean. For all of the segments in (b, f), the solid coloured lines are CMIP6 models, and the dashed lines are other models (i.e., EMICs, CMIP5-era models). Vertical dashed lines indicate peak CO_2 and when CO_2 again reaches pre-industrial value. The number of CMIP6 and non-CMIP6 models used is indicated in each panel. The time series for the multi-model means (b, f) and the normalized anomalies (a) are terminated when data from all models are not available, in order to avoid the discontinuity in the time series. Further details on data sources and processing are available in the chapter data table (Table 4.SM.1).

Delayed climate response to CDR-caused net negative CO_2 emissions

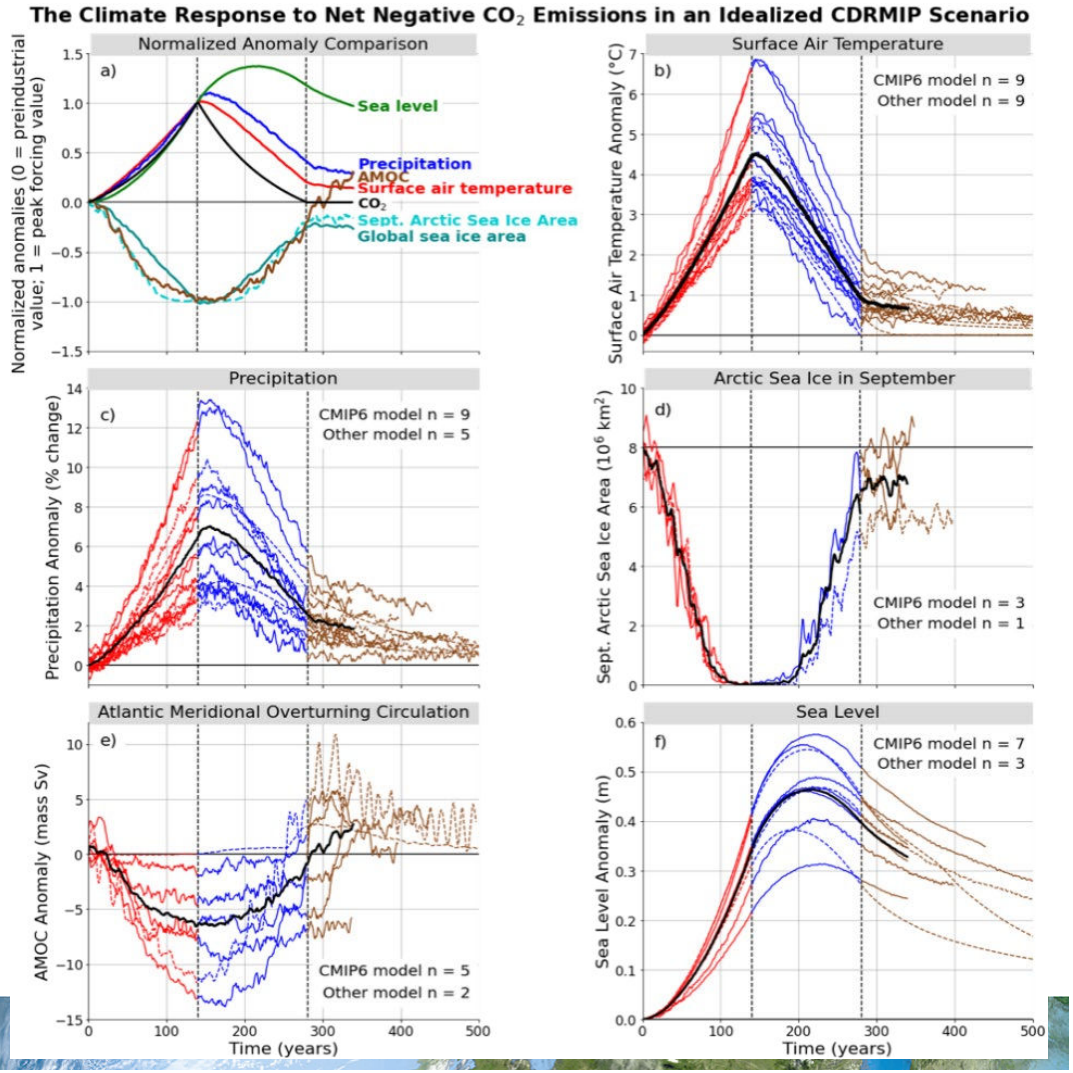

IPCC 2021, Chap. 4

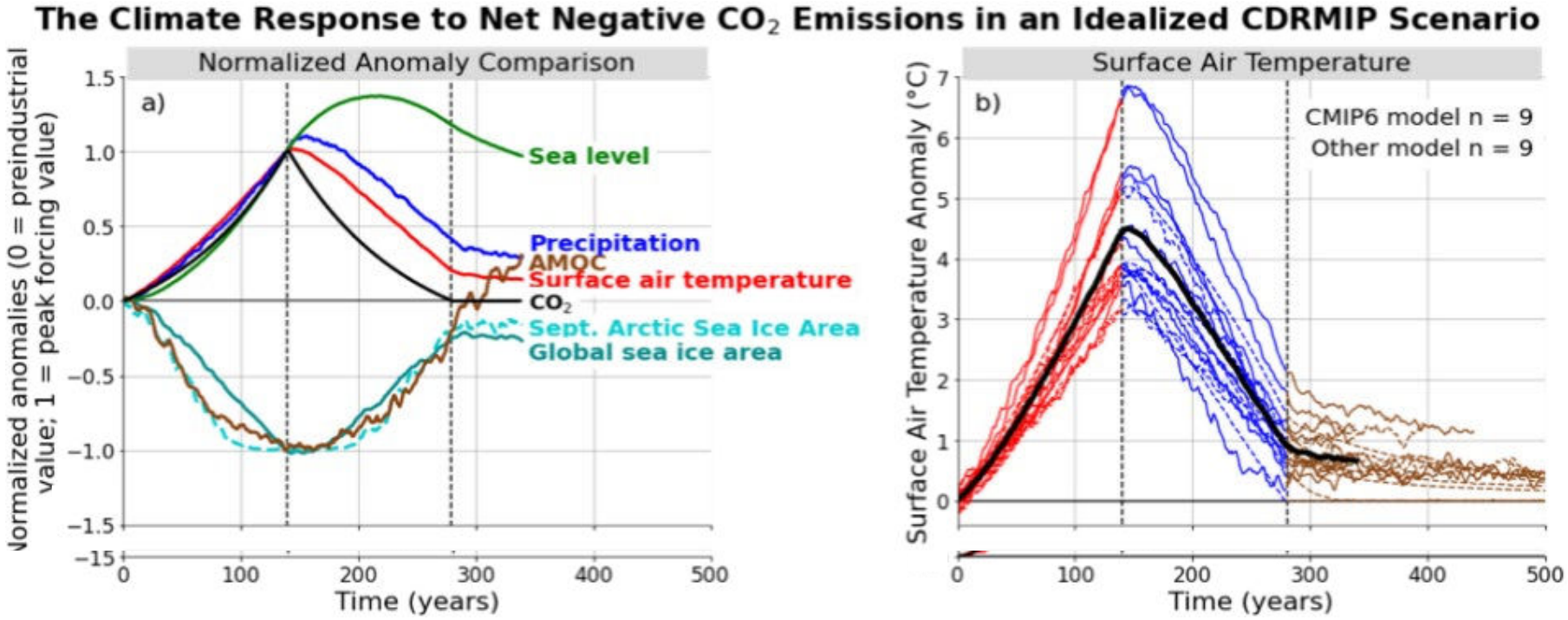

IPCC 2021, Chap. 4

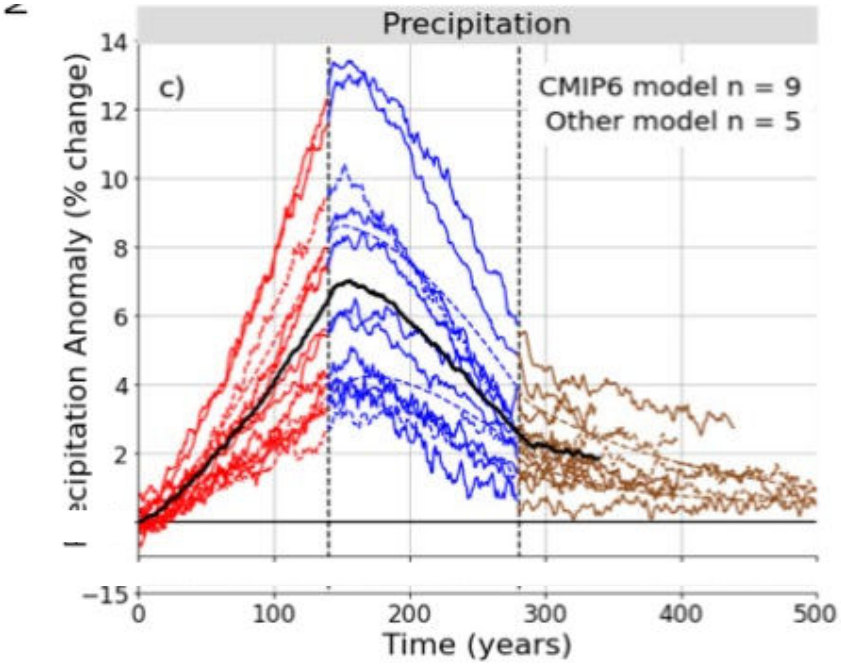

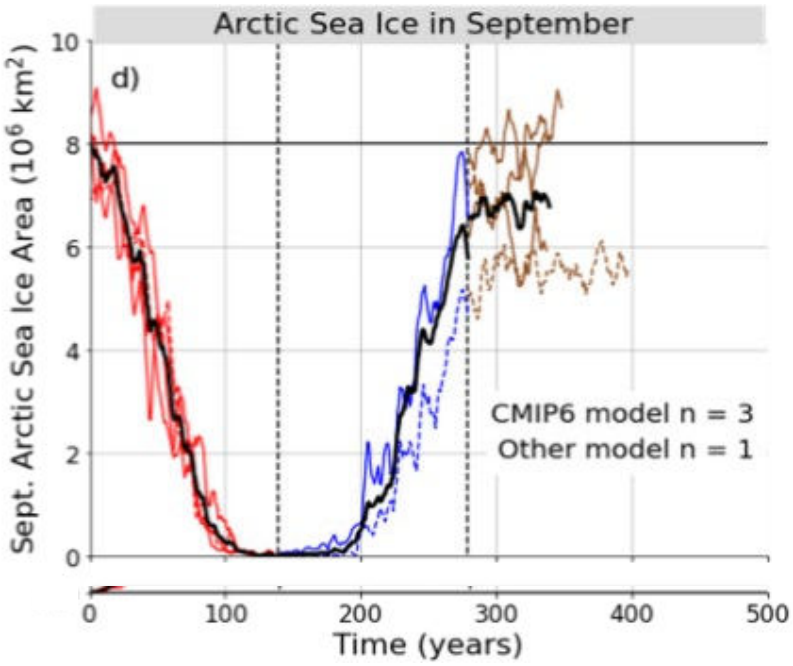

IPCC 2021, Chap. 4

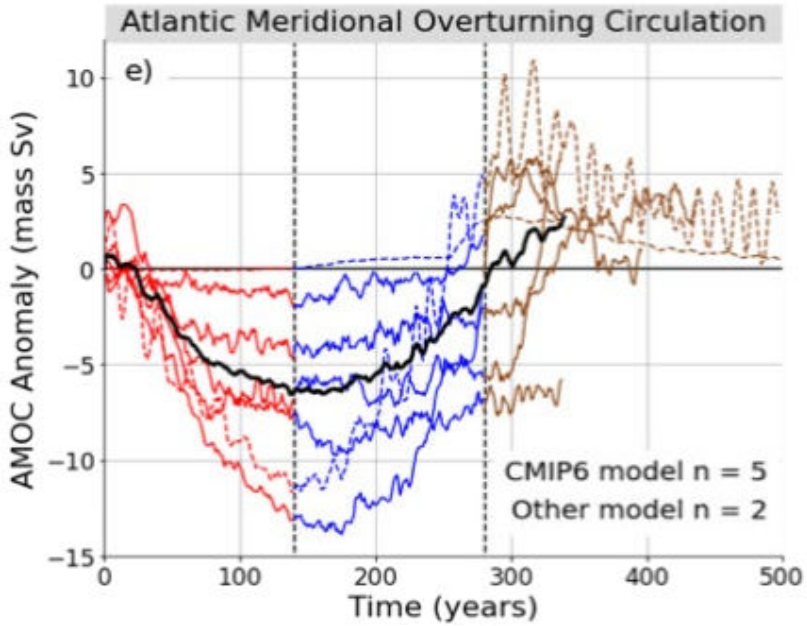

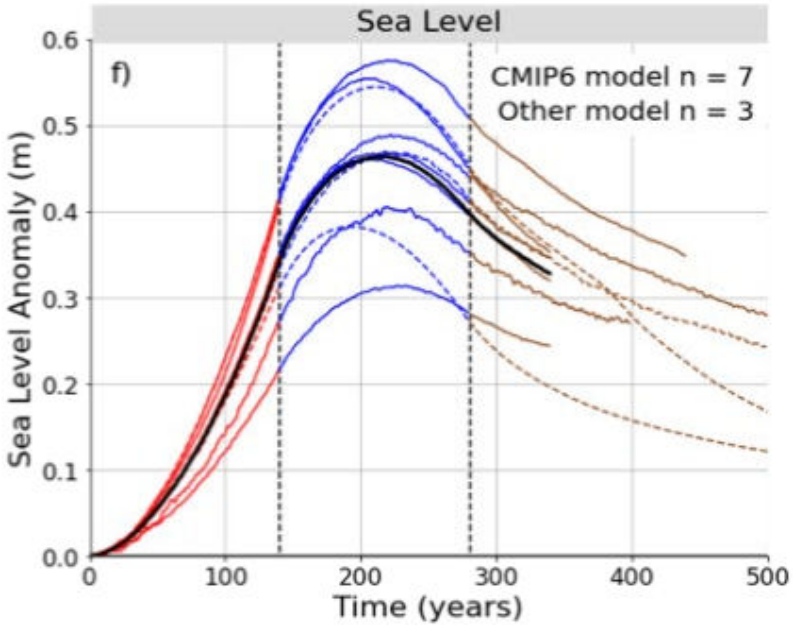

IPCC 2021, Chap. 4

Statements in the Executive Summary

Climate Response to Emission Reduction, Carbon Dioxide Removal, and Solar Radiation Modification (3)

Solar radiation modification (SRM) could offset some of the effects of anthropogenic warming on global and regional climate, but there would be substantial residual and overcompensating climate change at the regional scale and seasonal timescale (*high confidence*), and there is *low confidence* in our understanding of the climate response to SRM, specifically at the regional scale. Since the AR5, understanding of the global and regional climate response to SRM has improved, due to modelling work with more sophisticated treatment of aerosol-based SRM options and stratospheric processes. Improved modelling suggests that multiple climate goals could be met simultaneously. A sudden and sustained termination of SRM in a high-emission scenario such as SSP5-8.5 would cause a rapid climate change (*high confidence*). However, a gradual phase-out of SRM combined with emissions reductions and CDR would *more likely than* not avoid larger rates of warming. {4.6.3}

IPCC 2021, Chap. 4

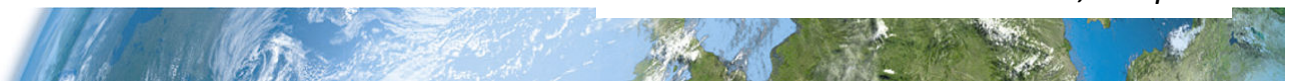

Multi-model response per degree global mean cooling in temperature and precipitation in response to CO_2 forcing and SRM forcing

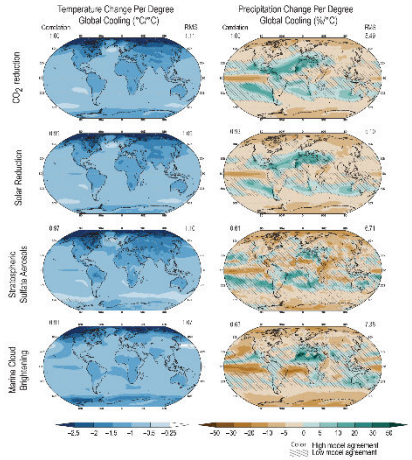

Figure 4.38 | Multi-model response per degree global mean cooling in temperature and precipitation in response to CO_2 forcing and SRM forcing. Top row shows the response to a CO_2 decrease, calculated as the difference between pre-industrial control simulation and *abrupt4xCO_2* simulations where the CO_2 concentration is quadrupled abruptly from the pre-industrial level (11-model average); **second row** shows the response to a globally uniform solar reduction, calculated as the difference between GeoMIP experiment G1 and *abrupt4xCO_2* (11-model average); **third row** shows the response to stratospheric sulphate aerosol injection, calculated as the difference between GeoMIP experiment G4 (a continuous injection of 5 Tg SO_2 $year^{-1}$ at one point on the equator into the lower stratosphere against the RCP4.5 background scenario) and RCP4.5 (six-model average); and the **bottom row** shows the response to marine cloud brightening, calculated as the difference between GeoMIP experiment G4cdnc (increase cloud droplet concentration number in marine low cloud by 50% over the global ocean against RCP4.5 background scenario) and RCP4.5 (eight-model average). All differences (average of years 11–50 of simulation) are normalized by the global mean cooling in each scenario, averaged over years 11–50. Diagonal lines represent regions where fewer than 80% of the models agree on the sign of change. The values of correlation represent the spatial correlation of each SRM-induced temperature and precipitation change pattern with the pattern of change caused by a reduction of atmospheric CO_2. RMS (root mean square) is calculated based on the fields shown in the maps (normalized by global mean cooling). Further details on data sources and processing are available in the chapter data table (Table 4.SM.1).

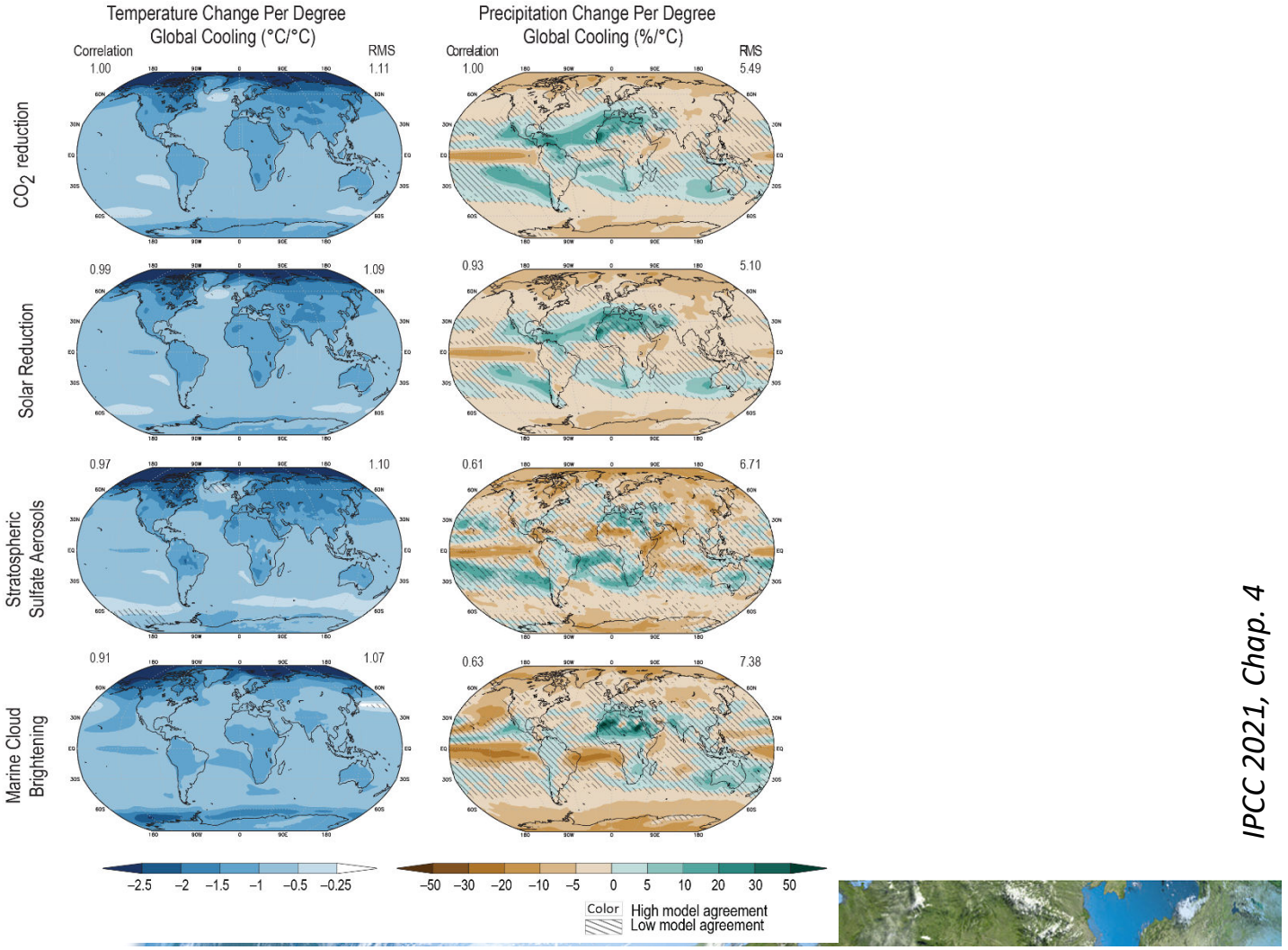
Temperature Change Per Degree
Global Cooling (°C/°C)
Precipitation Change Per Degree
Global Cooling (%/°C)
Correlation
RMS
CO_2 reduction
1.00
1.11
1.00
5.49
Solar Reduction
0.99
1.09
0.93
5.10
Stratospheric
Sulfate Aerosols
0.97
1.10
0.61
6.71
Marine Cloud
Brightening
0.91
1.07
0.63
7.38
−2.5 −2 −1.5 −1 −0.5 −0.25
−50 −30 −20 −10 −5 0 5 10 20 30 50
Color
High model agreement
Low model agreement

Statements in the Executive Summary

Climate Change Commitment and Change Beyond 2100 (1)

Earth system modelling experiments since AR5 confirm that the zero CO_2 emissions commitment (the additional rise in GSAT after all CO_2 emissions cease) is small (*likely* less than 0.3°C in magnitude) on decadal time scales, but that it may be positive or negative. There is *low confidence* in the sign of the zero CO_2 emissions commitment. Consistent with SR1.5, the central estimate is taken as zero for assessments of remaining carbon budgets for global warming levels of 1.5°C or 2°C. {4.7.2, 5.5.2}.

Overshooting specific global warming levels such as 2°C has effects on the climate system that persist beyond 2100 *(medium confidence*). Under one scenario including a peak and decline in atmospheric CO_2 concentration (SSP5-3.4-OS), some climate metrics such as GSAT begin to decline but do not fully reverse by 2100 to levels prior to the CO_2 peak (*medium confidence*). GMSL continues to rise in all models up to 2100 despite a reduction in CO_2 to 2040 levels. {4.6.3, 4.7.1, 4.7.2}

IPCC 2021, Chap. 4

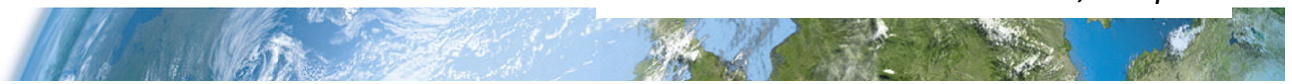

Statements in the Executive Summary

Climate Change Commitment and Change Beyond 2100 (2)

Using extended scenarios beyond 2100, projections show *likely* warming by 2300, relative to 1850–1900, of 1.0°C–2.2°C for SSP1-2.6 and 6.6°C–14.1°C for SSP5-8.5. By 2300, warming under the SSP5-3.4-OS overshoot scenario decreases from a peak around year 2060 to a level very similar to SSP1-2.6. Precipitation over land continues to increase strongly under SSP5-8.5. GSAT projected for the end of the 23rd century under SSP2-4.5 (2.3–4.6°C) has not been experienced since the mid-Pliocene, about 3 million years ago. GSAT projected for the end of the 23rd century under SSP5-8.5 (6.6–14.1°C) overlaps with the range estimated for the Miocene Climatic Optimum (5°C–10°C) and Early Eocene Climatic Optimum (10°C–18°C), about 15 and 50 million years ago, respectively (*medium confidence*). {2.3.1.1, 4.7.1}

IPCC 2021, Chap. 4

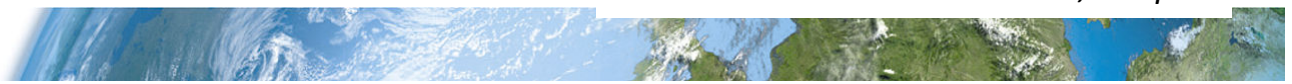

Simulated climate changes up to 2300 under the extended SSP scenarios

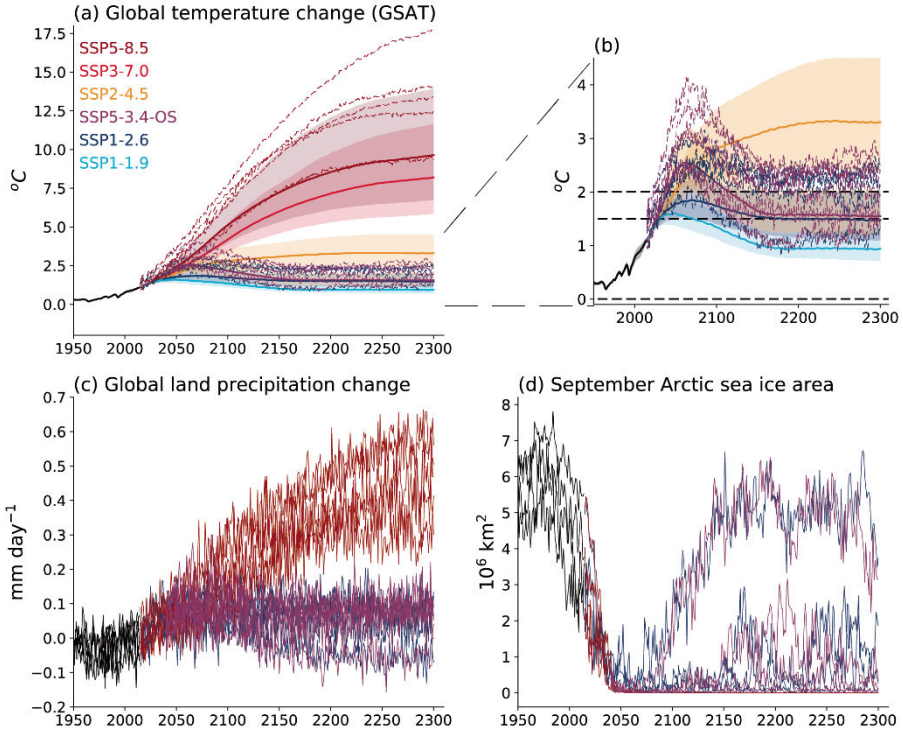

Figure 4.40 | Simulated climate changes up to 2300 under the extended SSP scenarios. Displayed are **(a)** projected global surface air temperature (GSAT) change, relative to 1850–1900, from CMIP6 models (individual lines) and MAGICC7 (shaded plumes); **(b)** as (a) but zoomed in to show low-emissions scenarios; **(c)** global land precipitation change; and **(d)** September Arctic sea ice area. Further details on data sources and processing are available in the chapter data table (Table 4.SM.1).

Simulated climate changes up to 2300 under the extended SSP scenarios

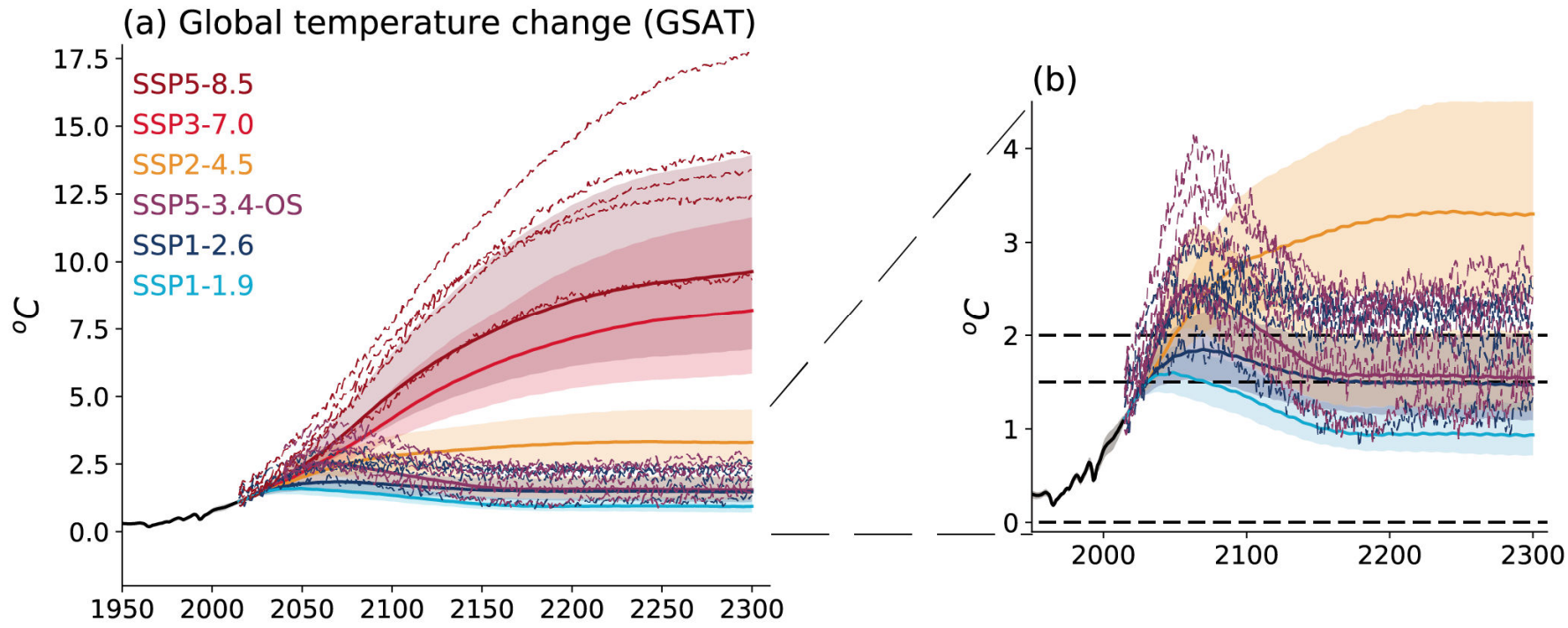

IPCC 2021, Chap. 4

Simulated climate changes up to 2300 under the extended SSP scenarios

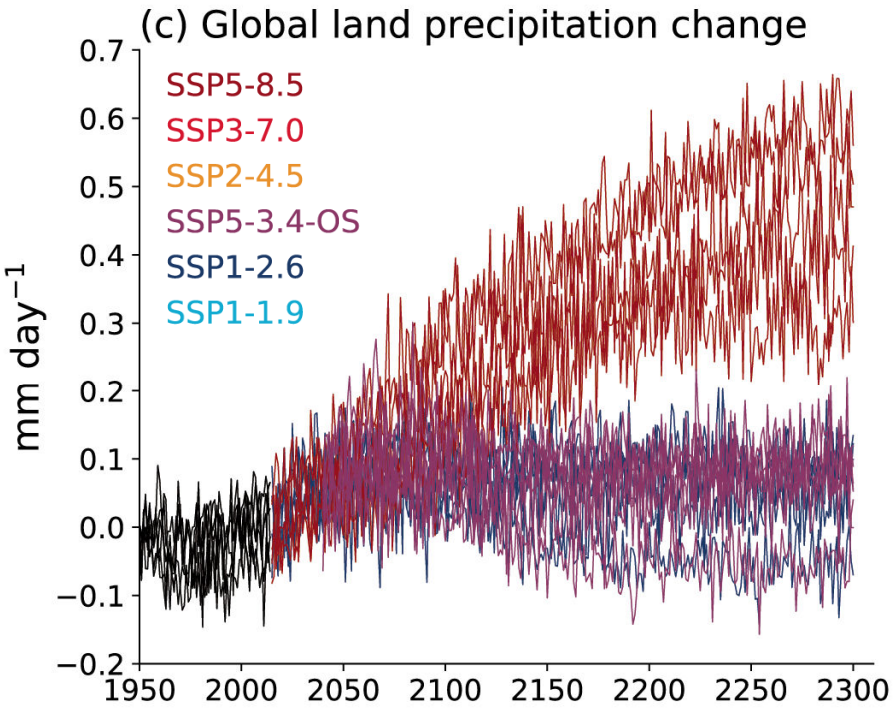

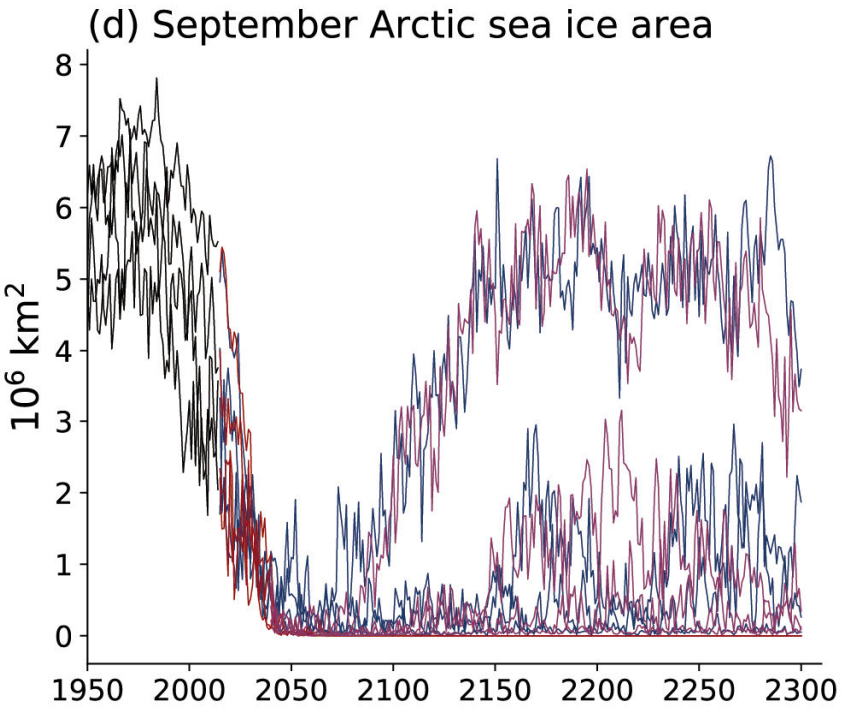

IPCC 2021, Chap. 4